THEORETICAL INVESTIGATION OF THE OPTICAL KERR EFFECT AND THIRD-HARMONIC GENERATION IN AU-VO_2 THIN-FILMS.

MULUNDA FRANLY NKULU

A Dissertation submitted to the Faculty of Science
University of the Witwatersrand, Johannesburg
in fulfilment of the requirement of the degree of
Master of Science

November, 2004

DECLARATION

I declare that this dissertation is my own, unaided work.

It is being submitted for the degree of Master of Science in the University of the Witwatersrand, Johannesburg. It has not been submitted previously for any degree or examination in any other university.

_____ Signature of Candidate

November 23, 2004

ACKNOWLEDGMENT

I would like to thank my supervisor, Prof. A. G. Every for his guidance, patience as well as scientific input and financial support during my work. I acknowledge his meticulousness in every discussion that resulted in much of the material in this thesis. I am highly indebted to him for boosting my confidence, in general, and in tackling difficult problems, in particular.

I would like to thank Dr. M. Maaza for proposing this research project and for initiating me into the ideas and literature of the subject. Thanks to Dr. O. Nemraoui for many fruitful discussion and guidance in search for information on nonlinear optics. Thanks to Dr. G. Hearne for provision of a bursary in my first year of MSc and to Dr. C. Wafo Soh for his constant encouragement.

I am grateful to the National Research Foundation (NRF) as well as the University of the Witwatersrand through the Postgraduate Merit Award for their financial support that made this work possible.

I would like to express my gratitude to my family, especially my father M. F. Nkulu and my uncle U. B. Kambele who have been a source of inspiration and encouragement to me. Last but not least, I would also like to thank my fianceé as well as my fellows from Harvest House Church International for their invaluable support.

Abstract

The theoretical investigation of the Optical Kerr Effect (OKE) and Third-Harmonic Generation (THG) of Au-VO_2 nanocomposite thin-films undertaken in this project is motivated by the potential use of the Au-VO_2 nanocomposite in nonlinear optical (NLO) devices. NLO devices are a driving force in today's high technology industry. In this thesis the OKE is estimated and computed and will be compared later to the measured OKE using the Z-scan interferometric laser technique [47]. This is a simple yet highly sensitive single-beam experimental technique used to determine the real part of the dielectric susceptibility.

The study of the OKE in these composites has shown that it has a high value, comparable to that found in Au-SiO_2, Au-TiO_2 and Au-Al_2O_3 thin-films [29, 33]. This is despite the fact that the Au volumetric concentration in the Au-VO_2 composites considered here is 10 percent at most, whereas in the other above mentioned composite thin-films the volumetric concentration range was between $5 - 60$ percent. Moreover, it has been demonstrated that the OKE is thermally tunable in the Au-VO_2 thin-films, owing to the thermally tunable optical properties of the VO_2 [8, 38]. It is found that the magnitude of the OKE is of the order of 10^{-6} esu when the composite is below 68 ^{0}C and it is of the order of 10^{-7} esu when the nanocomposite thin-film is above 68 ^{0}C.

The large enhancement of the OKE is due to the surface plasmon resonance (SPR) of the nanogold particles. Its fast response, which is of the order of few picoseconds [4, 6, 7], makes the Au-VO_2 nanocomposite a good candidate as a fast thermally tunable optical switch or modulator.

The modelling here of high-order harmonic generation in strongly absorbing media, as regards the amplitude of the primary beam, takes into account *pump attenuation* only, due to the absorption of light by the media. It is not concerned with *pump depletion* which is a consequence of the transfer of energy to the harmonics and which is small by comparison with attenuation in absorbing media. The modelling is applied to the so-called transmission and reflection configurations. The former refers to the case in which the high-order harmonic wave is monitored in the same direction as the input fundamental wave, whereas the latter describes the situation in which the fundamental wave is in the opposite direction to the high-order harmonic one.

To analyse high-order harmonic generation one has to relate the high-order harmonic intensity to the fundamental intensity [1, 9, 10, 34-36]. In so doing, a general formula for analysing high-order harmonic generation is obtained and

reduced to the particular case pertaining to THG in strongly absorbing media.

The ratio of the third-harmonic intensity to the fundamental intensity is termed the *conversion coefficient* or the *conversion efficiency*, and it is denoted by η [23, 34]. It is useful in the sense that it expresses quantitatively the amount of input light of frequency ω converted into light of frequency $n\omega$, where n is the order of nonlinear polarisation [1].

It is found that the THG conversion coefficient is higher the higher the laser intensity. It is thus advantageous to use a pulsed laser, which achieved very high intensities for short periods, separated by long off periods. The net harmonic output in this case is much higher than one would obtain with a continous laser of the same average output. It is found here that η is greater in the reflection configuration compared to the transmission one above and below T_t in the photon energy range $1.0 - 3.0$ eV, see Fig. 5.1 to 5.8.

However, the conversion efficiency for THG in the Au-VO_2 nanocomposites for the picoseconds laser illumination we have considered, is still extremely low, and it is difficult to see a potential use for this system as a tunable frequency converter. The situation would become more favorable with the use of femtosecond laser pulses, where for the same pulse energy the intensity is much greater. The laser pulse energy must be limited to avoid excessive heating of the thin-film.

The heat generated as a consequence of the illumination of the thin-film by the laser [23] may be controlled by using a simple cooling device which consists of a substrate on which the thin-film is deposited. The choice of such a substrate depends on whether THG is monitored in the transmission or reflection configuration. In the former a transparent substrate must be used (for example diamond) whereas in the latter an opaque substrate may be used (for example Ag). Calculations pertaining to the removal of heat from the illuminated film are reported, and show that thermal control is manageable but only within limits. To avoid a temperature rise of more than 5 ^{0}K the peak laser intensity we found must not exceed 7.4 $\times 10^5 \mathrm{Wcm}^{-2}$ with a pulse duration of 5 ps.

Contents

List of Figures

List of Tables

Chapter 1

Introduction

The realm of nonlinear optics becomes accessible under the illumination of a medium by an intense optical field such as that obtained with a laser. Under such conditions the linear polarization model fails to describe the measured polarization, which mediates the interaction between the medium and the light or optical field.

The induced polarization (linear and nonlinear polarization) is analysed by means of the susceptibility tensors formalism that may be viewed as an higher order correction of the linear polarization model by means of extra anharmonic terms; quadratic correction, cubic correction and so on. The susceptibility tensors are greatly simplified through their relevant symmetric properties.

According to J. E. Sipe and R. W. Boyd [2], one may obtain optical systems with desirable nonlinear optical properties in three ways:

1. Molecular Engineering: One attempts to find or to design at the molecular levels, materials with the intrinsic nonlinear optical properties of interest.

2. Propagation Design: The geometry of the system results in light propagation which enhances the effect of nonlinearities. An optical fiber is an example.

3. Materials Architecture: Materials are combined to form a composite optical material.

The Au-VO_2 nano-composite system under investigation in this thesis is a good example of the last mentioned. It is a system that conforms to the well-known Maxwell-Garnett topology, with Au particles embedded in a host matrix of VO_2 in such a way that the radius of the inclusions, denoted a, is very small compared to the distance between particles, which we shall call b, which in turn is small compared to the wavelength λ of the illuminating optical field (light) i.e $a \ll b \ll \lambda$. see Fig. 1.1.

This is the Rayleigh regime of Mie scattering theory where the induced polarization in the small spherical particles is a "dipole" and the propagation of the incident optical field through the medium may be studied by means of electrostatics theory. This is the "quasi-static approximation"[4] by means of which the induced nonlinear polarization of the composite material may be determined with respect to the one of the inclusions (gold nanoparticles).

The third-order nonlinear susceptibility $\chi^{(3)}$ which relates the tripled frequency induced nonlinear polarization of the composite medium to the incident optical field $\mathbf{E}$ may be defined with respect to that of the gold nanoparticles $\chi^{(3)}_{gold}$ by means of the quasi-static approximation, within the "effective medium theory approach"[2] and in particular the linear Maxwell-Garnett effective medium theory whose topology is shown below.

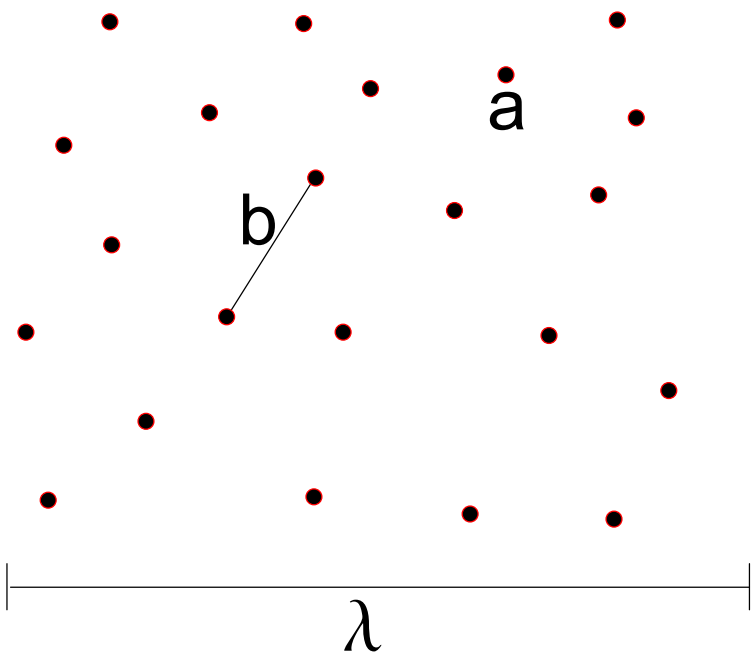

Figure 1.1: Maxwell-Garnett composite topology after J. Sipe and R. W. Boyd [1]

There exist other effective medium theories that describe different composite geometries (topologies) such as the Bruggeman theory. There are two main variants of the Bruggeman topology. One is were the two different components are mixed on an equal footing, which is referred to as the Bruggeman symmetric topology. The other Bruggeman topology is of two unequivalently mixed

components, which is the Bruggeman asymmetric geometry. With respect to the second; if the lowest concentrated component has a volumetric percentage p such that $p \ll .1$ the Bruggeman asymmetric theory reduces to the Maxwell-Garnett theory. There exist also other mixing topologies described by means of the effective medium theory approaches [5, 19, 20].

The third-order nonlinear susceptibility which is of interest in this work manifests itself in different ways depending on the origin and the mechanism underlying the nonlinear polarization [1]. In this work the calculated third order nonlinear susceptibility $\chi^{(3)}_{composite}$ of the Au-VO_2 nano-composite will be used to estimate the efficiencies of the third harmonic generation (THG), and to estimate the nonlinear refractive index. The latter underlies the optical Kerr effect (OKE).

THG and OKE represent just two of the many phenomena which are manifestations of $\chi^{(3)}$. These phenomena [1, 9-11, 34-35] depend either on the intensity of the input light such as two-photon absorption (TPA), stimulated Raman scattering, degenerate four-wave mixing,.... Or, they arise as a consequence of the interactions and recombination of different waves in the medium. The physical meaning of the latter is the following: An incident optical field of frequency ω induces a dipolar polarization. The dipoles oscillate coherently in such a way that they add up to each other to emit a macroscopic field with frequency $n\omega$. The number n represents the order of nonlinearity. If $n = 2$ we have second-harmonic generation (SHG), $n = 3$ represents third-harmonic generation (THG). This is known as sum-frequency generation. In the case where the coherent oscillations of the dipoles get subtracted from one another for example third-order difference mixing, the phenomena are known as difference-frequency mixing [1, 9-11, 34-35]. In this respect *high-order harmonic generation* may be understood as a sum-frequency generation of n waves each of frequency ω. Consequently the resulting wave has frequency $n\omega$.

There exist numerous techniques in nonlinear optics for the measurements of the nonlinear phenomena. To measure OKE, one may use the nonlinear interferometry method [42], the degenerate four-wave mixing [43], the nearly degenerate three-wave mixing [44], the beam-distortion measurements [45] and the Z-scan interferometry [46] method to name a few. The last mentioned is a simple and highly sensitive single-beam technique used to determine the real part of $\chi^{(3)}$. THG may be estimated using picoseconds p-polarised Nd:YAG pulses [32] or a picosecond pulse train from a mode-locked Nd-glass laser [39]. Anna et al. [47] provides a review of experimental techniques for measuring THG.

Many physical mechanisms are responsible for these nonlinear optical phenomena [4, 6]. They are listed in Table 1.1. Metal based nanocomposites are formed of nanoscaled and quasispherical metallic particles embedded in a host

Mechanism	OKE $\chi^{(3)}_{xxxx}$(esu)	Response Time(sec)
Electronic polarisation	$10^{-14} - 10^{-12}$	$10^{-15} - 10^{-12}$
molecular orientation	10^{-12}	10^{-12}
Electrostriction	10^{-12}	10^{-9}
Saturated atomic absorption	10^{-10}	10^{-8}
Thermal effects	10^{-4}	10^{-3}

Table 1.1: Typical values of the OKE $\chi^{(3)}_{xxxx}$ after R. W. Boyd [9] and F. Hache et al. [6]

dielectric matrix [29, 33], for example TiO_2 as shown in Fig. 1.2. The OKE and THG in small metal particles and metal colloids in the case of Au have been successfully investigated by F. Hache et al. [6,7] and D. Ricard et al. [4].

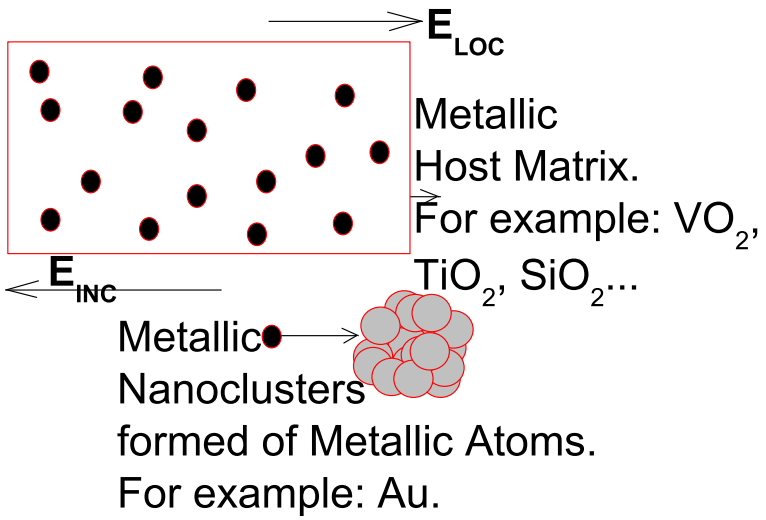

Figure 1.2: Au-Matrix Nanocomposite [29, 33]

Electrons in each nano-particle are well localised. There is spatial confinement within the nanometric volume of the metal nano-particles. This confinement becomes important when the size of the nanoscaled metallic dots is less than 10 Å in the case of Au [1]. It manifests itself as a broadening and shift at the surface plasmon resonance (SPR) energy (see next page). This is known as *quantum confinement effect* or *quantum size effect.*

The SPR condition may be understood as follows: The electric field inside the metal nano-particles is called the *local electric field*, E_{LOC}. The electric

field inside the matrix is different from that of the metal nano-particles. Well away from the particles it is the incident field, E_{INC}. On the assumption that the metallic nanoparticles are spherical, E_{LOC} and E_{INC} are related to each other through the so-called *local field factor* [2, 4, 6]

In this thesis the local field factor enters the expression of the effective $\chi^{(3)}$ of the metal nanocomposite under the assumption that the third-order susceptibility of the inclusion is much greater than that of the host matrix i.e $\chi_i^{(3)} \gg \chi_h^{(3)}$ and the nanoparticles are spherically shaped and their volume fraction $p \ll .10$ we get [2, 8]:

$$\chi^{(3)} = p|\frac{3\epsilon_h(\omega)}{\epsilon_i(\omega) + 2\epsilon_h(\omega)}|^2[\frac{3\epsilon_h(\omega)}{\epsilon_i(\omega) + 2\epsilon_h(\omega)}]^2\chi_i^{(3)}$$

or

$$\chi^{(3)} = p|\frac{\epsilon(\omega) + 2\epsilon_h(\omega)}{\epsilon_i(\omega) + 2\epsilon_h(\omega)}|^2[\frac{\epsilon(\omega) + 2\epsilon_h(\omega)}{\epsilon_i(\omega) + 2\epsilon_h(\omega)}]^2\chi_i^{(3)}$$

where
$\chi^{(3)}$ and $\chi_i^{(3)}$ are the third-order nonlinear susceptibilities of the composite medium and the metallic inclusion respectively, and ϵ, ϵ_i and ϵ_h are the dielectric functions of the composite medium, the metallic inclusion and that of the host matrix.

The expressions $\frac{3\epsilon_h(\omega)}{\epsilon_i(\omega)+2\epsilon_h(\omega)}$ and $\frac{\epsilon(\omega)+2\epsilon_h(\omega)}{\epsilon_i(\omega)+2\epsilon_h(\omega)}$ represent the so-called local field factor according to D. Ricard et al. [8] and J. E. Sipe and R. W. Boyd [2]. It is easy to see that the frequency dependence of these local field factors become colossal i.e $f(\omega) \gg 0$ when the condition below known as *Surface Plasmon Resonance* (SPR) is satisfied at the so-called SPR frequency; ω_S.

$$\epsilon_i(\omega_S) + 2\epsilon_h(\omega_S) \simeq 0.$$

Consequently the effective $\chi^{(3)}$ of the nanocomposite can reach *giant* values when the SPR condition holds. This enhancement is reinforced by the power 4 of $f(\omega)$, which is known as the *local field effect*. As such the effective OKE $\chi^{(3)}$ of the nanocomposite is greater than that of the classical bulk materials as shown in the Tables 1.2 and 1.3 for the various Au-dielectric composites [29]. In this work the hope was to have the effective OKE $\chi^{(3)}_{\mathrm{Au-VO_2}}$in esu near the high end of this scale. This is despite the fact that the volumetric concentration of nano Au particles in the composite is in the range $p \leq .1$.

Thin − Films	Synthesis	Radius(Å)	Au Vol. Conc.	OKE $\chi^{(3)}$in esu
$Au - SiO_2$	Co − Sputtering	30 − 800	5 − 63 percent	-2.10×10^{-6}
$Au - SiO_2$	Ion − Implantation	50 − 250	5 percent	$+2.90 \times 10^{-6}$
$Au - Al_2O_3$	Co − Sputtering	100 − 2500	25 − 60percent	$+1.20 \times 10^{-6}$
$Au - TiO_2$	Ion − Implantation	100 − 2500	15 − 60percent	$+8.60 \times 10^{-6}$

Table 1.2: Values of the OKE $\chi^{(3)}_{xxxx}$ for $Au - SiO_2$, $Au - TiO_2$ and $Au - Al_2O_3$ thin-films nanocomposites, with different Au Volumetric Concentration [29].

Classical Third Order Nonlinear Materials in esu.
OKE $\chi^{(3)}$ for Bulk $SiO_2 \mid + 3.10^{-14}$
OKE $\chi^{(3)}$ for Bulk $CS_2 \mid + 2.10^{-12}$

Table 1.3: Values of the OKE $\chi^{(3)}_{xxxx}$ for pure bulk SiO_2 and CS_2.

N. A. Papadogiannis et al. [32] have shown that THG may be achieved with moderally intense input pump laser beam of the order 5 GW/cm^2 [32] by reflection from bulk gold. Their measured THG efficiencies on a Au surface is reported to be in the range $(10^{-10} - 10^{-13})$. In this work the hope was to have THG efficiencies of the Au-VO_2 thin-films close to this above mentioned range. This is despite the strongly absorbing nature of VO_2 and the fact that the value of the overall THG third-order nonlinear susceptibility of pure gold is: THG $\chi^{(3)}_{(nanogold)}$= THG $\chi^{(3)}_{(inter)}$+THG$\chi^{(3)}_{(intra)} \approx 10^{-12}$ esu [6].

The theoretical background chapter presents the relevant nonlinearities underlying the optical Kerr effect (OKE) and third-harmonic generation (THG) in Au nanoparticles. The various mechanisms contributing to them are discussed in the light of the work of F. Hache et al. [6, 7] and D. Ricard et al. [4]. They were able to ascertain with great confidence the origin of the nonlinear response. It was shown to be of hot-electron, intraband and interband origin and mostly absorptive near the resonance frequency.

The optical Kerr effect which depends upon the intensity of the incident optical field (light) propagating through a medium and third-harmonic generation which results from the coupling of three incoming waves each of fundamental frequency ω that produces an outgoing wave of frequency 3ω will be defined and described. Moreover the mathematical and physical properties pertaining to the OKE and THG with relevance to our Au-VO_2 nanocomposite system is elucidated.

Finally, the linear Maxwell-Garnett effective medium theory and its various extensions to nonlinear cases will be discussed.

The next chapter is organised as follows. Section 2.1 presents the mathematical formalism of the most general n-th order susceptibility tensor, in preparation for Section 2.2, which deals with the physical properties of the n-th order susceptibility tensor in general, the OKE and the THG susceptibility tensor in particular. Section 2.3 describes the optical Kerr effect and the third-harmonic generation. Section 2.4 deals with the origin of the nonlinearity of gold nanoparticles based on the work of F. Hache and co-workers [6,7]. Finally, section 2.5 presents the linear Maxwell-Garnett effective medium theory and its nonlinear extensions pertaining in the *dipole approximation.*

Chapter 2

Theoretical Background

2.1 The Mathematical Formalism of $\chi^{(3)}$

This section describes the mathematical properties of the susceptibility and polarization tensors required to describe the optical Kerr effect(OKE) and third-harmonic generation (THG). It is by no means complete. A more detailed treatment on the subject may be found in the book of P.N. Butcher and D. Cotter [1], on which this section is largely based.

The constitutive relations we are about to derive do not include spatial dispersion i.e the $\mathbf{k}$ dependence of $\chi^{(\mathbf{n})}$. This is because the properties of the gold nanoparticles are similar to that of a molecule i.e $ka \ll 1$, where k is the optical wave vector and a is the radius of the spherical inclusion [3]. Therefore the spatial term of the monochromatic field reduces to 1 because $\exp(-ika) = \exp(ika) \simeq 1$. It means that the field to which the sphere is exposed is approximately uniform over the region occupied by the sphere [3]. Moreover it has a corresponding size dependent nonzero dipolar $\chi^{(\mathbf{3})}$ [4].

The fundamental formalism that describes nonlinear optics is the constitutive relation which relates at a given time t the polarization $\mathbf{P}$(t) and the incident electrical field at earlier time t' denoted by $\mathbf{E}$(t'). It is formulated in two closely-linked approaches: Firstly in terms of time domain response functions, secondly as susceptibilities tensors (e.g F. Hache et al. [6]). The choice of these is based on various factors such as the bandwidth or pulse duration of the applied field and the speed of response of the nonlinear medium [1]. As we shall see later F. Hache and co-workers [6] have used the susceptibility tensor formalism which is a frequency domain approach as the nonlinear response under investigation was shown to be fast on a $5ps$ time scale. Moreover the frequency domain approach is suitable for monochromatic or quasi-monochromatic fields i.e monochromatic fields varying slowly with time. They both may be obtained from a continous-wave single-mode lasers such as those used by F. Hache et al. [6].

2.1.1 The Susceptibility Tensors

The nonlinear optical properties of a medium may be described by time-domain polarization response functions in all orders. An alternative approach based on the so-called frequency-domain response functions also known as the susceptibility tensors is a more widely used description. The choice of these has been discussed in the previous subsection (section 1.1). In this thesis we adopt the susceptibility tensor formalism for two reasons:

Firstly, it is used by F. Hache et al. [6, 7] to account for the fast nonlinear response of the nanogold particles i.e the measured nonlinear response that takes only 5 ps [1, 4, 6, 7]. It was concluded that in the case of nanogold particles, the electrons were responsible for the nonlinearity. It could have resulted from molecular reorientation, thermal effects due to lattice heating or electrostriction (compression of a material in the presence of an electromagnetic field) to name a few [9]. This work is restricted to the $fast$ nonlinear response due to electrons only.

Secondly, the mode-locked laser that was used by F. Hache et al. [6, 7] radiates monochromatic or quasi-monochromatic fields. Such electromagnetic fields are well described as functions of the frequency since they are periodic functions, whose amplitudes vary slowly with time [1].

Relation between $\mathbf{E}(\mathrm{t})$ and $\mathbf{E}(\omega)$

According to P. N. Butcher and D. Cotter [1] the susceptibility tensors arise when the electric field $\mathbf{E}(\mathrm{t})$ is defined in terms of its Fourier transform $\mathbf{E}(\omega)$ through the Fourier integral identity:

$$\mathbf{E}(\mathrm{t}) = \int_{-\infty}^{+\infty} \mathbf{E}(\omega)\exp(-\mathrm{i}\omega\mathrm{t}) \tag{2.1}$$

where

$$\mathbf{E}(\omega) = \frac{1}{2\pi}\int_{-\infty}^{+\infty} \mathbf{E}(\mathrm{t})\exp(+\mathrm{i}\omega\mathrm{t}). \tag{2.2}$$

We use of the above Fourier transform to define the third-order susceptibility.

Definition of the third order susceptibility

The 3^{rd} order susceptibility is defined as [1]:

$$\mathbf{P}^{(3)}(\mathrm{t}) = \epsilon_0 \int_{-\infty}^{+\infty} \mathrm{d}\ \omega_1 \int_{-\infty}^{+\infty} \mathrm{d}\ \omega_2 \int_{-\infty}^{+\infty} \mathrm{d}\ \omega_3 \underline{\chi}^{(3)}(-\omega_\sigma;\omega_1,\omega_2,\omega_3) \times \mathbf{E}(\omega_1)\mathbf{E}(\omega_2)\mathbf{E}(\omega_3)\exp(-\mathrm{i}\omega_\sigma\mathrm{t}). \tag{2.3}$$

where

$$\underline{\chi}^{(3)}(-\omega_\sigma;\omega_1,\omega_2,\omega_3) = \int_{-\infty}^{+\infty}\mathrm{d}\tau_1\int_{-\infty}^{+\infty}\mathrm{d}\tau_2\int_{-\infty}^{+\infty}\mathrm{d}\tau_3 \mathbf{R}^{(3)}(\mathrm{t}-\tau_1,\mathrm{t}-\tau_2,\mathrm{t}-\tau_3)\exp[\mathrm{i}\sum_{\mathrm{j}=1}^{3}\omega_\mathrm{j}\tau_\mathrm{j}] \tag{2.4}$$

and

$$\omega_\sigma = \omega_1+\omega_2+\omega_3. \tag{2.5}$$

Eq. (2.4) defines the third-order susceptibility tensor. Its component form is denoted by $\chi^{(\mathrm{n})}_{\mu\alpha\beta\gamma}(-\omega_\sigma;\omega_1,\omega_2,\omega_3)$ (see Eq. (2.11)). P. N. Butcher and D. Cotter [1] have shown that it remains invariant under all 3! permutations of the 3 pairs $(\alpha,\omega_1),(\beta,\omega_2),(\gamma,\omega_3)$. This is known as the *intrinsic permutation symmetry.*

The causality principle [1] implies that $\underline{\chi}^{(3)}$ vanishes when all the frequencies lie in the upper half of the complex plane, while the reality condition requires that:

$$[\underline{\chi}^{(3)}(-\omega_\sigma;\omega_1,\omega_2,\omega_3)]^* = \underline{\chi}^{(3)}(-\omega_\sigma^*;\omega_1^*,\omega_2^*,\omega_3^*). \tag{2.6}$$

Relation between $\mathbf{P}(\mathrm{t})$ and $\mathbf{P}(\omega)$

Consider $\mathbf{P}(\mathrm{t})$ and $\mathbf{P}(\omega)$ which are related through the Fourier integral identity:

$$\mathbf{P}(\mathrm{t}) = \int_{-\infty}^{+\infty}\mathbf{P}(\omega)\exp(-\mathrm{i}\omega\mathrm{t}) \tag{2.7}$$

where

$$\mathbf{P}(\omega) = \frac{1}{2\pi}\int_{-\infty}^{+\infty}\mathbf{P}(\mathrm{t})\exp(+\mathrm{i}\omega\mathrm{t}). \tag{2.8}$$

Consider the following identity:

$$\frac{1}{2\pi}\int_{-\infty}^{+\infty}dx\exp[ix(\tau-t)] = \delta(\tau-t). \tag{2.9}$$

It follows that Eq. (2.3) becomes:

$$\mathbf{P}^{(3)}(\mathrm{t}) = \epsilon_0\int_{-\infty}^{+\infty}\mathrm{d}\ \omega_1\int_{-\infty}^{+\infty}\mathrm{d}\ \omega_2\int_{-\infty}^{+\infty}\mathrm{d}\ \omega_3\underline{\chi}^{(3)}(-\omega_\sigma;\omega_1,\omega_2,\omega_3) \times\mathbf{E}(\omega_1)\mathbf{E}(\omega_2)\mathbf{E}(\omega_3)\exp(-\mathrm{i}\omega_\sigma\mathrm{t})\delta(\omega-\omega_\sigma) \tag{2.10}$$

Alternatively in suffix notation:

$$[P^{(3)}]_\mu = \epsilon_0\sum_{\alpha\beta\gamma}\int_{-\infty}^{+\infty}d\omega_1\int_{-\infty}^{+\infty}d\omega_2\int_{-\infty}^{+\infty}d\omega_3\chi_{\mu\alpha\beta\gamma}(-\omega_\sigma;\omega_1,\omega_2,\omega_3) \times[E(\omega_1)]_\alpha[E(\omega_1)]_\alpha[E(\omega_1)]_\alpha\delta(\omega-\omega_\sigma) \tag{2.11}$$

where α,β and γ are to be summed over x,y and z.

Polarization induced by Monochromatic fields

A combination of monochromatic waves each of frequency ω' which takes on different positive values or zero may be written as:

$$\mathbf{E}(\mathrm{t}) = \frac{1}{2}\sum_{\omega'\geq 0}[\mathbf{E}_{\omega'}\exp(-\mathrm{i}\omega'\mathrm{t}) + \mathbf{E}_{-\omega'}\exp(+\mathrm{i}\omega'\mathrm{t})]. \tag{2.12}$$

By the reality condition we have that $\mathbf{E}_{\omega'} = \mathbf{E}^*_{\omega'}$. Combining Eq. (2.10) and Eq. (2.12) we obtain the Fourier transform of $\mathbf{E}(\mathrm{t})$:

$$\mathbf{E}(\omega) = \frac{1}{2}\sum_{\omega'\geq 0}[\mathbf{E}_{\omega'}\delta(\omega-\omega') + \mathbf{E}_{-\omega'}\delta(\omega+\omega')]. \tag{2.13}$$

It has the unit of Vsm^{-1}, while $\mathbf{E}_{\omega'}$ has unit of Vm^{-1}. For a single monochromatic wave with frequency ω' the intensity is:

$$\begin{aligned} I_{\omega'} = \quad & \epsilon_0 cn(\omega') < \frac{1}{2}[\mathbf{E}_{\omega'}\exp(-\mathrm{i}\omega'\mathrm{t}) + \mathbf{E}^*_{\omega'}\exp(+\mathrm{i}\omega'\mathrm{t})] \\ \times \quad & \frac{1}{2}[\mathbf{E}_{\omega'}\exp(-\mathrm{i}\omega'\mathrm{t}) + \mathbf{E}^*_{\omega'}\exp(+\mathrm{i}\omega'\mathrm{t})] > \\ = \quad & \frac{1}{2}\epsilon_0 cn(\omega')|E_{\omega'}|^2, \end{aligned} \tag{2.14}$$

where the angle brackets denote a cycle average, and $n(\omega')$ is the refractive index at frequency ω'. If $\mathbf{E}(\mathrm{t})$ is given by Eq. (2.12). It follows that Eq. (2.3) becomes:

$$\mathbf{P}^{(3)}(\mathrm{t}) = \frac{1}{2}\sum_{\omega'\geq 0}[\mathbf{P}^{(3)}_{\omega'}\exp(-\mathrm{i}\omega'\mathrm{t}) + \mathbf{P}^{(3)}_{-\omega'}\exp(+\mathrm{i}\omega'\mathrm{t})] \tag{2.15}$$

Since $\mathbf{P}^{(3)}(\mathrm{t})$ is real, $\mathbf{P}^{(3)}_{-\omega} = (\mathbf{P}^{(3)}_{\omega})^*$. Alternatively by dropping $\frac{1}{2}$ Eq. (2.15) may written as Eq. (2.16) for $\mathbf{E}(\mathrm{t})$ given by Eq. (2.17):

$$\mathbf{P}^{(3)}(\mathrm{t}) = \sum_{\omega'\geq 0}[\mathbf{P}^{(3)}_{\omega'}\exp(-\mathrm{i}\omega'\mathrm{t}) + \mathbf{P}^{(3)}_{-\omega'}\exp(+\mathrm{i}\omega'\mathrm{t})] \tag{2.16}$$

$$\mathbf{E}(\mathrm{t}) = \sum_{\omega'\geq 0}[\mathbf{E}_{\omega'}\exp(-\mathrm{i}\omega'\mathrm{t}) + \mathbf{E}_{-\omega'}\exp(+\mathrm{i}\omega'\mathrm{t})]. \tag{2.17}$$

Substituting Eq. (2.13) into the form of Eq. (2.10) it follows that:

$$\begin{aligned} [P^{(3)}(\omega)]_\mu = 2\epsilon_0 \sum_{\alpha\beta\gamma}[\chi^{(3)}_{\mu\alpha\beta\gamma}(-\omega_\sigma;\omega_1,\omega_2,\omega_3) \\ \times(\frac{1}{2}E(\omega_1))_\alpha(\frac{1}{2}E(\omega_2))_\beta(\frac{1}{2}E(\omega_3))_\gamma + \\ \chi^{(3)}_{\mu\alpha\beta\gamma}(-\omega_\sigma;\omega_1,\omega_2,\omega_3) \\ \times((\frac{1}{2}E(\omega_2))_\alpha\frac{1}{2}E(\omega_1))_\beta(\frac{1}{2}E(\omega_3))_\gamma + \\ \text{other possible arrangements }], \end{aligned} \tag{2.18}$$

where $\omega_\sigma = \omega_1 + \omega_2 + \omega_3$ and $\omega_n \geq 0$ for $1 \leq n \leq 3$.
The frequencies ω_1, ω_2 and ω_3 may be positive or negative for a.c fields or zero for d.c fields.

The Numerical Factor $K(-\omega_\sigma; \omega_1, \ldots, \omega_n)$

By taking into account the intrinsic permutation symmetry the most general form of Eq. (2.18) becomes:

$$\begin{aligned}[P^{(n)}(\omega)]_\mu = 2\epsilon_0 \quad & \sum_{\alpha_1 \ldots \alpha_n} [\chi^{(n)}_{\mu\alpha_1\ldots\alpha_n}(-\omega_\sigma; \omega_1, \ldots, \omega_n). \\ & (\frac{1}{2}E(\omega_1))_{\alpha_1}(\frac{1}{2}E(\omega_2))_{\alpha_2} \ldots (\frac{1}{2}E(\omega_n))_{\alpha_n} + \\ & \chi^{(n)}_{\mu\alpha_1\ldots\alpha_n}(-\omega_\sigma; \omega_1, \ldots, \omega_n). \\ & (\frac{1}{2}E(\omega_2))_{\alpha_1}(\frac{1}{2}E(\omega_1))_{\alpha_2} \ldots (\frac{1}{2}E(\omega_n))_{\alpha_n} + \\ & \text{other possible arrangements}].\end{aligned}$$

To keep track of terms arising from all possible arrangements due to permutation Eq (2.18) may be written as:

$$[P^{(n)}_{\omega_\sigma}(\omega)]_\mu = \epsilon_0 \sum_{\mu\alpha_1\ldots\alpha_n} \sum_{\omega} K(-\omega_\sigma; \omega_1, \ldots, \omega_n)\chi^{(n)}_{\mu\alpha_1\ldots\alpha_n}(-\omega_\sigma; \omega_1, \ldots, \omega_n) \quad (2.19)$$
$$E(\omega_1)_{\alpha_1} \ldots E(\omega_2)_{\alpha_2} E(\omega_n)_{\alpha_n}.$$

In vector notation:

$$\mathbf{P}^{(\mathrm{n})}_{\omega_\sigma}(\omega) = \epsilon_{\mathbf{0}} \sum_{\omega} \mathbf{K}(-\omega_\sigma; \omega_{\mathbf{1}}, \ldots, \omega_{\mathbf{n}})\underline{\chi}^{(\mathbf{n})}_{\mu\alpha_{\mathbf{1}}\ldots\alpha_{\mathbf{n}}}(-\omega_\sigma; \omega_{\mathbf{1}}, \ldots, \omega_{\mathbf{n}}) \quad (2.20)$$
$$\mathbf{E}_{\omega_1} \ldots \mathbf{E}_{\omega_2} \mathbf{E}_{\omega_\mathrm{n}}.$$

In the summation $\sum_{\alpha_1\ldots\alpha_n}$ the $\alpha_1 \ldots \alpha_n$ are summed over x, y, and z, whereas $\sum_\omega$ means that we are summing over all frequencies $\omega_1, \ldots, \omega_n$. If $\mathbf{E}(\mathbf{t})$is given by (2.13) the numerical term is found to be:

$$K(-\omega_\sigma; \omega_1, \ldots, \omega_n) = 2^{l+m-n}p, \quad (2.21)$$

where p is the number of distinct permutations of $\alpha_1 \ldots \alpha_n$, n is the order of nonlinearity, m is the set of frequency $\omega_1, \ldots, \omega_n$ that are zero (d.c field) and l is 1 if $\omega_\sigma \neq 0$ and 0 otherwise. For an a.c field i.e $m = 0$. Hence,

$$K(-\omega_\sigma; \omega_1, \ldots, \omega_n) = 2^{l-n}p. \quad (2.22)$$

By some authors the summation $\sum_\omega$ is dropped for convenience and K is taken to be 1 as the experimentally measured susceptibility incorporates all other possible arrangements i.e

$$\chi^{(n)}_{experimental}(-\omega_\sigma; \omega_1, \ldots, \omega_n) = K(-\omega_\sigma; \omega_1, \ldots, \omega_n)\chi^{(n)}(-\omega_\sigma; \omega_1, \ldots, \omega_n).$$

See for example F. Hache et al. [6]. We adopt the same approximation in this work.

Scalar form of the Susceptibility

The component form of the susceptibility tensor is often preferred to its vector form for a practical reason. It lightens the notation and therefore makes the computations easier. Let $\mathbf{E}_{\omega_\mathrm{j}} = \mathbf{e}_\mathrm{j}\mathrm{E}_{\omega_\mathrm{j}}$, where E_{ω_j} is a complex scalar, $\mathbf{e}_\mathrm{j}$ is a unit vector in the direction of the polarization field which is complex for elliptically polarized field and real for linearly polarized fields, with the property $\mathbf{e}_\mathrm{j}.\mathbf{e}_\mathrm{j}^* = \mathbf{1}$. The Nd:YAG laser beam used by F. Hache et al. [6] is linearly polarized. The component form of the n-th order susceptibility tensor is defined in the following way:

$$\begin{aligned}\chi^{(n)}(-\omega_\sigma;\omega_1,\ldots,\omega_n) &= \mathbf{e}_\sigma^*.\underline{\chi}^{(\mathrm{n})}(-\omega_\sigma;\omega_1,\ldots,\omega_\mathrm{n}).\mathbf{e}_1\ldots\mathbf{e}_\mathrm{n} \\ &= \sum_{\mu\alpha_1\ldots\alpha_n}\chi^{(n)}_{\mu\alpha_1\ldots\alpha_n}(-\omega_\sigma;\omega_1,\ldots,\omega_\mathrm{n}) \\ &\times\ (e_\sigma^*)_\mu(e_1)_{\alpha_1}\ldots(e_\mathrm{n})_{\alpha_n},\end{aligned} \tag{2.23}$$

where $\mathbf{e}_\sigma$ is the direction of the polarization of the field $\mathbf{E}_{\omega_\sigma}$. The scalar form of the polarization may be defined by substituting Eq. (2.23) into Eq. (2.19).

$$[P^{(n)}_{\omega_\sigma}(\omega)]_\mu = \epsilon_0\sum_\omega K(-\omega_\sigma;\omega_1,\ldots,\omega_n)\chi^{(n)}(-\omega_\sigma;\omega_1,\ldots,\omega_\mathrm{n})E_1\ldots E_n, \tag{2.24}$$

where the complex scalar amplitude $P^{(n)}_{\omega_\sigma}$ is defined as: $\mathbf{P}^{(\mathrm{n})}_{\omega_\sigma} = \mathbf{e}_\sigma\mathrm{P}^{(\mathrm{n})}_{\omega_\sigma}$. We set $K = 1$ and drop $\sum_\omega$ and μ for convenience. It follows that in electrostatic units (esu) i.e $\epsilon_0 = 1$ Eq. (2.24) becomes:

$$P^{(n)}_{\omega_\sigma}(t) = \chi^{(n)}(-\omega_\sigma;\omega_1,\ldots,\omega_\mathrm{n})E_1\ldots E_n. \tag{2.25}$$

Eq. (2.25) is the key result of this chapter, it represents the n-th order polarization term of the induced "dipole" of the illuminated medium. Our composite material which conforms to the Maxwell-Garnett topology may be consider as a *weakly nonlinear* medium with a polarization of the form [9]:

$$P^{(3)}_{\omega_\sigma} = \chi^{(3)}(-\omega_\sigma;\omega_1,\omega_2,\omega_3)EEE, \tag{2.26}$$

where $\omega_\sigma = \omega_1 + \omega_2 + \omega_3$ and $E_1 = E_2 = E_3 = E$.
In the case of OKE for which $\omega_\sigma = \omega_1 = -\omega_2 = \omega_3 = \omega$ (2.36) becomes:

$$P^{(3)}_{\omega} = \chi^{(3)}(-\omega;\omega,-\omega,\omega)EE^*E. \tag{2.27}$$

whereas in the case of THG, $\omega_1 = \omega_2 = \omega_3 = \omega$ and $\omega_\sigma = 3\omega$ (2.36) reads:

$$P^{(3)}_{3\omega} = \chi^{(3)}(-3\omega;\omega,\omega,\omega)EEE. \tag{2.28}$$

2.2 Physical Properties of the OKE and THG

This section describes the properties of the OKE and THG susceptibility tensor in an isotropic medium.

As mentioned earlier in our Au-VO_2 composite system the gold particles represent a low concentration of spherical inclusions i.e $p \ll .1$ embedded in the VO_2 matrix as shown in Fig. 1.1. As a consequence of the randomness in which the spherical particles are distributed in the matrix its physical properties are invariant under rotation. This is known as *isotropy*. The physical properties of the composite medium are also invariant under translation, that is to say *homogeous*. This section describes the OKE and THG susceptibility tensors under rotational symmetry operations.

We now proceed to describe the third order susceptibility $\chi^{(3)}$ under rotation. The discussion is based on the book of P. N. Butcher and D. Cotter [1]. They define the term rotation operation to be inversion symmetry (centrosymmetry[9]), reflection and rotation. We investigate the rotation operation as follows: First, Neumann's principle will be stated. Next, the symmetry that arises as a consequence of reflection will be studied. Finally, the Neumann's principle will be evoked to understand inversion and rotation symmetry.

2.2.1 Rotation Operation

Statement of the Neumann's principle: Any physical property must be invariant under all the point-symmetry operations (rotation, translation,...) characteristic of the system. From this it follows that the physical property of our composite system i.e $\chi^{(3)}$ must include rotation, inversion and reflection operations which follow from isotropy. Our discussion is closely related to that of P. N. Butcher and D. Cotter [1].

Symmetry due to Reflection

Reflection symmetry may be defined through the following coordinate transformation in the yz-plane.
Let $(x, y, z) \rightarrow (-x, y, z)$. It follows that any component of $\chi^{(3)}$ with an odd number of x components vanishes. Consider for example $\chi^{(3)}_{xyyz}$ which transforms to $\chi^{(3)}_{(-x)yyz} = -\chi^{(3)}_{xyyz}$. Hence: $\chi^{(3)}_{xyyz} = -\chi^{(3)}_{xyyz} = 0$. A similar argument applies to reflection through the xy and yz planes. Therefore any component of $\chi^{(3)}$ with an odd number of x, y or z components vanishes. As a consequence of reflection symmetry, the 81 terms of $\chi^{(3)}$ which arise from the fact that there are three different choices x, y or z for each of the four terms in the fourth rank tensor $\chi^{(3)}_{\mu\alpha\beta\gamma}(2.23)$, reduce to 21 terms only.

$\chi^{(3)}_{x\alpha\beta\gamma}$	$\chi^{(3)}_{y\alpha\beta\gamma}$	$\chi^{(3)}_{z\alpha\beta\gamma}$
$\chi^{(3)}_{xxxx}$	$\chi^{(3)}_{yyyy}$	$\chi^{(3)}_{zzzz}$
$\chi^{(3)}_{xxyy}$	$\chi^{(3)}_{yyxx}$	$\chi^{(3)}_{zzxx}$
$\chi^{(3)}_{xxzz}$	$\chi^{(3)}_{yyzz}$	$\chi^{(3)}_{zzyy}$
$\chi^{(3)}_{xyxy}$	$\chi^{(3)}_{yxyx}$	$\chi^{(3)}_{zxzx}$
$\chi^{(3)}_{xzxz}$	$\chi^{(3)}_{yzyz}$	$\chi^{(3)}_{zyzy}$
$\chi^{(3)}_{xyyx}$	$\chi^{(3)}_{yxxy}$	$\chi^{(3)}_{zxxz}$
$\chi^{(3)}_{xzzx}$	$\chi^{(3)}_{yzzy}$	$\chi^{(3)}_{zyyz}$

Table 2.1: Components of $\chi^{(3)}_{xxxx}$ after P. N. Butcher and D. Cotter [1].

This follows from the fact that all tensor components with an odd number of x, y or z must be zero may also be understood by saying that all tensor components with an even number of x, y or z do not vanish. They have either two or four terms in x, y or z since we have a fourth rank tensor. Consider the case of the x term only, as the same argument applies to the y and z terms. There is only one term that contains four x i.e $\chi^{(3)}_{xxxx}$. Next the tensor term that contains two x components will appear as $\chi^{(3)}_{xx\alpha\beta}$, $\chi^{(3)}_{x\alpha x\beta}$ and $\chi^{(3)}_{x\alpha\beta x}$ where the indices α and β may either be y or z. For a tensor component not to vanish we require that it has an even number of y or z, therefore we must demand that $\alpha = \beta$ where $\alpha = y$ or z. It follows that: $\chi^{(3)}_{xx\alpha\beta}$ represents either $\chi^{(3)}_{xxyy}$ or $\chi^{(3)}_{xxzz}$, similarly $\chi^{(3)}_{x\alpha x\alpha}$ represents either $\chi^{(3)}_{xyxy}$ or $\chi^{(3)}_{xzxz}$ and $\chi^{(3)}_{x\alpha\alpha x}$ represents either $\chi^{(3)}_{xyyx}$ or $\chi^{(3)}_{xzzx}$. So under reflection the term $\chi^{(3)}_{\mu\alpha\beta\gamma}$ represents 7 distinct terms: $\chi^{(3)}_{xxxx}$, $\chi^{(3)}_{xxyy}$, $\chi^{(3)}_{xxzz}$, $\chi^{(3)}_{xyxy}$, $\chi^{(3)}_{xzxz}$, $\chi^{(3)}_{xyyx}$ and $\chi^{(3)}_{xzzx}$. A similar argument to the case $\mu = x$ may be applied for $\mu = y$ or $\mu = z$. The results are shown in Table 2.1:

Rotation and Inversion Symmetry

Inversion Symmetry

The susceptibility tensor is described using the transformation laws of polar tensors. Two coordinate may be related through a proper and improper rotation. In the first one a coordinate system remains unchanged before and after the operation, whereas in the second one the right-handed and the left-handed coordinate system interchange (they involve an inversion operation).

As a consequence of the Newmann's principle a polar tensor of rank n transforms as follows:

$$\chi'^{(n)}_{\mu\alpha_1\ldots\alpha_n}(-\omega_\sigma;\omega_1,\ldots,\omega_n) = R_{\mu u}R_{\alpha_1 a_1}R_{\alpha_2 a_2}\ldots R_{\alpha_n a_n} \times\chi^{(n)}_{ua_1\ldots a_n}(-\omega_\sigma;\omega_1,\ldots,\omega_n). \tag{2.29}$$

Note that the elements of the transformation $\mathbf{R}$ are given by the directions cosines

$R_{\alpha a} = \cos\theta_{\alpha a}$, where $\theta_{\alpha a}$ is the angle between the α and a axes. In particular the OKE and THG tensors are written as:

$$\chi'^{(3)}_{\mu\alpha\beta\gamma}(-\omega;\omega,-\omega,\omega) = R_{\mu u}R_{\alpha a}R_{\beta b}R_{\gamma c} \times\chi^{(3)}_{uabc}(-\omega;\omega,-\omega,\omega) \tag{2.30}$$

$$\chi'^{(3)}_{\mu\alpha\beta\gamma}(3\omega;\omega,\omega,\omega) = R_{\mu u}R_{\alpha a}R_{\beta b}R_{\gamma c} \times\chi^{(3)}_{uabc}(3\omega;\omega,\omega,\omega), \tag{2.31}$$

with $R_{mn} = \cos\theta_{mn}$ is the angle between m and n for $m = \mu,\alpha,\beta,\gamma$ and $n = u,a,b,c$ respectively.

According to Neumann's principle the elements of the susceptibility tensor taken with respect to two coordinates, which are related by one of the symmetry operations of the medium, must be identical [1]:

$$\chi'^{(n)}_{\mu\alpha_1\ldots\alpha_n}(-\omega_\sigma;\omega_1,\ldots,\omega_n) = \chi^{(n)}_{\mu\alpha_1\ldots\alpha_n}(-\omega_\sigma;\omega_1,\ldots,\omega_n). \tag{2.32}$$

The usefulness of this equation above will be illustrated through the inversion operation for which $R_{\alpha\beta} = -\delta_{\alpha\beta}$; where $\delta_{\alpha\beta}$ is the Kronecker delta.

Combining Eq. (2.29) and Eq. (2.32) leads to:

$$\begin{aligned}\chi^{(n)}_{\mu\alpha_1\ldots\alpha_n}(-\omega_\sigma;\omega_1,\ldots,\omega_n) &= R_{\mu u}R_{\alpha_1 a_1}R_{\alpha_2 a_2}\ldots R_{\alpha_n a_n} \times\chi^{(n)}_{ua_1\ldots a_n}(-\omega_\sigma;\omega_1,\ldots,\omega_n) \\ &= (-\delta_{\mu u})(-\delta_{\alpha_1 a_1})(-\delta_{\alpha_2 a_2})\ldots(-\delta_{\alpha_n a_n}) \times\chi^{(n)}_{ua_1\ldots a_n}(-\omega_\sigma;\omega_1,\ldots,\omega_n) \\ &= (-1)^{n+1}\chi^{(n)}_{ua_1\ldots a_n}(-\omega_\sigma;\omega_1,\ldots,\omega_n).\end{aligned} \tag{2.33}$$

It is clear that Eq. (2.33) vanishes for n even. This is the reason why the first nonlinear term in an isotropic medium is of order 3. Moreover for an *isotropic* medium only the *odd* polarization terms will survive. In particular the lowest nonlinear polarization term in the case of OKE and THG for a *weakly* nonlinear medium will be [9]:

$$P^{(3)}_{\omega}(t) = \chi^3(-\omega;\omega,-\omega,\omega)E(\omega)E^*(\omega)E(\omega) \tag{2.34}$$

$$P^{(3)}_{3\omega}(t) = \chi^3(-3\omega;\omega,\omega,\omega)E(\omega)E(\omega)E(\omega). \tag{2.35}$$

Rotation Symmetry

Consider first the case of a 90° rotation about the z-axis in the xy plane. The transformation of coordinate are $(1,2,3) \rightarrow (2,-1,3)$ as below in Fig. 2.1 and Fig. 2.2.

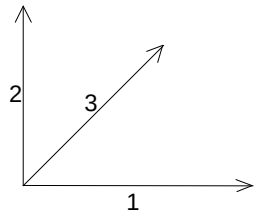

Figure 2.1: x, y and z axis before rotation

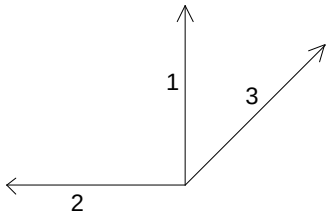

Figure 2.2: x, y and z axis after rotation

It is usual to represents such a transformation in matrix form as:

$$R = \begin{bmatrix} 0 & 1 & 0 \\ -1 & 0 & 0 \\ 0 & 0 & 1 \end{bmatrix}$$

For an arbitrary angle of rotation θ about the z-axis it follows that:

$$R = \begin{bmatrix} +\cos\theta & +\sin\theta & 0 \\ -\sin\theta & +\cos\theta & 0 \\ 0 & 0 & 1 \end{bmatrix}$$

Where $R_{33} = 1$ follows from the fact that 3 maps onto itself.

The case of the most general third order susceptibility tensor may be treated in a similar fashion. The OKE and THG are identically deduced from it.

Consider Eq. (2.29) with $n = 3$:

$$\begin{aligned} \chi'^{(3)}_{\mu\alpha_1\alpha_1\alpha_3}(-\omega_\sigma;\omega_1,\omega_2,\omega_3) = \quad & R_{\mu u}R_{\alpha_1 a_1}R_{\alpha_2 a_2}R_{\alpha_3 a_3} \\ & \times\chi^{(3)}_{ua_1a_2a_3}(-\omega_\sigma;\omega_1,\omega,\omega_3). \end{aligned} \tag{2.36}$$

According to R. W. Boyd [9], Eq. (2.36) leads the following general expression:

$$\chi^{(3)}_{\mu\alpha\beta\gamma} = \chi^{(3)}_{xxyy}\delta_{\mu\alpha}\delta_{\beta\gamma} + \chi^{(3)}_{xyxy}\delta_{\mu\beta}\delta_{\alpha\gamma} + \chi^{(3)}_{xyyx}\delta_{\mu\gamma}\delta_{\alpha\beta} \tag{2.37}$$

It follows that if $\mu = \alpha = \beta = \gamma = x$, Eq. (2.37) reduces to:

$$\chi^{(3)}_{xxxx} = \chi^{(3)}_{xxyy} + \chi^{(3)}_{xyxy} + \chi^{(3)}_{xyyx}. \tag{2.38}$$

Scalar Form of Third Order Susceptibility Tensor in an Isotropic Medium

Consider the scalar form of the n-th order susceptibility tensor defined by Eq. (2.33):

$$\begin{aligned}\chi^{(n)}(-\omega_\sigma;\omega_1,\ldots,\omega_n) &= \mathbf{e}^*_\sigma.\underline{\chi}^{(\mathrm{n})}(-\omega_\sigma;\omega_1,\ldots,\omega_\mathrm{n})|\mathbf{e}_1\ldots\mathbf{e}_\mathrm{n} \\ &= \sum_{\mu\alpha_1\ldots\alpha_n} \chi^{(n)}_{\mu\alpha_1\ldots\alpha_n}(-\omega_\sigma;\omega_1,\ldots,\omega_\mathrm{n})(e^*_\sigma)_\mu(e_1)_{\alpha_1}\ldots(e_\mathrm{n})_{\alpha_n}.\end{aligned}$$

For a general third order susceptibility tensor i.e $n = 3$ we have:

$$\begin{aligned}\chi^{(3)}(-\omega_\sigma;\omega_1,\omega_2,\omega_3) &= \mathbf{e}^*_\sigma.\underline{\chi}^{(3)}(-\omega_\sigma;\omega_1,\omega_2,\omega_\mathrm{n}).\mathbf{e}_1\mathbf{e}_2\mathbf{e}_3 \\ &= \sum_{\mu\alpha\beta\gamma} \chi^{(3)}_{\mu\alpha\beta\gamma}(-\omega_\sigma;\omega_1,\omega_2,\omega_3)(e^*_\sigma)_\mu(e_1)_\alpha(e_2)_\beta(e_3)_\gamma \\ &= \sum_{\mu\alpha\beta\gamma} \chi^{(3)}_{xxxx}(-\omega_\sigma;\omega_1,\omega_2,\omega_3)(e^*_\sigma)_x(e_1)_x(e_2)_x(e_3)_x \\ &= \chi^{(3)}_{xxxx}(-\omega_\sigma;\omega_1,\omega_2,\omega_3) \\ &= \chi^{(3)}_{xxyy}(-\omega_\sigma;\omega_1,\omega_2,\omega_3) + \chi^{(3)}_{xyxy}(-\omega_\sigma;\omega_1,\omega_2,\omega_3) \\ &+ \chi^{(3)}_{xyyx}(-\omega_\sigma;\omega_1,\omega_2,\omega_3) \quad \text{by} \quad (2.38).\end{aligned} \tag{2.39}$$

Note that the real unit vectors $\mathbf{e}_\sigma, \mathbf{e}_1, \mathbf{e}_2, \mathbf{e}_3$ satisfy $(e_\sigma)_j(e_1)_j(e_2)_j(e_3)_j = 1$ for $j = x, y, z$ in the case of *linearily* polarized laser beam such as that obtained from an Nd:YAG laser [1,6].

OKE Susceptibility Tensor in an Isotropic Medium

The OKE susceptibility tensor in an isotropic medium is obtained by applying the intrinsic permutation symmetry to the choice of the following frequencies $(-\omega;\omega,-\omega,\omega)$ that pertain in the case of the OKE. Alternatively it could be written as $(\omega = \omega - \omega + \omega)$ [9].

Recall that the intrinsic permutation symmetry requires that all independent tensor components remain unchanged under all possible permutations [1]. This is done as follows: Consider a given independent tensor component $\chi^{(3)}_{xxyy}$ for example to which is associated the set of frequencies $(\omega = \omega - \omega + \omega)$ in the OKE case. One may establish a one-to-one relation between each tensor i-term and the corresponding frequency (see R. W. Boyd [9]). As such x is associated with ω we write $x \leftrightarrow \omega$, $x \leftrightarrow \omega$, $y \leftrightarrow -\omega$ and $y \leftrightarrow \omega$. This is written in a more compact form as follows: $(x,x,y,y) \leftrightarrow (\omega,\omega,-\omega,\omega)$. Similarly, $(x,y,x,y) \leftrightarrow (\omega,\omega,-\omega,\omega)$ and $(x,y,y,x) \leftrightarrow (\omega,\omega,-\omega,\omega)$. In Table 2.2 we present all the above three possibilities.

$(\mu,\alpha,\beta,\gamma) \leftrightarrow (\omega,\omega,-\omega,\omega)$
$(x,x,y,y) \leftrightarrow (\omega,\omega,-\omega,\omega)$
$(x,y,x,y) \leftrightarrow (\omega,\omega,-\omega,\omega)$
$(x,y,y,x) \leftrightarrow (\omega,\omega,-\omega,\omega)$

Table 2.2: Components of the OKE $\chi^{(3)}_{xxxx}$ after P. N. Butcher and D. Cotter [1].

Simple inspection leads us to the following conclusion: x maps onto ω in the first and the third term, and unto both ω and $-\omega$ in the second independent term, whereas y maps unto both ω and $-\omega$ in the first and the third term, and unto ω only in the second one; by the *intrinsic permutation symmetry* we require that $(x,x,y,y) = (x,y,x,y)$. Hence $\chi^{(3)}_{xxyy}$ remain unchanged under any permutation since:

$$\chi^{(3)}_{xxyy} = \chi^{(3)}_{xyxy} \tag{2.40}$$

So now there are only two independent components. We now proceed to define the OKE polarization tensor in an isotropic medium in the μ-direction. In esu i.e $\epsilon_0 = 1$ it is found by letting $\omega_\sigma = \omega_1 = -\omega_2 = \omega_3 = \omega$, dropping $\sum_\omega$ for convenience and setting $K(-\omega_\sigma;\omega,-\omega,\omega) = 1$. Equation (1.48) becomes

$$\begin{aligned}
[P^{(3)}_\omega]_\mu &= \sum_{\mu\alpha\beta\gamma} \chi^{(3)}_{\mu\alpha\beta\gamma}(-\omega_\sigma;\omega_1,\omega_2,\omega_3)(e^*_\sigma)_\mu(e_1)_\alpha(e_2)_\beta(e_3)_\gamma E_\alpha(\omega_1)E_\beta(\omega_2)E_\gamma(\omega_3) \\
&= \sum_{\mu\alpha\beta\gamma} \chi^{(3)}_{\mu\alpha\beta\gamma}(-\omega;\omega,-\omega,\omega)E_\alpha(\omega)E_\beta(-\omega)E_\gamma(\omega) \\
&= \sum_{\mu\alpha\beta\gamma} \chi^{(3)}_{\mu\alpha\beta\gamma}(-\omega;\omega,-\omega,\omega)E_\alpha(\omega)E^*_\beta(\omega)E_\gamma(\omega) \quad \text{since} \quad \mathrm{E}(-\omega) = \mathrm{E}^*(\omega) \\
&= \sum_{\mu\alpha\beta\gamma} (\chi^{(3)}_{xxyy}\delta_{\mu\alpha}\delta_{\beta\gamma} + \chi^{(3)}_{xyxy}\delta_{\mu\beta}\delta_{\alpha\gamma} + \chi^{(3)}_{xyyx}\delta_{\mu\gamma}\delta_{\alpha\beta})E_\alpha(\omega)E^*_\beta(\omega)E_\gamma \\
&= \chi^{(3)}_{xxyy}E_\mu(\omega)E^*_\beta(\omega)E_\beta(\omega) + \chi^{(3)}_{xyxy}E_\beta(\omega)E^*_\mu(\omega)E_\beta(\omega) \\
&+ \chi^{(3)}_{xyyx}E_\beta(\omega)E^*_\beta(\omega)E_\mu(\omega) \\
&= \chi^{(3)}_{xxyy}E_\mu E^*_\beta E_\beta + \chi^{(3)}_{xyxy}E_\beta E^*_\mu E_\beta + \chi^{(3)}_{xyyx}E_\beta E^*_\beta E_\mu \\
&= \chi^{(3)}_{xyxy}E^*_\mu EE + 2\chi^{(3)}_{xxyy}E_\mu \mathbf{E}^*\mathbf{E}.
\end{aligned}$$

This follows from $\chi^{(3)}_{xxyy} = \chi^{(3)}_{xyxy}$ and $\mathbf{EE} = \mathrm{EE}$. Therefore the component form of the OKE polarization is [9]:

$$P_\mu = \chi^{(3)}_{xyxy}\mathrm{E}^*_\mu\mathrm{EE} + 2\chi^{(3)}_{xxyy}\mathrm{E}_\mu\mathbf{E}^*\mathbf{E}. \tag{2.41}$$

And its vector form is [9]:

$$\mathbf{P} = \chi^{(3)}_{xyxy}\mathbf{E}^*\mathrm{EE} + 2\chi^{(3)}_{xxyy}\mathbf{EE}^*\mathbf{E}. \tag{2.42}$$

$(\mu,\alpha,\beta,\gamma) \leftrightarrow (\omega,\omega,\omega,\omega)$
$(x,x,y,y) \leftrightarrow (\omega,\omega,\omega,\omega)$
$(x,y,x,y) \leftrightarrow (\omega,\omega,\omega,\omega)$
$(x,y,y,x) \leftrightarrow (\omega,\omega,\omega,\omega)$

Table 2.3: Components of the THG $\chi^{(3)}_{xxxx}$ after P. N. Butcher and D. Cotter [1].

THG Susceptibility Tensor in an Isotropic Medium

We invoke the intrinsic permutation symmetry as applied in the case of the OKE susceptibility. In this case the three independents terms $\chi^{(3)}_{xxyy}$, $\chi^{(3)}_{xyxy}$ and $\chi^{(3)}_{xyyx}$ are all associated with the same set of frequencies $(\omega,\omega,\omega,\omega)$ as shown in Table 2.3.

We note that both x, y maps unto ω in the first, second and third term ; one may easily conclude based on the intrinsic permutation symmetry that $(x,x,y,y) = (x,y,x,y) = (x,y,y,x)$. i.e $\chi^{(3)}_{xxyy} = \chi^{(3)}_{xyxy} = \chi^{(3)}_{xyyx}$.
In esu, i.e $\epsilon_0 = 1$, the THG polarization tensor in an isotropic medium in the μ-direction is found by letting $= \omega_1 = \omega_2 = \omega_3 = \omega$ and $\omega_\sigma = 3\omega$, we drop $\sum_\omega$ for convenience and set $K(-\omega_\sigma;\omega,-\omega,\omega) = 1$. Equation (1.48) becomes:

$$\begin{aligned}
[P^{(3)}_\omega]_\mu &= \sum_{\mu\alpha\beta\gamma} \chi^{(3)}_{\mu\alpha\beta\gamma}(-\omega_\sigma;\omega_1,\omega_2,\omega_3)(e^*_\sigma)_\mu(e_1)_\alpha(e_2)_\beta(e_3)_\gamma E_\alpha(\omega_1)E_\beta(\omega_2)E_\gamma(\omega_3) \\
&= \sum_{\mu\alpha\beta\gamma} \chi^{(3)}_{\mu\alpha\beta\gamma}(3\omega;\omega,\omega,\omega)E_\alpha(\omega)E_\beta(\omega)E_\gamma(\omega) \\
&= \sum_{\mu\alpha\beta\gamma} (\chi^{(3)}_{xxyy}\delta_{\mu\alpha}\delta_{\beta\gamma} + \chi^{(3)}_{xyxy}\delta_{\mu\beta}\delta_{\alpha\gamma} + \chi^{(3)}_{xyyx}\delta_{\mu\gamma}\delta_{\alpha\beta})E_\alpha(\omega)E_\beta(\omega)E_\gamma \\
&= \chi^{(3)}_{xxyy}E_\mu(\omega)E_\beta(\omega)E_\beta(\omega) + \chi^{(3)}_{xyxy}E_\beta(\omega)E_\mu(\omega)E_\beta(\omega) \\
&+ \chi^{(3)}_{xyyx}E_\beta(\omega)E_\beta(\omega)E_\mu(\omega) \\
&= \chi^{(3)}_{xxyy}E_\mu E_\beta E_\beta + \chi^{(3)}_{xyxy}E_\beta E_\mu E_\beta + \chi^{(3)}_{xyyx}E_\beta E_\beta E_\mu \\
&= 3\chi^{(3)}_{xxyy}E_\mu \mathbf{EE}
\end{aligned}$$

since, $\chi^{(3)}_{xxyy} = \chi^{(3)}_{xyxy} = \chi^{(3)}_{xyyx}$.
Hence the scalar form of the THG polarization is [9]:

$$P_\mu = \chi^{(3)}_{xxxx}E_\mu \mathbf{EE}; \tag{2.43}$$

whereas its vector form is equal to [9]:

$$\mathbf{P} = \chi^{(3)}_{xxxx}\mathbf{EEE}. \tag{2.44}$$

2.3 Optical Kerr Effect and Third-Harmonic Generation

When an intense optical field propagates through a medium, it induces a polarization which depends upon the intensity of the incident optical field (light). This gives rise to various intensity-dependent processes one of which is the optical Kerr effect. At such high intensity it may also happen that the waves mix with each other. Leading to the so-called frequency mixing phenomena (sum-and difference-mixing). In this respect harmonic generation is a special case of sum-mixing where the frequency of the mixing waves are all the same and equal to ω. If n such waves are involved in this process the resulting wave is of frequency $n\omega$. This is a degenerate case of the sum-frequency mixing, as each incoming wave has the same frequency. Third-harmonic generation results from the coupling of three waves each of frequency ω. Nonlinear phenomena dependent on the light intensity or resulting from coupling of waves are the central ideas that lie at the heart of nonlinear optics. A more complete treatment of the optical Kerr effect (OKE) and third-harmonic generation (THG) could be found in the books on nonlinear optics by P. N. Butcher and D. Cotter [1] and R. W. Boyd [9], on which this chapter greatly depends.

2.3.1 Parametric and Nonparametric Processes

Nonlinear processes are grouped into two categories: parametric and nonparametric processes. R. W. Boyd has pointed out that the origin of this terminology is obscure. They may be defined as follows: Parametric processes are those which involve a *virtual* energy transition of population from an initial to a final state. The initial and final state are quantum-mechanically identical. In order to represent the process Feynmann diagrams are used to describe the process step-by-step. Consider for example THG as shown in Fig. 2.3 where the left hand side represents three photons each of frequency ω ($\hbar = 1$) being absorbed, the right hand side represent a photon of frequency 3ω ($\hbar = 1$) being emitted. The process may happen in four ways as depicted in the figure. Note that since the initial and final state of the medium are identical, their photon energy is conserved and they may be described by a real susceptibility.

Nonparametric processes do involve *real* transitions from one level to another. Therefore they involve absorption. Hence their photon energy is not conserved and they may be described by means of complex susceptibility. Consider the nonlinear refractive index for instance. Its real part represents a parametric process i.e the optical Kerr effect $Re\chi^3(-\omega;\omega,-\omega,\omega)$, whereas the imaginary part describes processes such as two-photon absorption $Im\chi^3(-\omega;\omega,-\omega,\omega)$ or saturable absorption [6, 9] to name a few.

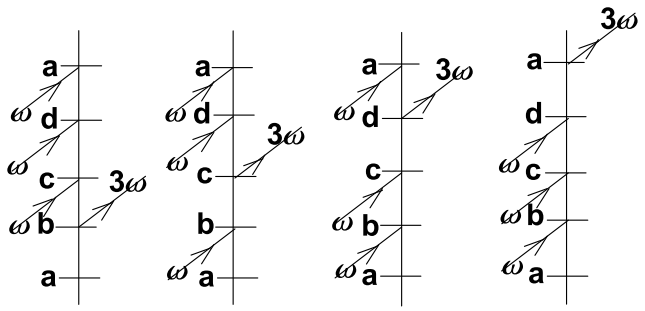

Figure 2.3: Feynman diagrams for THG processes after P. N. Butcher and D. Cotter [1]

2.3.2 Optical Kerr Effect

The Optical Kerr effect underlies the intensity-dependent refractive index[9] also known alternatively as nonlinear refraction coefficient [1]. It is an induced change of the refractive index $n(\omega)$ that results from an induced polarization caused by an intense optical field propagating through a material.

The intensity-dependent refractive index change in SI units is [1]:

$$\begin{aligned} n(\omega) &= n_0(\omega) + \delta n(\omega) \\ &= n_0(\omega) + n_2(\omega)|E|^2 \end{aligned} \tag{2.45}$$

where n_0 is the weak field refractive index, also known as low-intensity refractive index or linear refractive index, n_2 is the second-order index of refraction and E is the incident optical field (electromagnetic field).

Recall that by Eq. (2.12) monochromatic fields are of the form [1]:

$$\mathbf{E}(\mathrm{t}) = \frac{1}{2}\sum_{\omega' \geq 0}[\mathbf{E}_{\omega'}\exp(-\mathrm{i}\omega'\mathrm{t}) + \mathbf{E}_{-\omega'}\exp(+\mathrm{i}\omega'\mathrm{t})].$$

whereas a quasi-monochromatic fields is defined to be [1]:

$$\mathbf{E}(\mathrm{t}) = \frac{1}{2}\sum_{\omega' \geq 0}[\mathbf{E}(\mathrm{t})_{\omega'}\exp(-\mathrm{i}\omega'\mathrm{t}) + \mathbf{E}(\mathrm{t})_{-\omega'}\exp(+\mathrm{i}\omega'\mathrm{t})].$$

Let $\mathbf{E}_\omega = \mathbf{e}\mathrm{E}$ where E is a complex scalar amplitude and $\mathbf{e}$ is a unit vector in

the direction of the polarization P, where in SI units

$$\begin{aligned} P &= P^{(1)} + P^{(3)} \\ &= \epsilon_0[\chi^{(1)}(-\omega;\omega) + \chi^{(3)}(-\omega;\omega,-\omega,\omega)|E|^2]E. \end{aligned} \tag{2.46}$$

In esu the polarization P is:

$$\begin{aligned} P &= P^{(1)} + P^{(3)} \\ &= 4\pi[\chi^{(1)}(-\omega;\omega) + 4\pi\chi^{(3)}(-\omega;\omega,-\omega,\omega)|E|^2]E. \end{aligned} \tag{2.47}$$

2.3.3 The Nonlinear Refractive Index in SI units

Consider the linear refractive n_0 which is related to $\chi^{(1)}$ through [1],

$$n_0^2(\omega) = 1 + Re\chi^{(1)}(-\omega;\omega). \tag{2.48}$$

and the effective dielectric function which is defined by [1]:

$$\epsilon(\omega) = 1 + \chi^{(1)}(-\omega;\omega) + \chi^{(3)}(-\omega;\omega,-\omega,\omega)|E|^2. \tag{2.49}$$

By (2.48) we have that $n_0(\omega) = \sqrt{1 + Re\chi^{(1)}(-\omega;\omega)}$. In the same fashion (2.45) may written as:

$$n(\omega) = \sqrt{1 + Re\chi^{(1)}(-\omega;\omega) + Re\chi^{(3)}(-\omega;\omega,-\omega,\omega)|E|^2}. \tag{2.50}$$

As $n = n_0 + \delta n$ by Eq. (2.45), and considering Eq. (2.50) it follows that:

$$\begin{aligned} n_0(\omega) + \delta n(\omega) &= \sqrt{1 + Re\chi^{(1)}(-\omega;\omega) + Re\chi^{(3)}(-\omega;\omega,-\omega,\omega)|E|^2} \\ &= \sqrt{Re \quad \epsilon(\omega)}. \end{aligned}$$

Then

$$\begin{aligned} \delta n(\omega) &= \sqrt{1 + Re\chi^{(1)}(-\omega;\omega) + Re\chi^{(3)}(-\omega;\omega,-\omega,\omega)} - n_0(\omega) \\ &= \sqrt{1 + Re\chi^{(1)}(-\omega;\omega)}\sqrt{1 + \frac{Re\chi^{(3)}(-\omega;\omega,-\omega,\omega)}{1 + Re\chi^{(1)}(-\omega;\omega)}|E|^2} - n_0(\omega) \\ &\simeq \sqrt{1 + Re\chi^{(1)}(-\omega;\omega)} \quad [\quad 1 + \frac{Re\chi^{(3)}(-\omega;\omega,-\omega,\omega)}{2(1 + Re\chi^{(1)}(-\omega;\omega))}|E|^2 \quad] - n_0(\omega) \\ &= \quad \sqrt{1 + Re\chi^{(1)}(-\omega;\omega)} + \frac{Re\chi^{(3)}(-\omega;\omega,-\omega,\omega)}{2\sqrt{1 + Re\chi^{(1)}(-\omega;\omega)}}|E|^2 - n_0(\omega) \\ &= n_0(\omega) + \frac{Re\chi^{(3)}(-\omega;\omega,-\omega,\omega)}{2n_0}|E|^2 - n_0(\omega) \quad \text{by} \quad (2.48) \\ &= \frac{Re\chi^{(3)}(-\omega;\omega,-\omega,\omega)|E|^2}{2n_0} \\ &= n_2(\omega)|E|^2. \end{aligned}$$

This leads to:

$$n_2(\omega) = \frac{Re\chi^{(3)}(-\omega;\omega,-\omega,\omega)}{2n_0}. \tag{2.51}$$

We have used the binomial expansion on the assumption that $\delta n(\omega) \ll n_0(\omega)$, as the medium is *weakly* nonlinear [9]. Note that $n_2(\omega)$ has the same units as χ^3 (m^2V^{-2}) because n_0 is dimensionless [1].

The nonlinear refraction coefficient may alternatively be defined in terms of the intensity I_ω as:

$$n(\omega) = n_0(\omega) + n_2^I(\omega)I_\omega, \tag{2.52}$$

where the intensity I_ω is given by

$$I_\omega = \frac{1}{2}\epsilon_0 c n_0 |E|^2; \tag{2.53}$$

and $n_2(\omega)$ in units of m^2W^{-1} is

$$n_2^I = \frac{Re\chi^3(-\omega;\omega,-\omega,\omega)}{\epsilon_0 c n_0^2}. \tag{2.54}$$

2.3.4 The Nonlinear Refractive Index in esu

In electrostatics units the intensity-dependent refractive index is:

$$n(\omega) = n_0(\omega) + n_2(\omega)(\text{esu})|\mathrm{E}_\omega|^2. \tag{2.55}$$

The dimensions of n_2 in esu are stat.voltcm^{-1} with
1 statvoltcm^{-1} = (c/10^4)Vm^{-1} and $c = 3 \times 10^8$ms^{-1}.
Equation (2.49) becomes:

$$\epsilon(\omega) = 1 + 4\pi\chi_{esu}^{(1)}(-\omega;\omega) + 4\pi\chi_{esu}^{(3)}(-\omega;\omega,-\omega,\omega) \tag{2.56}$$

Moreover (2.51) and (2.54) reads:

$$n_2(\omega) = \frac{2\pi Re\chi_{esu}^{(3)}(-\omega;\omega,-\omega,\omega)}{n_0} \tag{2.57}$$

$$n_2^I(\omega) = \frac{160\pi^2 Re\chi_{esu}^{(3)}(-\omega;\omega,-\omega,\omega)}{c n_0^2}; \tag{2.58}$$

where $c, n_0(\omega)$ are the same as before.

2.3.5 Third-Harmonic Generation

High-order harmonic generation may be understood as follows: Consider a medium illuminated by an optical field that consists of waves each of frequency ω.

According to R. W. Boyd [9], due to the nonlinear response of atoms, they develop an oscillating dipole moment which contains a component with frequency $n\omega$ where n is the order of nonlinearity. As any material contains an huge number of such atomic dipoles each oscillating with a phase that depends upon that of the incident fields, and if the relative phasing of these dipoles is correct, it follows that the fields radiated by each dipole add constructively in the forward direction. This results into a radiation in the form of a well-defined beam with frequency $n\omega$.

Consider the component of the polarization which oscillate at ω. According to P. N. Butcher and D. Cotter [1] the phase of this component of the induced dipole moment is not constant throughout the medium it moves with a phase velocity equal to ω/k_ω, and in a similar way the phase velocity of the component which oscillate at $n\omega$ moves with a phase velocity equal to $n\omega/k_{n\omega}$. The phase-matching condition is satisfied when these two phase velocities are equal i.e $\Delta k = nk_\omega - k_{n\omega} = 0$.

Boyd [9] has pointed out that when this condition is met the electric field strength of the emitted radiation in the forward direction will be larger than that due to any one atom. The intensity in turn is proportional to the square of the incident field i.e $I \propto |E|^2$ [9].

According to P. N. Butcher and D. Cotter [1] THG may be analyzed by means the so-called "third-harmonic intensity" by relating the third-harmonic intensity $I_{3\omega}$ to the fundamental intensity I_ω.

Third-Harmonic Intensity

In a nonabsorptive medium the intensity of the third-harmonic wave after a distance L is related to the intensity of the fundamental wave I_ω through [1, 9, 12, 13]:

$$I_{3\omega}(L) = \frac{(3\omega)^2}{16\epsilon_0^2 c^4} \frac{|\chi^{(3)}(-3\omega;\omega,\omega,\omega)|^2}{n_\omega^3 n_{3\omega}} I_\omega^3 L^2 \mathrm{sinc}^2(\frac{\Delta \mathrm{kL}}{2}) \tag{2.59}$$

Eq.(2.59) is an oscillatory function of L, through the factor $\mathrm{sinc}^2(\Delta \mathrm{kL}/2)$ as shown below. Fig. 2.4 represents the plot of $\mathrm{sinc}^2(\Delta \mathrm{kL}/2)$ in units of $\Delta kL/2$ within the range from -5π to +5π.

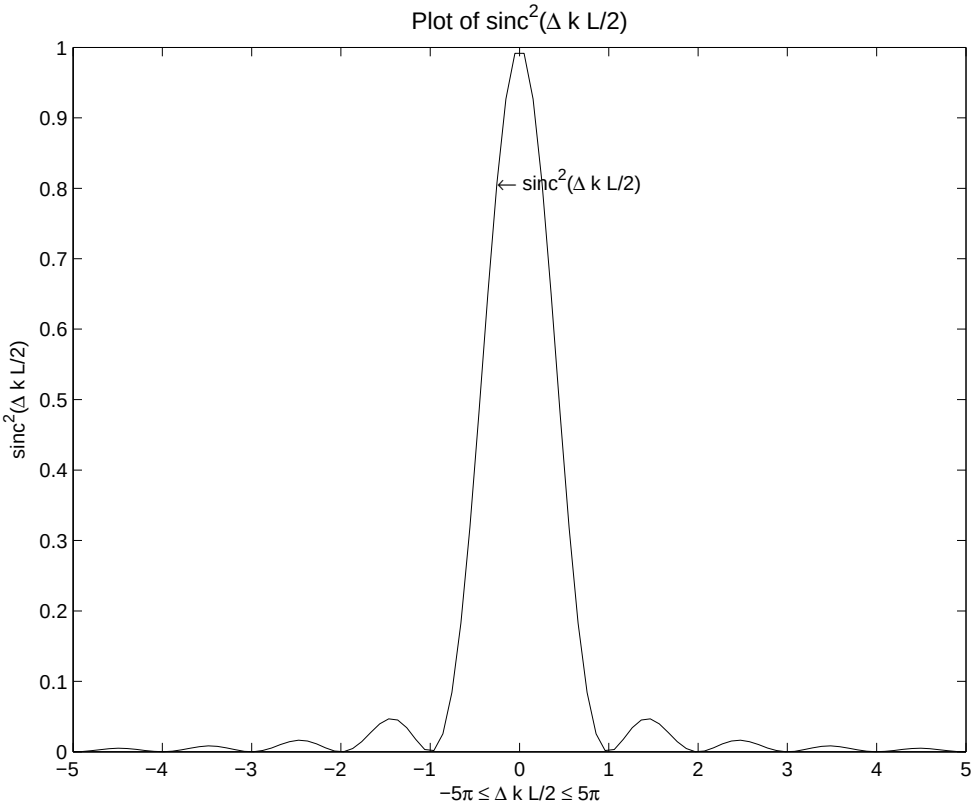

Figure 2.4: Plot of $\text{sinc}^2(\Delta kL/2)$

2.4 Optical Nonlinearity of Gold Nanoparticles

Frequency dependent properties of metals have been intensively investigated by means of the Drude and Drude-Sommerfeld models [3]. The latter is the extension of the original model due to Drude [14-17] and is based on the kinetic gas theory in the sense that a metal is modelled as a gas of electrons and it incorporates the Pauli principle into the original model due to Drude [16].

Despite its overwhelming success in describing the permittivity of metals at low frequencies or equivalently at low energies, the Drude-Sommerfeld model fails at higher frequencies, in particular at the so-called optical frequency region; near infrared, visible and ultraviolet region denoted by NIR-VIS-UV [17]. This is due to the fact that the DS model does not take into account the *interband* and *intraband* contributions to the permittivities i.e dielectric functions [17].

C. F. Bohren and D. R. Huffman [3] have represented schematically the optical properties of conductors and semiconductors by means of a continuum of energy states which is due to the large number of electrons in a solid. The energy levels are therefore grouped into the so-called *bands*. Insulators and semiconductors are called *nonconductors* as they possess a *band-gap* between "completely filled" and "completely empty" energy bands. In *conductors* a band of electron states is either "incompletely filled" or partly filled bands *overlap* in energy with partly empty bands. This is illustrated in Fig. 2.5.

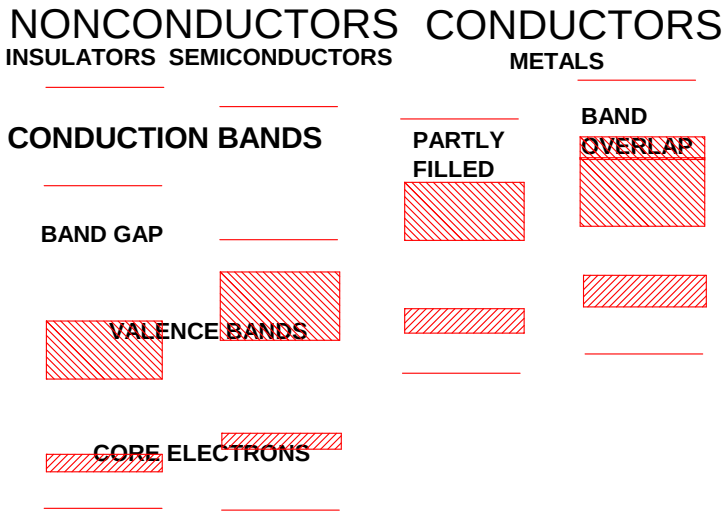

Figure 2.5: Electron energy bands in nonconductors and conductors. Adapted from C. F. Bohren and D. R. Huffman [3].

The mechanism through which electrons fill a vacant electron state in the same energy bands as a result of photon absorption is called *intraband absorption*.

This is due to the absorption of low-energy photons. If however the photon energies are greater than the band gap the valence electrons may fill the conduction band. This absorption is termed *interband absorption*. The intraband absorption is also called "conduction electron intraband contribution", whereas the interband one is called "interband contribution" [6].

In the sections that follow we present the key results due to F. Hache and co-workers [6]. The model that they used is that of N independents electrons in a spherical box of radius a [7]. We simply review the main results. For more information about the model the interested reader is referred to the authoritative papers of F. Hache et al. [6, 7].

2.4.1 The Conduction Electron Intraband Contribution

The $xxxx$ component of the OKE intraband tensor of pure nanogold spherical particles, whose radius a is within the range $50 - 500$ Å is equal to:

$$\chi^{(3)}_{xxxx(intra)} = -i\frac{64}{45\pi^2}T_1T_2\frac{1}{a^3}\frac{e^4}{m^2\hbar^5\omega^7}E_F^4 g_1(\nu)(1-\frac{a}{a_0}). \tag{2.60}$$

T_1 is the energy lifetime, T_2 is the dephasing time, e is the charge of a free electron, m is the mass of the electron, E_F is the Fermi energy. $g_1(\nu), g_2(\nu)$ and $g_3(\nu)$ are dimensionless quantities of the order 1 [7]. They are introduced for convenience in the model calculation. The constants T_1 and T_2 represent just two among the myriad of relaxation processes that tend to restore the ensemble to thermal equilibrium [1] and a_0 is given by

$$a_0 = T_2(2E_F/m)^{\frac{1}{2}}g_1/[g_2 + g_2]. \tag{2.61}$$

Recall that because of isotropy (2.38) we have $\chi^{(3)}_{xxxx} = \chi^{(3)}_{xxyy} + \chi^{(3)}_{xyxy} + \chi^{(3)}_{xyyx}$.

When $a \ll a_0$ equation (2.61) is strongly size dependent, varying as a^{-3}. This is due to the confinement of the electron also known as quantum size effect [22]. According to L. Genzel et al. [22] it may be understood as follows: The continous electronic conduction band of the gold breaks into observable discrete states as the dimensions of the metal particles becomes small enough.

This third-order nonlinear susceptibility is an electric dipole one as long as we remain in the Rayleigh regime [1, 3, 4, 6, 7]. In this regime the polarization of the material is described by a *dipole* $P = P^{(1)} + P^{(3)} + further\ terms$. Its cubic term is $P^{(3)} = \chi^{(3)}EEE$ where $\chi^{(3)}$ is the called the electric dipole susceptibility. F. Hache et al. [6, 7] have shown that for large particles the electric dipole

$\chi^{(3)}$ vanishes whereas a magnetic dipole and an electric multipole susceptibility become significant [6].

A calculation of the third-harmonic susceptibility tensor in the case of intra-band effects was found to be smaller than that of the Kerr susceptibility tensor by three order of magnitude i.e.

$$\frac{\chi^{(3)}(-\omega;\omega,-\omega,\omega)}{\chi^{(3)}(3\omega;\omega,\omega,\omega)} \propto 10^3.$$

Therefore for pure nanogold spherical particles,

$$\begin{aligned} \mathrm{OKE}\chi^{(3)}_{(intra)} &= -i10^{-10} \text{ esu}, \\ \mathrm{THG}\chi^{(3)}_{(intra)} &= -i10^{-13}\text{esu}. \end{aligned}$$

2.4.2 The Interband Contribution

The interband absorption of pure nanogold spherical particles is due to transitions between the d-valence band electrons and the $s-p$ conduction band. In the vicinity of the gold plasmon resonance $\hbar\omega \sim 2.33$eV the interband Kerr susceptibility tensor for gold particles within the range $50-500$ Å [7] is

$$\chi^{(3)}_{(inter)} = -i\frac{2\pi A}{3}T_1'T_2'\frac{e^4}{\hbar^2 m^4\omega^4}J(\omega)|\mathbf{P}|^{\mathbf{4}}, \tag{2.62}$$

where $J(\omega)$ is the joint density of states [6], $|\mathbf{P}|^2 = (\hbar\mathbf{G}\omega_{\mathrm{g}}/2\omega)^2$, $\mathbf{G}$ is the modulus of the reciprocal wave vector of the reciprocal lattice corresponding to the transition and $\hbar\omega_g$ is the gap energy $(1.7eV)$. T_1' and T_2' are the energy lifetime and dephasing time corresponding to the two-level system. A is an angular factor equal to $\frac{1}{5}$.

The interband third-harmonic susceptibility tensor as compared to the Kerr one is of the order of 4, this from:

$$\frac{\chi^{(3)}(-\omega;\omega,-\omega,\omega)}{\chi^{(3)}(3\omega;\omega,\omega,\omega)} \propto 10^4. \tag{2.63}$$

A direct evaluation of the Kerr susceptibility tensor at $\omega = 3.55\times10^{15}\ s^{-1}$ with $E_F = 5.5eV$, $T_1 = 10^{-13}$ s, $T_2 = 2\times10^{-14}$ s, $a_0 = 13.6nm$, $T_1' = 2\times10^{-13}$ s^{-1}, $T_2' = 2\times10^{-14}\ s^{-1}$ lead to the following results which agree in scale with the experimentally measured ones [6]:

$$\mathrm{OKE}\chi^{(3)}_{(inter)} = -i1.7\times10^{-8} \text{ esu} \tag{2.64}$$

$$\mathrm{THG}\chi^{(3)}_{(inter)} = -i1.7\times10^{-12}\text{esu}. \tag{2.65}$$

2.4.3 The Hot-Electron Contribution in the Unsaturated Regime

The hot-electron contribution in the unsatured regime is

$$\chi^{(3)}_{hot \quad electron} \approx \frac{\omega_P^2}{\omega^2}\frac{\tau_0}{\tau_{eff}}\frac{1}{24\pi^2\gamma T}\frac{\partial\epsilon"_L}{\partial T}. \tag{2.66}$$

This accounts for the change of the dielectric function $\delta\epsilon_m$ of the small gold nanoparticles caused by the incident laser beam whose frequency is close to the gold surface plasmon frequency ω_S. The metallic spheres absorb some part of the energy whereas another part is absorbed by d-band electrons of the L point of the Brillouin zone for which the "gap" is $\hbar\omega'_g \simeq 2.4eV$ is closer to the photon energy $2.33eV$. As a result d band electrons are promoted to the conduction band.

As opposed to the "intraband" and "interband" absorption this "hot-electron" absorption is imaginary positive hence it increases the imaginary part of the third-order susceptibility of the gold metal. Moreover the hot-electron process is not coherent, therefore it does not contribute to THG, but to the OKE only. F. Hache et al. [6] have reported that the OKE $\chi^{(3)}_{hot \quad electron} \approx 1.1 \times 10^{-7}$ esu. Note that Eq. (2.66) is restricted to the unsaturated regime for which the laser intensity is below 10^8 W/cm^2. Therefore for pure nanogold spherical particles,

$$\begin{aligned} \text{OKE}\chi^{(3)}_{(hot-electron)} &= -i1.1 \times 10^{-7} \text{ esu}, \\ \text{THG}\chi^{(3)}_{(hot-electron)} &= 0 \text{ esu}. \end{aligned}$$

2.4.4 Other Possible Mechanisms

Electrostriction

According to R. W. Boyd [9] there is the tendency for a material to compress under in the presence of an electric field. This effect induces a change of the optical properties of a material. In the case of gold nanoparticles F. Hache et al.[6] have shown that it would require a longer time as compared to nonlinear response that takes a few picoseconds ps [4, 6].

Reorientation and Thermal Effect Nonlinearity due to reorientation arises as a results of the disproportionality of the shape of a molecule for example a cigar-shaped molecule [9]. In the case of spheres it is not possible. Normal thermal effect due to lattice heating does not contribute, it is slower than the measured time scale of 5 ps [6].

2.5 The Maxwell-Garnett Effective Medium Theory

This section presents the Maxwell-Garnett effective medium theory. It applies to composite materials in which a dilute concentration $p \ll .1$ of spherical metallic inclusions with permittivity ϵ_i and radius size a are embedded in a matrix material with permittivity ϵ_h. The inclusions are separated by a distance b which is very small compared to the wavelength of the incident optical field λ. As shown in Fig. 2.6.

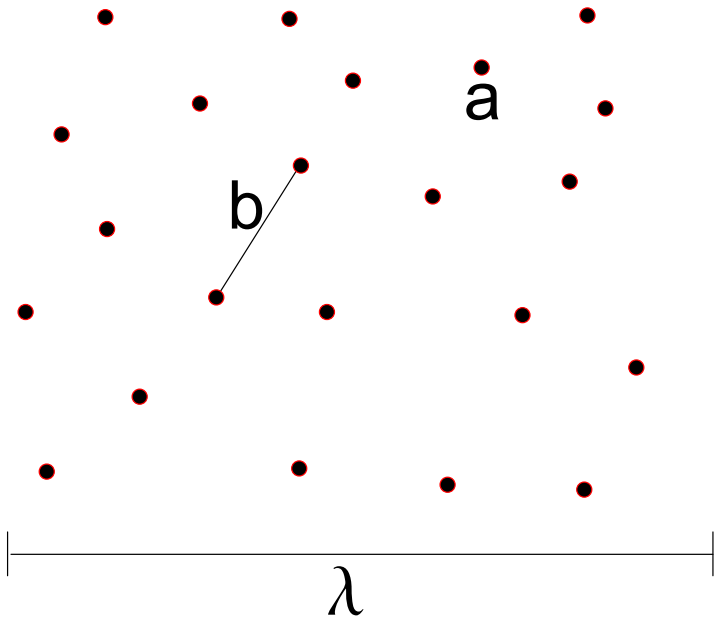

Figure 2.6: Maxwell-Garnett composite topology. Adapted from J. Sipe and R. W. Boyd [2]

The geometry of the composite material comforms to the Rayleigh regime of Mie scattering theory [3]. At this limit the propagation of light is suitably described by electrostatics theory. This is the *quasi-statics* or $effective\ medium\ theory\ approach$ that may be used to calculate the permittivity of the composite material $\epsilon_{composite}$. R. W. Boyd et al. [5] provide a topical review of effective medium theories. The original theory due to Maxwell-Garnett is linear [18]. There exist however many nonlinear extensions of the Maxwell-Garnett theory [19, 20]. Here we present only two of them: The nonlinear extension of the MG model of J. Sipe and R. W. Boyd [2] and D. Ricard et al. [4].

Quasi-Static Approximation

According to C. F. Bohren and D. R. Huffman [3] the illuminating optical electric field to which the spherical inclusion is exposed is approximately uniform over the region occupied by the sphere. This is because $\mathbf{ka} \ll 1$ and as a consequence $\exp(-i\mathbf{k}.\mathbf{a}) = \exp(\mathbf{ik}.\mathbf{a}) \approx \mathbf{1}$. A direct consequence of this approximation is the following:

$$\begin{aligned}\mathbf{E}(\mathbf{x},\mathrm{t}) &= \sum_{\omega\geq 0} \mathbf{E}(\mathrm{t})\exp[-\mathrm{i}(\mathbf{k}.\mathbf{x}-\omega\mathrm{t})] + \mathbf{E}^{*}\exp[+\mathrm{i}(\mathbf{k}.\mathbf{x}-\omega\mathrm{t})] \\ &= \sum_{\omega\geq 0} \mathbf{E}(\mathrm{t})\exp(-\mathrm{i}\omega\mathrm{t}) + \mathbf{E}^{*}\exp(+\mathrm{i}\omega\mathrm{t}).\end{aligned}$$

Effective Medium Theories in the Maxwell-Garnett Topology context

The study of the Maxwell-Garnett geometry has been a subject of intense research since the pioneering work of Maxwell-Garnett in 1904 [18]. Nonlinear extensions of the MG theories were developed shortly after the discoveries of the laser, and due to their potential use in nonlinear optical devices [2]. The effective dielectric function of the composite medium predicted by the Maxwell-Garnett theory is the following:

$$\frac{\epsilon-\epsilon_h}{\epsilon+2\epsilon_h} = p\frac{\epsilon_i-\epsilon_h}{\epsilon_i+2\epsilon_h}, \tag{2.67}$$

where in esu:

$$\epsilon = 1+4\pi\chi(esu), \tag{2.68}$$

$$\epsilon_i = 1+4\pi\chi_i(esu), \tag{2.69}$$

$$\epsilon_h = 1+4\pi\chi_h(esu). \tag{2.70}$$

$p \ll .1$ is the volumetric concentration of inclusions also known as fill fraction of the inclusions [2] or overall occupancy of inclusions [4].

The Rayleigh Regime and the Surface Plasmon Resonance

In the Rayleigh regime which corresponds to the quasi-statics approximation [3], one may calculate the surface plasmon resonance which is also termed Rayleigh-type plasmon resonance.

The plasmon resonance occurs where the condition $\epsilon_i(\omega_S) + 2\epsilon_h(\omega_S) \simeq 0$ is satisfied, where ϵ_i is the complex dielectric permittivity of the spherical particles inclusion and ϵ_h is the complex dielectric permittivity of the matrix. Note that this surface plasmon resonance condition (SPR) holds in the dipole approximation only [3]. It is the frequency at which optical effects due to the molecules in the matrix or close to a rough surface experience a spectacular increase.

It is worth pointing out that L. Genzel et al. [22] have shown that the most dramatic effect observed when the particle size is decreased down to 10Å is a *broadening* and *shift* of the plasma resonance peak. These effects are called *quantum size effects*. They are qualitatively accounted for by a decreased electron mean free path due to the scattering off the particle surface [22].

Nonlinear Extension of Maxwell-Garnett Theories

Nonlinear extensions of the MG theory treat the nonlinearity in either or both the inclusion and the host matrix material [2], while others are restricted to the nonlinearity of the inclusion [4]. A nonlinear extension of the MG theory may also take into account the size dependence of the spherical inclusions [19, 20]. These are the various models that we present in the next section. They all relate the susceptibility of the inclusion ϵ_i to that of the composite ϵ through the so-called *local field factor*, which differs between each theory as they have different formulations.

The Nonlinear Extended Maxwell-Garnett Theory due to J. E. Sipe and R. W. Boyd [2]

J. E. Sipe and R. W. Boyd [2] have developed a full generalisation of the Maxwell-Garnett theory in which either or both components (inclusions and host matrix) posses a nonlinear response. We simply present the one in which the inclusion is nonlinear. The third-order susceptibility of the composite medium is related to that of the metallic inclusion through:

$$\chi^{(3)} = p|\frac{\epsilon + 2\epsilon_h}{\epsilon_i + 2\epsilon_h}|^2[\frac{\epsilon + 2\epsilon_h}{\epsilon_i + 2\epsilon_h}]^2\chi_i^{(3)}, \tag{2.71}$$

where $\chi^{(3)}$, $\chi_i^{(3)}$, $\chi_h^{(3)}$ are the third-order nonlinear susceptibilities of the composite medium, the metallic inclusion and that of the host matrix. The quantity,

$$\frac{\epsilon + 2\epsilon_h}{\epsilon_i + 2\epsilon_h}, \tag{2.72}$$

is defined as the field factor.

The Nonlinear Extended Maxwell-Garnett Theory due to D. Ricard et al. [4].

D. Ricard et al. [4] have used an approach based on a local field argument where the local field prevailing over the metallic particle E_1 is related to the incident field E by:

$$E_1 = \frac{3\epsilon_h}{\epsilon_i + 2\epsilon_h} E, \tag{2.73}$$

where

$$\frac{3\epsilon_h}{\epsilon_i + 2\epsilon_h} \tag{2.74}$$

is the local field factor. In their theories, the third-order susceptibility is related to that of the inclusion by:

$$\chi^{(3)} = p|\frac{3\epsilon_h}{\epsilon_i + 2\epsilon_h}|^2[\frac{3\epsilon_h}{\epsilon_i + 2\epsilon_h}]^2\chi_i^{(3)}. \tag{2.75}$$

Chapter 3

Model Calculation of the Optical Kerr Effect.

3.1 Optical Functions of Au-VO_2 Thin-Films

3.1.1 Introduction

This and the following chapters aim at predicting through model calculation the OKE and THG in Au-VO_2 thin-films and modelling high-order harmonic generation in strongly absorbing media. Chapter 5 also investigates the heat generated in the Au-VO_2 nano-composite thin-films of thickness $L = 80$ Å.

The chapters are organized as follows. Chapter 3 presents the energy loss functions of Au-VO_2 thin-films below and above 68 ^{0}C. It also deals with the model calculation of the OKE. The modelling of high-harmonic generation in strongly absorbing media is presented in chapter 4 and the model calculation of the THG in Au-VO_2 thin-films below and above 68 ^{0}C is the subject of chapter 5. Chapter 5 is also concerned with the heat dissipation in the Au-VO_2 thin-films below and above 68 ^{0}C.

3.1.2 Complex Dielectric Function of Au

The complex dielectric function of Au is calculated from the complex refractive index of Au [26]. The real and imaginary part of the complex refractive index, n and k respectively, are available in the literature in the energy range 0.1-30 eV. The real and imaginary part of the complex dielectric function $Re(\epsilon)$ and $Im(\epsilon)$ are related to n and k through [1, 3, 8-11, 25, 26]:

$$\begin{aligned} Re(\epsilon) &= n^2 - k^2, \\ Im(\epsilon) &= 2nk. \end{aligned}$$

This follows from the fact that $Re(\epsilon) + Im(\epsilon) = (n + ik)^2$. The Figure below presents the real and imaginary part of the dielectric function of Au in the photon

energy range $0 - 7$ eV. According to P. B. Johnson and R. W. Christy [41] the imaginary part of the dielectric function of Au displays mainly two interband absorptions around 2.5 and 5 eV as shown in Fig. 3.1.

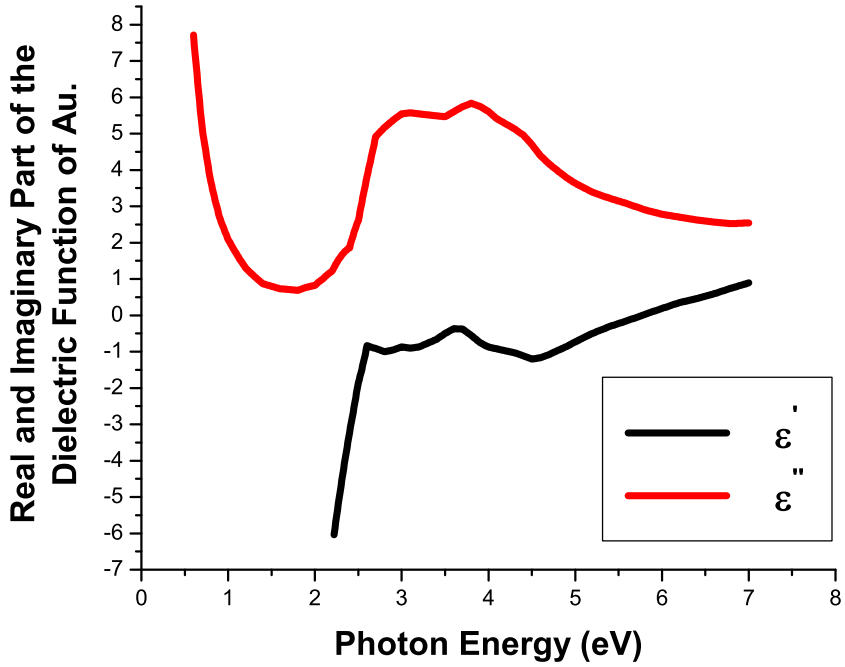

Figure 3.1: Real and Imaginary Part of the Dielectric Function of Au after P. B. Johnson and R. W. Christy [41]

3.2 The Optical Properties VO_2 Thin-Films

Rutile VO_2 shows a dramatic change of its physical properties (complex refractive index and resistivity) at 68 ^{0}C.

This section describes the reason why the complex dielectric function of VO_2 thin-films varies over the so-called transition temperature of 68 ^{0}C. It is based on the work of H. W. Verleur et al. [23]. They have investigated experimentally the optical properties of VO_2 thin-films of 1000Å thickness and have interpreted the results using the simple band model shown in Fig. 3.2.

The oxygen $2p$ levels form the *valence* band separated by a gap of approximately $2.5eV$ from a partially filled *conduction* band that consists of $3d$ vanadium levels. They are responsible for the high energy absorption that peaks at 2.8 and

3.6 eV in both the metallic and the semiconductor phase. The two absorption peaks at 0.85 and 1.3 eV result from transitions between the lowest $3d$ bands.

Unfortunately the model does not predict the origin of the *phase transition* at 68 ^{0}C where the physical properties (electrical resistance, magnetic susceptibility) of the VO_2 rutile like crystal (tetragonal) changes from metal to semiconductor behaviour [23].

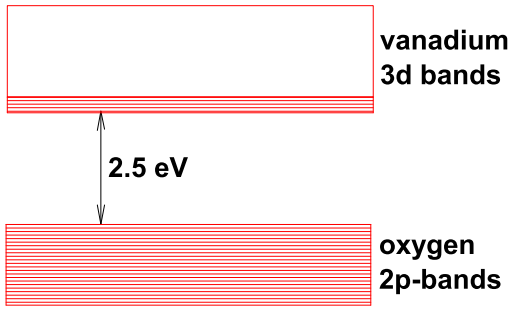

Figure 3.2: Energy-band of VO_2 after H. W. Verleur et al. [8]

3.2.1 The Metallic (rutile) phase $T > T_t$

In the metallic phase, vanadium dioxide has a tetragonal crystal structure also known as rutile since it is similar to that of the TiO_2 [23] rutile with a and $b = 0.453\ nm$, whereas $c = 0.286\ nm$ [24] as shown in Fig. 3.3. The unit cell of the crystal contains two vanadium ions V^{4+}. It follows that the solid has ten $3d$-type energy bands.The two absorption peaks at 0.85 and 1.3 eV result from transitions between the lowest $3d$ bands.

Furthermore the d band with the lowest energy overlaps at least with one of the other nine bands in such a way they are partially occupied by an extra d electron per vanadium ion. This is the reason why this phase should be termed "semimetal" rather than "metal".

The two high-energy peaks that occur at 2.8 eV and 3.6 eV are caused by the *interband* transitions of electrons between the oxygen $2p$ valence bands and the empty $3d$ conduction bands. On the other hand the absorption peak centered near $0.7eV$ is due to the quasi-free electrons.

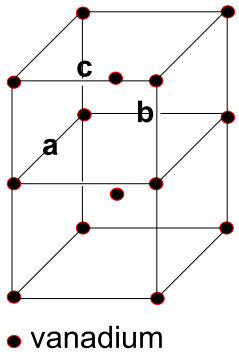

Figure 3.3: Tetragonal Crystal Structure of VO_2 after G. J. Hyland [24]

3.2.2 The Semiconductor (monoclinic) phase $T < T_t$

In this phase the vanadium dioxide presents a monoclinic crystal structure which results from a distortion of the rutile structure. As a consequence there is a "pairing" of vanadium ions and the doubling of the size of the metal cell [23] with $a = 0.547\ nm$, $b = 0.451\ nm$ and $c = 0.537\ nm$ [24] as shown in Fig. 3.4.

The energy gap between the oxygen $2p$ bands and the vanadium $3d$ bands remains the same, however the number of bands doubles as the size of the monoclinic crystal unit cell is double that of the tetragonal crystal unit cell. Therefore there are 20 $3d$ bands as there are four vanadium ions per unit cell. The energy gap between the two filled bands and the remaining eighteen bands is finite and equal to $0.6eV$. It is responsible for the absorption peaks at 0.85 and 1.3 eV.

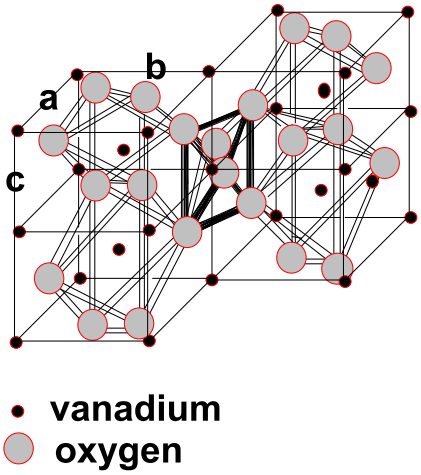

Figure 3.4: Monoclinic Crystal Structure of VO_2 after G. J. Hyland [24]

3.2.3 Complex Dielectric Function of VO_2

The complex dielectric function of VO_2 has been determined in a similar way to that used by H. W. Verleur et al. [8, 38]. They used an automatic curve-fitting computer program based on the well-known dispersion relation [8, 38]:

$$\epsilon(\omega) = \epsilon_\infty - \frac{\omega_n^2}{\omega^2 + i\omega_c\omega} + \sum_{i=1}^{N} \frac{s_i}{1 - \omega^2/\omega_i^2 - i\Gamma_i\omega/\omega_i}.$$

Here
ω is the frequency in eV,
ω_n is the carrier density parameter related to the plasma frequency,
ω_c is the collision frequency,
s_i is the strength of the i'th harmonic oscillator,
ω_i is the frequency of the i'th oscillator,
Γ_i is the linewidth of the i'th oscillator.

According to Verleur et al. [8] the physical significance of the three terms is the following: The first term ϵ_∞ represents a constant contribution to $Re(\epsilon(\omega))$ from high-frequency electronic transitions. The second term accounts for the free carrier contribution to the dielectric function. The third term represents the sum over Lorenz or classical oscillators and accounts for the non-monotonic contribution to the dielectric function within the spectral region of interest.

The real and imaginary part of the dielectric function are computed using the appropriate parameters displayed in the table below for the case above and below 68 ^{0}C. The parameters are the same as those of Verleur et al. [8] within the photon energy range $0.25 - 5$ eV these parameters are displayed above the horizontal line see Table 3.1. Above 5 eV, the parameters are chosen in such a way that their so-called energy loss functions (the probability a fast electron will lose energy $E = \hbar\omega$ in a single inelastic scattering) below and above 68 ^{0}C have the same trend as those of Thomas and Chain [28] as is depicted in Fig. 3.5 and 3.6.

According to H. W. Verleur et al. [8]: Below 68 ^{0}C there are four prominent absorption peaks near photon energies 0.85, 1.3, 2.8 and 3.6 eV see Fig. 3.7. Above 68 ^{0}C there are three prominent absorption peaks near photon energies below 2.0, 3.0 and 4.0 eV as shown in Fig. 3.8.

ω_{iAbove}	s_{iAbove}	Γ_{iAbove}	ω_{iBelow}	s_{iBelow}	Γ_{iBelow}
1.02	0.79	0.55	1.02	0.79	0.55
1.30	0.47	0.55	1.30	0.47	0.55
1.50	0.48	0.50	1.50	0.48	0.50
3.03	0.58	0.22	2.75	0.53	0.22
3.46	1.36	0.47	3.49	1.31	0.47
3.53	1.08	0.38	3.76	1.06	0.38
4.60	1.05	0.49	5.10	0.84	0.79
5.20	1.05	1.10	6.00	1.10	1.10
			7.00	2.60	0.60
			8.60	1.65	3.00
			9.50	0.60	3.30
			14.00	0.20	9.00

Table 3.1: Parameters of the Complex Dielectric Function of VO_2 below and above 68 ^{0}C.

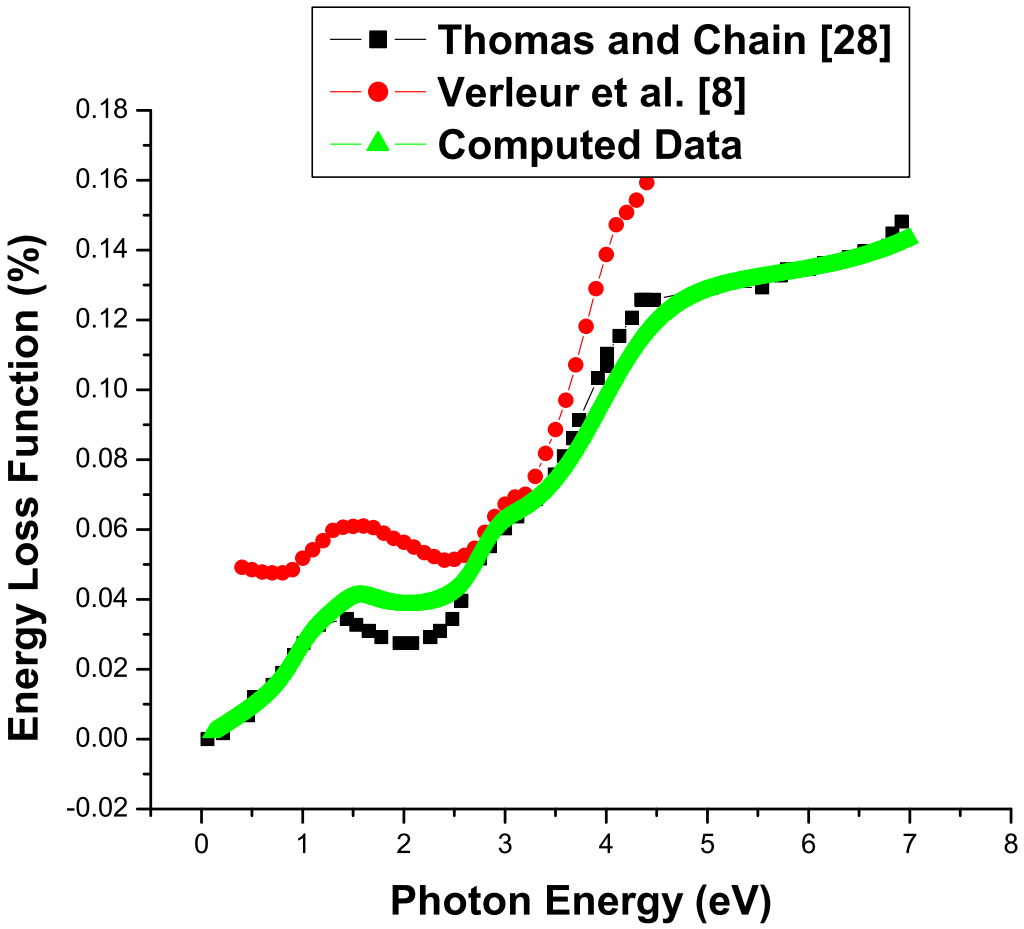

Figure 3.5: Comparison between the Energy Loss Functions of VO_2 Thin-Films below 68 ^{0}C after Thomas and Chain [28] , Verleur et al. [8] and the Computed Data.

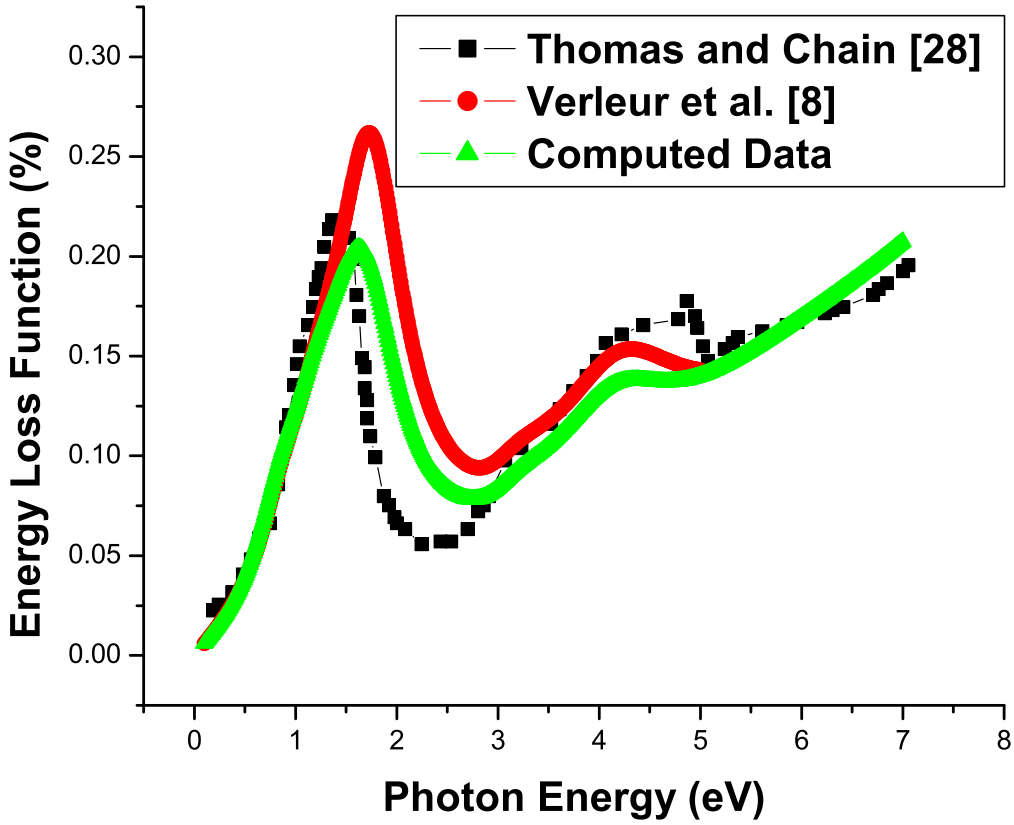

Figure 3.6: Comparison between the Energy Loss Functions of VO_2 Thin-Films above 68 ^{0}C after Thomas and Chain [28] , Verleur et al. [8] and the Computed Data.

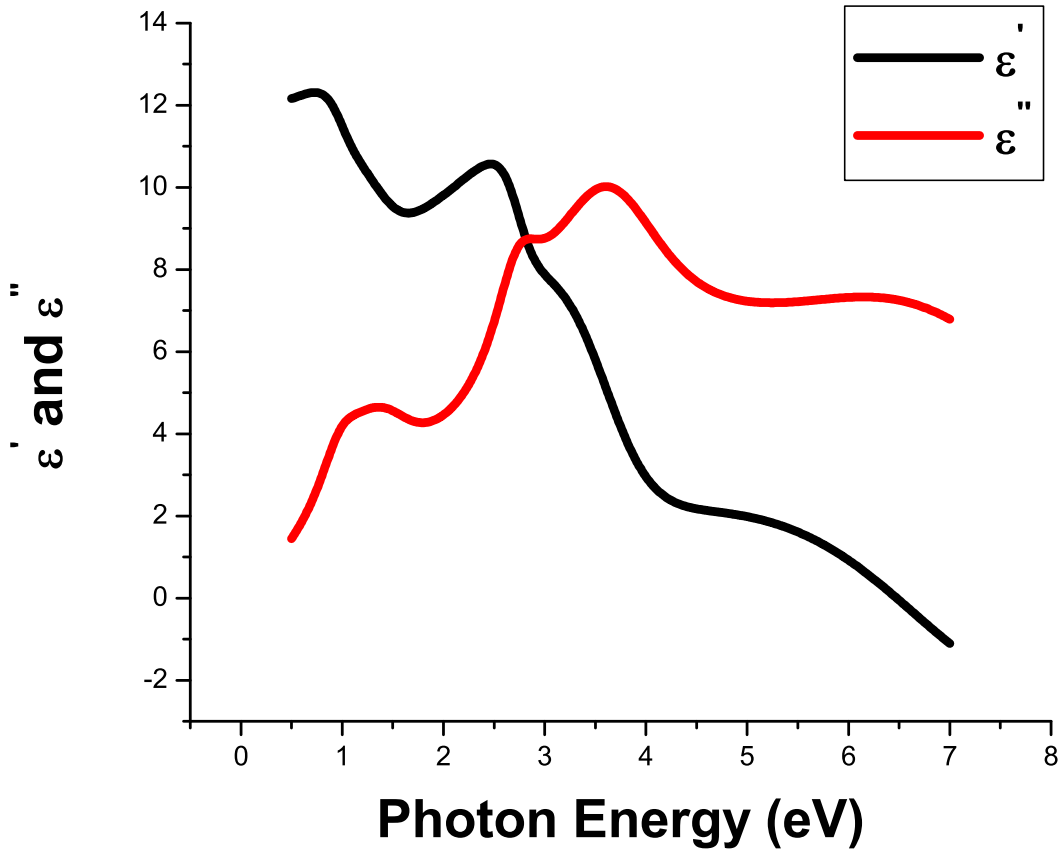

Figure 3.7: Computed Real ($\epsilon^{'}$) and Imaginary ($\epsilon^{''}$) part of the Dielectric Functions of VO_2 Thin-Films below 68 ^{0}C.

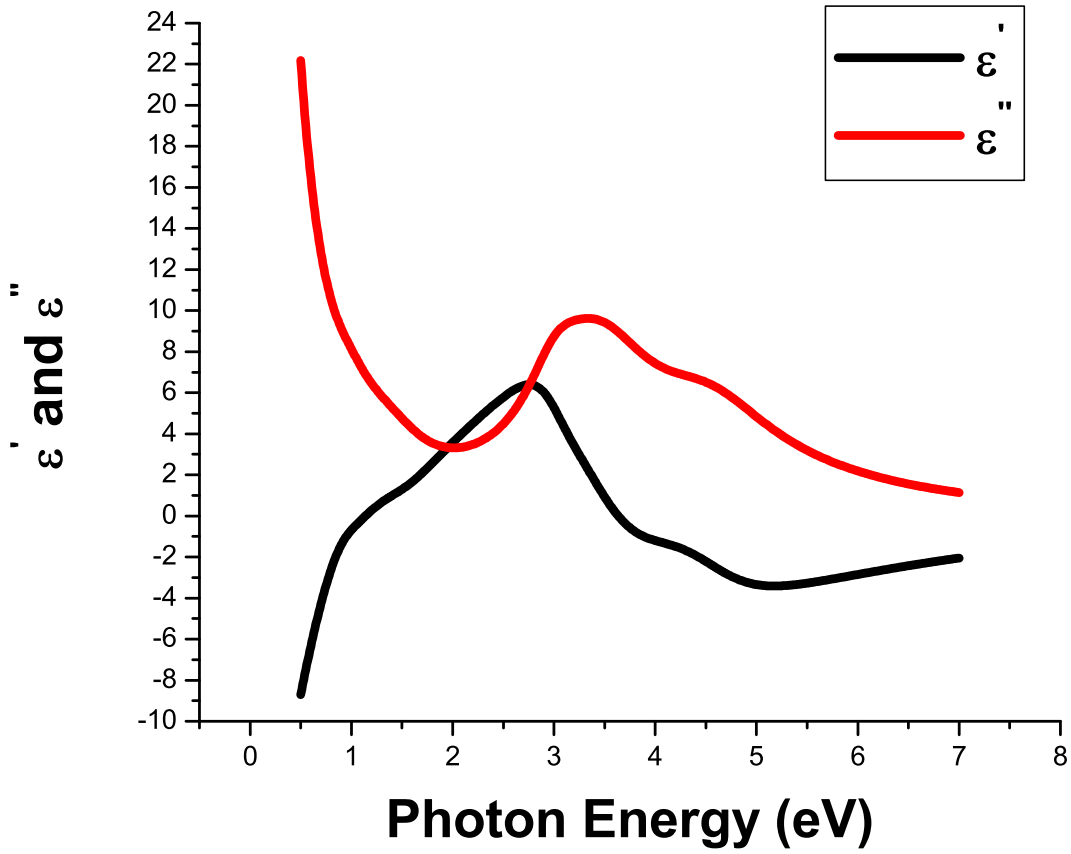

Figure 3.8: Computed Real ($\epsilon^{'}$) and Imaginary ($\epsilon^{''}$) part of the Dielectric Functions of VO_2 Thin-Films above 68 ^{0}C.

3.2.4 Absorption Coefficient of Au-VO_2 Thin-Films

Consider a composite made of metallic inclusions in a host matrix of volumetric concentration or fill fraction, p, of the metallic inclusions in the host material [2, 4, 6, 11, 18].

In the Maxwell-Garnett configuration for which $p \leq .1$, the complex dielectric function of the composite ϵ is related to that of the metallic inclusions ϵ_i and the host material ϵ_h through the relation [2, 4, 11, 18]

$$\epsilon = \epsilon_h \frac{\epsilon_i(1+2p) + 2\epsilon_h(1+p)}{\epsilon_i(1-p) + \epsilon_h(2+p)}.$$

In particular for $p \ll .1$ the above formula reduces to:

$$\epsilon = \epsilon_h + 3p\epsilon_h \frac{\epsilon_i - \epsilon_h}{\epsilon_i + \epsilon_h}.$$

The dielectric function of the Au-VO_2 thin-film may be calculated by means of the above formula for $p \leq .1$ where $\epsilon_i = \epsilon_{Au}$ and $\epsilon_h = \epsilon_{VO_2}$. In particular one may obtain the real and imaginary part of the Au-VO_2 thin-films both below and above the transition temperature of 68 ^{0}C.

It is customary to study the absorption by means of the so-called *absorption coefficient* [3, 5, 9, 23] which is defined as

$$\alpha = \frac{2\omega Im(\epsilon)}{n(\omega)c}$$

where
ω is the frequency in Hz,
ϵ is the complex dielectric function of the composite,
$n(\omega)$ is the real part of the complex index of refraction,
c is the velocity of light in vacuum.

Fig. 3.9 and 3.10 represent the absorption coefficient of Au-VO_2 thin-films below and above 68 ^{0}C.

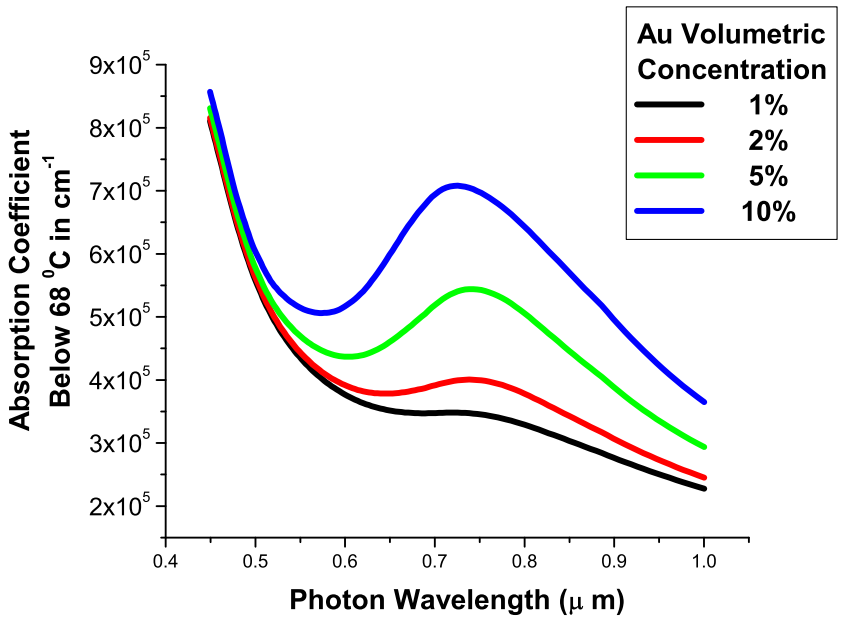

Figure 3.9: Absorption Coefficient of Au-VO_2 Thin-Films below 68^0 C.

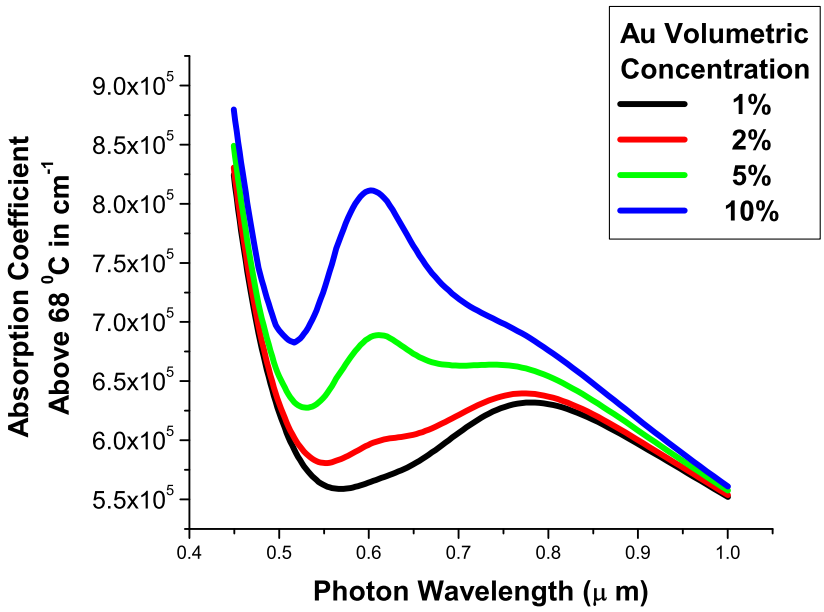

Figure 3.10: Absorption Coefficient of Au-VO_2 Thin-Films above 68^0 C.

3.2.5 Conclusion

The complex dielectric function of VO_2 below and above the transition temperature of 68 ^{0}C has been computed in the energy range 0-7 eV.

It is in good agreement with the results of H. W. Verleur et al. [8] in the energy range from 0.25 to 5 eV on one hand and that of M. Thomas and E. E. Chain [28] in the energy range from 5 to 7 eV on the other. For Au-VO_2 thin-film the peak of the absorption coefficient occurs around 0.7 μm when the Au-VO_2 thin-film is below 68 ^{0}C and about 0.6 μm when it is above 68 ^{0}C.

The SPR energy of Au-SiO_2 composite which occurs at 2.33 eV or 532 μm in [4] shifts towards the red in the Au-VO_2 composite. This is due to the fact that the value of the imaginary part of the complex refractive index of VO_2 is greater than that of SiO_2.

3.3 Model Calculation of the OKE in Au-VO_2 Thin-Films

3.3.1 Introduction

The origins of the mechanisms underlying the Kerr-susceptibility tensor $\chi^{(3)}(-\omega;\omega,-\omega,\omega)$ near the SPR of gold have been described in Chapter 2. Here we merely recall the key results.

It was found that the intraband part was mostly imaginary negative and proportional to a^3 where a is the nanoparticle radius. It accounts for the electronic transitions within the conduction band [6, 11, 27]. According to F. Hache et al. [6] the value of the OKE $\chi^{(3)}_{(intra)} = -i1.0 \times 10^{-10}$esu around the SPR energy of 2.33 eV for gold nanoparticles of size 50Å in a glass matrix.

The interband part was found to be imaginary negative too. It arises as the consequence of electronic transitions from the d-bands to the s-band (conduction band)[6, 11, 27]. It is reported that the OKE $\chi^{(3)}_{(inter)} = -i1.7 \times 10^{-8}$ esu in the vicinity of the SPR energy.

The hot-electron part of the OKE $\chi^{(3)}$ which is imaginary positive is equal to $+i1.1 \times 10^{-7}$. It is due to non equilibrium heating of the conduction electrons [6, 11, 27]. This contribution accounts for the change of the dielectric function $\delta\epsilon_m$ of the small gold nanoparticles caused by the incident laser beam whose frequency is close to the gold surface plasmon frequency ω_S.

3.3.2 Local Field Effect in Au-VO_2 Thin-Films

There is a local field effect that arises as a result of the induced polarization in a nanocomposite under the illumination of an intense optical field [2-6, 9-11, 19, 20, 25, 27]. The electrical field inside the nanoparticle is called "$Local \quad Electrical \quad Field$" whereas the field in the surrounding matrix is the same as the incident one. Finally the electrical field in the vicinity of the nanoparticle is known as the "$Effective \quad Electrical \quad Field$".

On the assumption that the nanoparticle inclusions have a given shape and by means of electrostatic arguments one can relate the effective electrical field to the local one. This is known as effective medium theory (EMT).

There exist many EMT's [2-4, 18-21]. In this work we make use of two, which are simple and appropriate for our Au-VO_2 nanocomposite where the inclusions are spherical.

The first model is due to Ricard et al. [4] and the second one is the model of Sipe and Boyd [2]. They are both nonlinear extensions of the original Maxwell-Garnett theory which is linear [18]. It takes into account the first order susceptibility which is related to the complex refractive index.

The model of Maxwell-Garnett has succeeded in predicting the SPR of gold - doped glasses [2, 6, 19, 27]. Its nonlinear extensions lead to expressions of the form:

$$\chi_{eff}^{(3)} = pf^2|f|^2\chi_i^{(3)},$$

where
$\chi_{eff}^{(3)}$ is the effective third-order susceptibility of the nanocomposite,
$\chi_i^{(3)}$ is the third-order susceptibility of the inclusion,
f is the local field factor,
p is the volumetric concentration of the inclusion.

The local field effect, also called the field factor f is therefore a measure of the enhancement of the local field and differs from one EMT to another.

In the model of Ricard et al. [4], interaction among particles is assumed to be negligible. By means of electrostatic arguments the local field factor is found to be

$$f = \frac{3\epsilon_h}{\epsilon_i + 2\epsilon_h}.$$

The theory of Ricard et al. [4] leads to the following result:

$$\chi_{eff}^{(3)} = p(\frac{3\epsilon_h}{\epsilon_i + 2\epsilon_h})^2 |\frac{3\epsilon_h}{\epsilon_i + 2\epsilon_h}|^2 \chi_i^{(3)}.$$

In the model of Sipe and Boyd [2] the interaction among particles is also regarded as negligible, and the local field factor is found by means of a mesoscopic and macroscopic fields argument.

The mesoscopic field refers to the electrical field in the neighbourghood of an inclusion whereas the macroscopic field is an average of the mesoscopic field over a given region in space. The local field is equal to:

$$f = \frac{\epsilon + 2\epsilon_h}{\epsilon_i + 2\epsilon_h}.$$

The theory of Sipe and Boyd [2] takes into accounts the nonlinearity of both the inclusion and the host matrix. They found that in such a case the effective third-order susceptibility is the sum of the effective third-order susceptibility due to the inclusion on one hand and the host matrix on the other. In particular the effective third-order susceptibility due to the inclusion which is of interest in this work is

$$\chi_{eff}^{(3)} = p(\frac{\epsilon + 2\epsilon_h}{\epsilon_i + 2\epsilon_h})^2 |\frac{\epsilon + 2\epsilon_h}{\epsilon_i + 2\epsilon_h}|^2 \chi_i^{(3)}.$$

The local field factor is independent of the volumetric concentration of the nanoparticle, p according to model of Ricard et al. [4] as opposed to the model of Sipe and Boyd [2].

3.3.3 Discussion

Calculation of the effective OKE in Au-VO_2 thin-films at both below and above the transition temperature of VO_2 thin-films at 68 ^{0}C are performed using the EMT of D. Ricard et al. [4] and Sipe and Boyd [2] for different volumetric concentration of Au ranging from 0.01 to 0.10. Note that for Au nanoparticles the overall OKE $\chi^{(3)}$ =OKE $\chi_{(intra)}^{(3)}$ + OKE $\chi_{(inter)}^{(3)}$ + OKE $\chi_{(hot-electron)}^{(3)} = 1.2\times10^{-7}$ esu.

A direct comparison between each specific calculation using either the model of Sipe and Boyd [2] or that of Ricard et al. [6] leads one to the following conclusions:

The calculated magnitudes of the real and imaginary parts of the effective nonlinear susceptibilities increase monotonically with respect to the gold volumetric concentration. This follows from the fact that Au is responsible for the optical nonlinearity.

It is worth pointing out that the calculations were performed by taking into account the size dependence of the gold nanoparticle which affects the intraband contribution only. It is found that this size effect due to the intraband absorption is negligible when compared to the interband and hot-electron absorptions. As a consequence the overall susceptibility which is the sum of each one of them is almost size independent for nanogold particles within the range 50-500Å. See Fig. 3.11 to 3.18.

The real part of the effective $\chi^{(3)}$ presents two peaks, a first one around 1.4 eV of magnitude -3×10^{-7} esu and a second one, whose magnitude is 1.6×10^{-6} esu. The latter occurs at the SPR energy 1.7 eV. This shift from that reported by F. Hache et al. [6] about 2.3 eV in Au-glass composite is due to the higher value of the refractive index of VO_2 below T_t. When the VO_2 is above T_t there is only one peak at 2.1 eV with magnitude $+2.0 \times 10^{-7}$ esu. The SPR energy in this phase is closer to that of F. Hache et al. [6]. This follows from the fact that the value of the refractive index of VO_2 in this metallic phase is less than that in the semiconductor one.

The imaginary part of the effective $\chi^{(3)}$ presents two peaks, a first one around 1.6 eV of magnitude -1.4×10^{-6} esu and a second one, whose magnitude is $+4.0 \times 10^{-7}$ esu occurring at the SPR energy 1.8 eV. This latter shift towards red is more pronounced in this semiconducting phase compared the metallic one where the two peaks occur at 2.0 and 2.2 eV with magnitude -1.0×10^{-7} and $+8.0 \times 10^{-8}$ esu respectively. The reason for this is the same as that evoked in the previous paragraph.

The computed values of either the real or imaginary part of the effective $\chi^{(3)}$ is higher using the model of Ricard et al. [6] than that of Sipe and Boyd [2]. This is due to the difference of their respective local field effect $f(\omega)$. In the former $f(\omega) = \frac{3\epsilon_h}{\epsilon_i + 2\epsilon_h}$, but in the latter $f(\omega) = \frac{\epsilon + 2\epsilon_h}{\epsilon_i + 2\epsilon_h}$. This last quantity is less than the previous one as the magnitude of the dielectric of the composite, ϵ, is less than that of the host matrix, ϵ_h, if the volumetric concentration of the inclusions is less than 10 percent i.e $p \leq .1$.

The value of the real part of the effective $\chi^{(3)}$ is of the order of 10^{-6} esu when measured below the transition temperature T_t and it is of the order of 10^{-7} esu when measured above T_t. The value of the imaginary part of the effective $\chi^{(3)}$ is higher when measured below than above the transition temperature T_t.

It is of the order of 10^{-7} esu in both phases. This is probably due to the high value of the local field effect resulting from the fact that the refractive indices of VO_2 below and above T_t are bigger than those of SiO_2, TiO_2 and Al_2O_3 [29, 33].

These values are big despite the fact that the maximum volumetric concentration of nanogold particles is 10 percent and the particles size is between $50 - 500$Å. Note that such a high value has already been reported previously [29, 33]. However the Au volumetric concentration was generally above 10 percent and the nanogold particles was mostly bigger than 500Å.

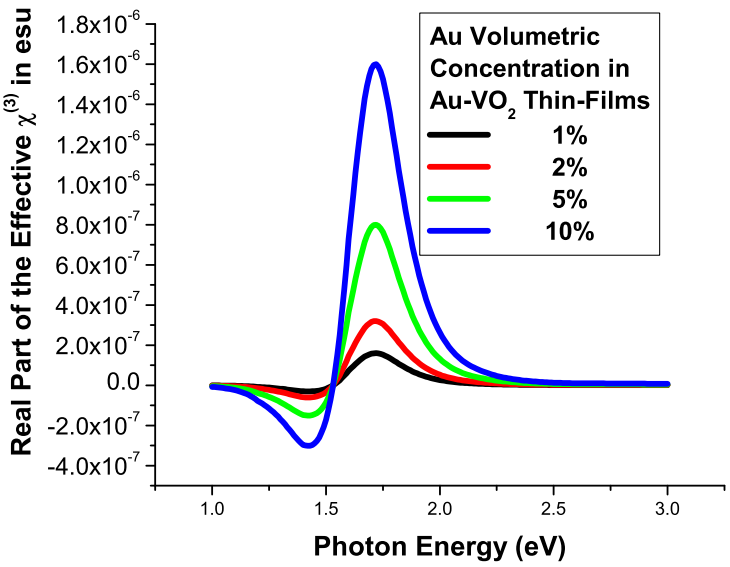

Figure 3.11: Calculation of the Real Part of the overall Effective OKE $\chi^{(3)}$ of Au-VO_2 Thin-Film below 68 ^{0}C using the Model of Ricard et al. [4]. The size of the nanogold particles is within the range 50Å-500Å.

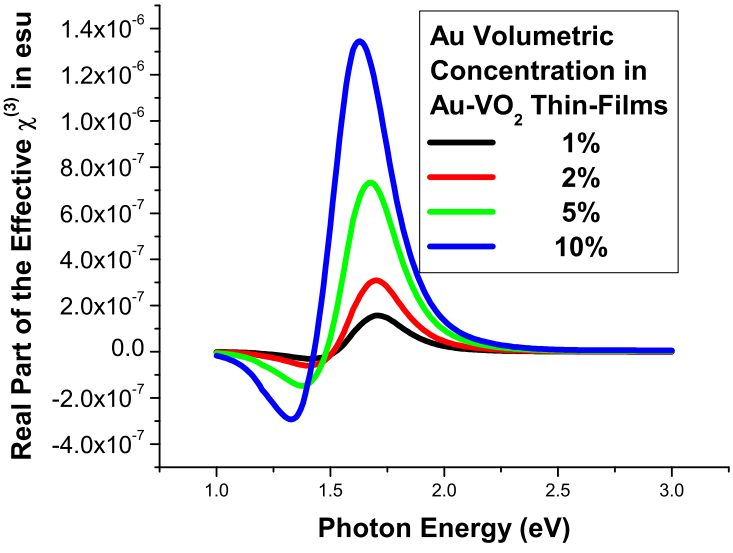

Figure 3.12: Calculation of the Real Part of the overall Effective OKE $\chi^{(3)}$ of Au-VO_2 Thin-Film below 68 ^{0}C using the Model of Sipe and Boyd [2]. The size of the nanogold particles is within the range 50Å-500Å.

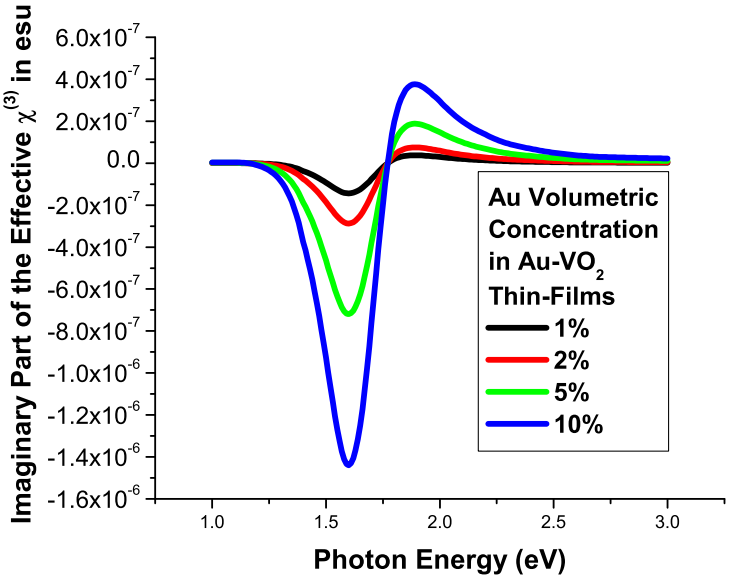

Figure 3.13: Calculation of the Imaginary Part of the overall Effective OKE $\chi^{(3)}$ of Au-VO_2 Thin-Film below 68 ^{0}C using the Model of Ricard et al. [4]. The size of the nanogold particles is within the range 50Å-500Å.

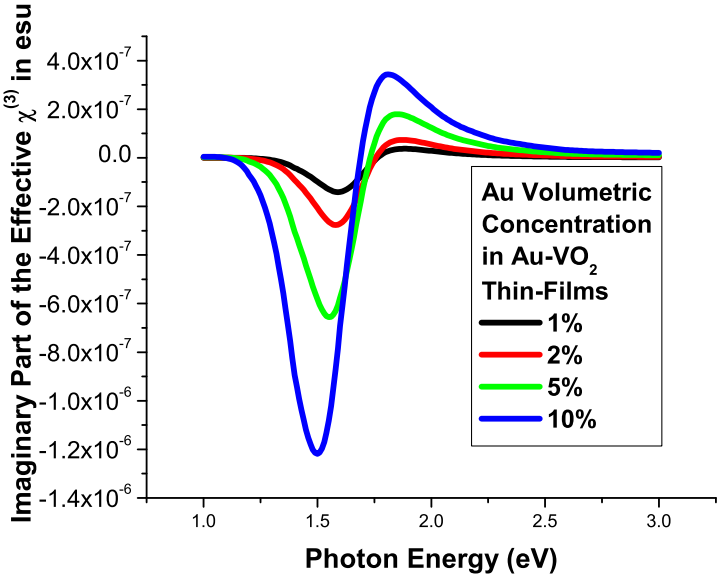

Figure 3.14: Calculation of the Imaginary Part of the overall Effective OKE $\chi^{(3)}$ of Au-VO_2 Thin-Film below 68 ^{0}C using the Model of Sipe and Boyd [2]. The size of the nanogold particles is within the range 50Å-500Å.

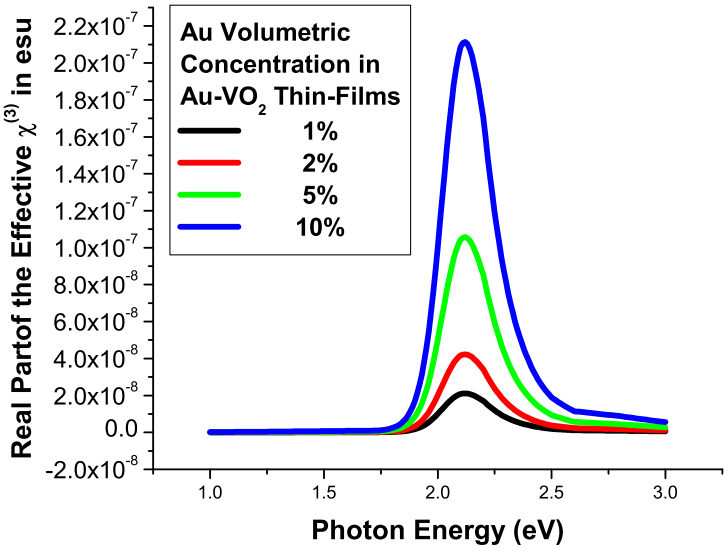

Figure 3.15: Calculation of the Real Part of the overall Effective OKE $\chi^{(3)}$ of Au-VO_2 Thin-Film above 68 ^{0}C using the Model of Ricard et al. [4]. The size of the nanogold particles is within the range 50Å-500Å.

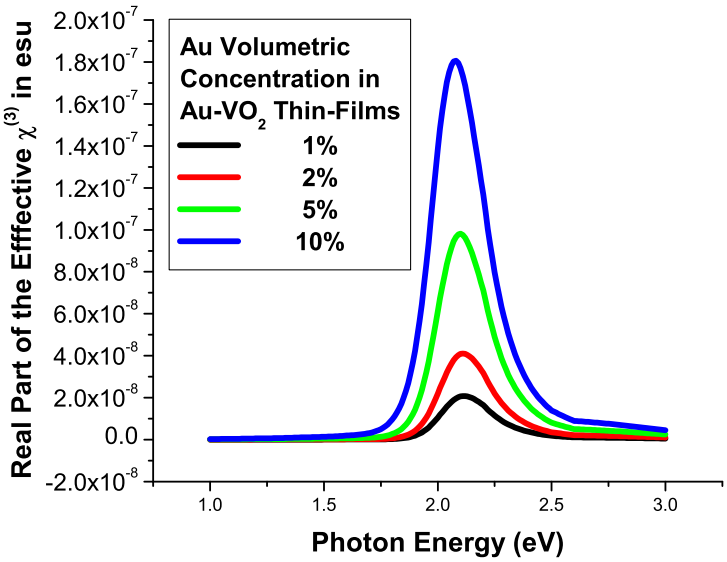

Figure 3.16: Calculation of the Real Part of the overall Effective OKE $\chi^{(3)}$ of Au-VO_2 Thin-Film above 68 ^{0}C using the Model of Sipe and Boyd [2]. The size of the nanogold particles is within the range 50Å-500Å.

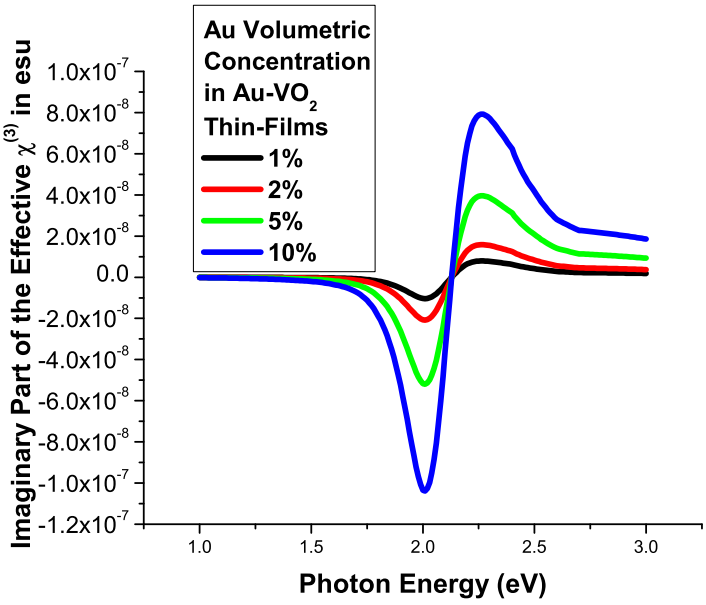

Figure 3.17: Calculation of the Imaginary Part of the overall Effective OKE $\chi^{(3)}$ of Au-VO_2 Thin-Film above 68 ^{0}C using the Model of Ricard et al. [4]. The size of the nanogold particles is within the range 50Å-500Å.

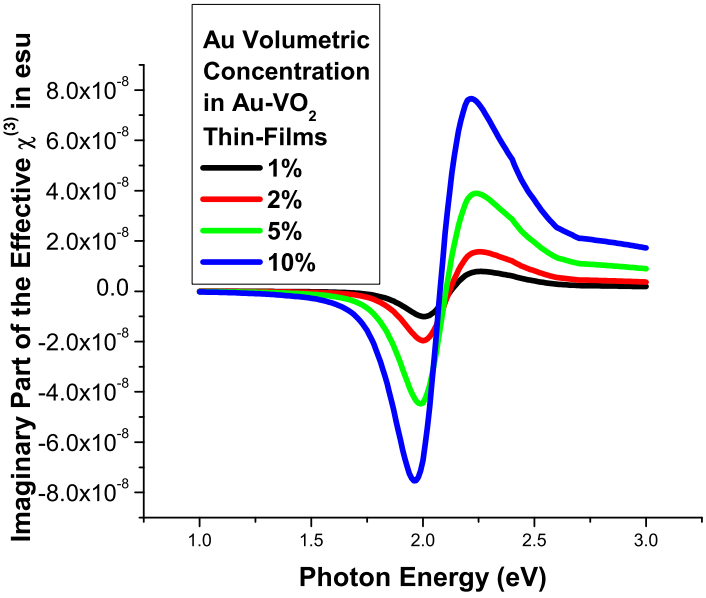

Figure 3.18: Calculation of the Imaginary Part of the overall Effective OKE $\chi^{(3)}$ of Au-VO_2 Thin-Film above 68 ^{0}C using the Model of Sipe and Boyd [2]. The size of the nanogold particles is within the range 50Å-500Å.

3.3.4 Conclusion

The main feature of the model calculations of the real and imaginary parts of the effective nonlinear susceptibilities is their monotonically increasing magnitudes as the gold volumetric concentration increases. This follows from the fact that the gold is responsible for the optical nonlinearity.

It should be noted that the value of the overall effective OKE nonlinear susceptibilities is of the order of 10^{-6} esu when the Au-VO_2 thin-films is below 68 ^{0}C. To our knowledge such a high value has been observed in composite with high Au concentration in the range $.05 - .60$ [29, 33]. The Au concentration of our composites is at most 10 percent. The value of the real and imaginary part of the overall effective nonlinear susceptibilities is of the order of 10^{-7} esu when the Au-VO_2 thin-films is above T_t.

Our computed results of the effective third-order nonlinear susceptibility of Au-VO_2 nanocomposite are in some respect similar to those of L. Banyai et al. [30]. Although the main feature of theirs is the fact that their nanocomposite consists of semiconductor inclusions embedded in a glass matrix, whereas in this work the nanocomposite is formed of metallic inclusions embedded into either a metallic matrix (VO_2 above 68 ^{0}C) or a semiconductor matrix (VO_2 below 68 ^{0}C).

Chapter 4

Modelling of High-Order Harmonic Generation in Strongly Absorbing Media

4.1 Introduction

When an intense optical field propagates through a medium, it induces a polarization, which is the origin of several kinds of phenomena. Firstly, it accounts for the change of the optical properties of the material which depend on the input light intensity, for example the OKE [1, 9, 10]. Secondly, it describes the interaction among different waves or between waves and the medium, this is known as frequency mixing [1, 2, 9, 34, 35], for example high-order harmonic generation from which third-harmonic generation is a particular case.

High-order harmonic generation is analysed quantitatively by means of the *susceptibility tensor formalism* [1] in the following way: The induced polarization in the medium which depends on the electrical field of the incident light is written as [1, 3, 5, 8]:

$$\begin{aligned} P(\omega) &= \epsilon_0\chi^{(1)}(-\omega;\omega)E(\omega) + \epsilon_0\chi^{(2)}(-2\omega;\omega,\omega)E(\omega)E(\omega) \\ &+ \epsilon_0\chi^{(3)}(-3\omega;\omega,\omega,\omega)E(\omega)E(\omega)E(\omega) + \dots \end{aligned}$$

where
$P(\omega)$ is the induced polarization of the medium.
$E(\omega)$ is the incident electrical field.
$\chi^{(1)}(-\omega;\omega)$, $\chi^{(2)}(-2\omega;\omega,\omega)$ and $\chi^{(3)}(-3\omega;\omega,\omega,\omega)$,... are the fundamental, the second-, third- and higher -order harmonic susceptibility tensors.

High-order harmonic generation is a very active area of research due to its use in nonlinear optical (NLO) devices such as frequency up-conversion of some nonlinear optical crystals [23], near-UV emitters, ultra-fast UV light modulators

[36] to name a few applications.

The possibility of generating strong vacuum UV (VUV) and x-ray radiation has been one of the main reason for investigating SHG [23]. THG aims at producing coherent VIS radiation from laser source emitting in NIR range and VUV radiation from VIS and UV lasers [1].

Until recently SHG in opaque crystals was not investigated [23]. THG on the other hand has been investigated in vapors and gases for generating VUV radiation using visible and UV lasers [1]. This section addresses high-order harmonic generation in opaque media. It is assumed that the input pump beam suffers attenuation due to absorption only. This is justified because the amount of energy transferred into the harmonic is very much less than that absorbed.

4.2 The Slowly Varying Envelope Approximation

Consider the wave equation for the electric field $\mathbf{E}_\omega$ propagating in a given medium.

$$\nabla \times \nabla \times \mathbf{E}(\omega) = \frac{\omega^2}{\mathrm{c}^2}\mathbf{E}(\omega) + \omega^2 \mu_0 \mathbf{P}(\omega), \tag{4.1}$$

where
ω is the frequency,
μ_0 is the permeability,
c is the velocity of light in vacuum,
$\mathbf{E}(\omega)$ is the electric field of the fundamental wave,
$\mathbf{P}(\omega)$ is the induced polarization in the medium due to $\mathbf{E}(\omega)$.

The functions $\mathbf{E}$ and $\mathbf{P}$ are both dependent on ω and the spatial coordinates $\mathbf{r}$ although they are written as $\mathbf{E}(\omega)$ and $\mathbf{P}(\omega)$ for convenience [1].

Consider next the induced polarization $\mathbf{P}(\omega)$ which is written as the sum of the linear and the remaining nonlinear terms:

$$\mathbf{P}(\omega) = \epsilon_0 \underline{\chi}^{(1)}(-\omega;\omega).\mathbf{E}(\omega) + \mathbf{P}^{\mathrm{NL}}(\omega), \tag{4.2}$$

where

$$\mathbf{P}^{\mathrm{NL}}(\omega) = \epsilon_{\mathbf{0}} \underline{\chi}^{(\mathrm{n})}(-\mathrm{n}\omega;\omega,\omega,\ldots,\omega).\mathbf{E}(\omega)\mathbf{E}(\omega)\ldots\mathbf{E}(\omega) \quad \text{for} \quad \mathrm{n} \geq 2 \tag{4.3}$$

One may substitute Eq. (4.2) into Eq. (4.1) to get Eq. (4.4) for $n = 2, 3, \ldots$

$$\nabla \times \nabla \times \mathbf{E}(\omega) = \frac{\omega^2}{\mathrm{c}^2}\epsilon(\omega)\mathbf{E}(\omega) + \omega^2 \mu_0 \mathbf{P}^{\mathrm{NL}}(\omega). \tag{4.4}$$

Eq. (4.4) may be rewritten by introducing the envelope function $\mathcal{E}$ (ω). It is a complex quantity which consists of both the amplitude and the phase of the wave as pointed out by P. N. Butcher and D. Cotter [1]. Moreover, it is a function of all the three spatial coordinates through its dependence on $\mathbf{k}.\mathbf{r}$.

Hence Eq. (4.4) becomes [1]

$$\nabla \times \nabla \times [\mathcal{E}(\omega)\exp(\mathrm{i}\mathbf{k}.\mathbf{r})] = \frac{\omega^2}{\mathrm{c}^2}\epsilon(\omega)\mathcal{E}(\omega)\exp(\mathrm{i}\mathbf{k}.\mathbf{r}) + \omega^2\mu_0\mathcal{P}^{\mathrm{NL}}(\omega). \tag{4.5}$$

In the plane wave approximation, the components of $\mathcal{E}(\omega)$ in Eq. (4.5) are wave propagating collinearly in some direction $\mathbf{z}$. It follows that $\mathcal{E}(\omega)$ is a function of $\mathbf{z}$ only and $\mathbf{k}.\mathbf{r} = \pm\mathrm{k.z}$ where $+$ indicates the direction of the forward travelling waves in the z direction and the $-$ for the backward one.

Therefore, $\nabla \times \nabla \times \mathcal{E}(\omega)$ may be replaced by $-\frac{\partial^2\mathcal{E}(\omega)}{\partial z^2}$ and Eq. (4.5) becomes

$$-\frac{\partial^2}{\partial z^2}[\mathcal{E}(\omega)\exp(\mathrm{ikz})] = \frac{\omega^2}{\mathrm{c}^2}\epsilon(\omega)\mathcal{E}(\omega)\exp(\mathrm{ikz}) + \omega^2\mu_0\mathcal{P}^{\mathrm{NL}}(\omega). \tag{4.6}$$

If the wave envelope $\mathcal{E}(\omega)$ varies slowly with the distance z we have

$$|\frac{\partial^2\mathcal{E}(\omega)}{\partial z^2}| \ll |k\frac{\partial\mathcal{E}(\omega)}{\partial z}|. \tag{4.7}$$

This is the *slowly varying envelope approximation* (SVEA) [1, 9, 34, 35].

Given that

$$\begin{aligned}\frac{\partial^2}{\partial z^2}[\mathcal{E}(\omega)\exp(\mathrm{ikz})] &= -2ik\frac{\partial\mathcal{E}(\omega)}{\partial z}\exp(ikz) + k^2\mathcal{E}(\omega)\exp(\mathrm{ikz}) \\ &\quad + \frac{\partial^2\mathcal{E}(\omega)}{\partial z^2}\exp(\mathrm{ikz}),\end{aligned} \tag{4.8}$$

it follows from the SVEA that

$$\frac{\partial^2}{\partial z^2}[\mathcal{E}(\omega)\exp(\mathrm{ikz})] \approx -2\mathrm{ik}\frac{\partial\mathcal{E}(\omega)}{\partial\mathrm{z}}\exp(\mathrm{ikz}) + \mathrm{k}^2\mathcal{E}(\omega)\exp(\mathrm{ikz}). \tag{4.9}$$

Therefore Eq. (4.6) reduces to

$$\begin{aligned} -2ik\frac{\partial\mathcal{E}(\omega)}{\partial z}\exp(ikz) + k^2\mathcal{E}(\omega)\exp(\mathrm{ikz}) &= \frac{\omega^2}{c^2}\epsilon(\omega)\mathcal{E}(\omega)\exp(\mathrm{ikz}) \\ &+ \omega^2\mu_0\mathcal{P}^{\mathrm{NL}}(\omega). \end{aligned} \tag{4.10}$$

Substituting $k^2 = \frac{\omega^2}{c^2}n^2$ and $\epsilon(\omega) \simeq n(n + i2\kappa)$ in Eq. (4.10) leads to the following ordinary differential equation [1, 9] in SI units

$$\frac{\partial\mathcal{E}(\omega)}{\partial z} = -\frac{\omega}{c}\kappa\mathcal{E}(\omega) + i\frac{\omega^2\mu_0}{2\kappa}\mathcal{P}(\omega)\exp(ikz). \tag{4.11}$$

Alternatively, in esu units Eq. (4.11) is rewritten as:

$$\frac{\partial\mathcal{E}(\omega)}{\partial z} = -\frac{4\pi\omega}{c}\kappa\mathcal{E}(\omega) + i\frac{2\pi\omega^2\mu_0}{\kappa c^2}\mathcal{P}(\omega)\exp(ikz). \tag{4.12}$$

Eq. (4.11) and (4.12) describe the propagation of the waves envelopes of both the fundamental and nth order harmonic waves in an absorbing media whereas Eq. (4.13) and (4.14) describe the propagation of the waves envelopes of both the fundamental and nth order harmonic waves in an nonabsorbing media. It is easy to see that in a lossless medium Eq. (4.13) agrees with the result of P. N. Butcher and D. Cotter [1] in SI units:

$$\frac{\partial\mathcal{E}(\omega)}{\partial z} = i\frac{\omega^2\mu_0}{2\kappa}\mathcal{P}(\omega)\exp(ikz). \tag{4.13}$$

In a similar way in a lossless medium Eq. (4.11) reduces to the same equation obtained by Y. R. Shen [35] in esu:

$$\frac{\partial\mathcal{E}(\omega)}{\partial z} = i\frac{2\pi\omega^2}{\kappa c^2}\mathcal{P}(\omega)\exp(ikz). \tag{4.14}$$

Eq. (4.12) essentially differs from Eq. (4.14) in the sense that it accounts for the absorption of the fundamental wave as a consequence of pump attenuation due to absorption only. There is no pump depletion due to the transfer energy to the harmonics in either of these two equations.

To analyse this absorption one needs to solve the ODE that describes the absorption of the fundamental wave.

$$\frac{\partial \mathcal{E}(\omega)}{\partial z} = -\frac{\omega}{c}\kappa \mathcal{E}(\omega).$$

Its solution is:

$$\mathcal{E}_\omega(\omega) = \mathcal{E}_\omega(0)\exp(-\frac{\alpha_\omega z}{2}); \tag{4.15}$$

where
z is the direction of the wave propagation,
α_ω is the absorption coefficient of the fundamental field,
$\alpha_\omega = -\frac{2\omega}{c}\kappa_\omega$ in SI units and $\alpha_\omega = -\frac{4\pi\omega}{2c}\kappa_\omega$ in esu.

On the assumption that for each frequency other than the fundamental one there is no pump attenuation or pump enhancement; it follows that for a particular frequency ω_σ, Eq. (4.13) may be written as [1]

$$\frac{\partial \mathcal{E}_{\omega_\sigma}}{\partial z} = i\frac{\omega_\sigma^2}{2k_P c^2}\chi^{(n)}\mathcal{E}_1 \ldots \mathcal{E}_n \exp(i\Delta k z) \tag{4.16}$$

with

$$\begin{aligned}
\Delta k &= k_P - k_\sigma, \\
k_P &= k_1 + k_2 + \ldots + k_n, \\
k_n &= \frac{n\omega n_\omega}{c}, \\
\mathcal{E}_i &= \mathcal{E}_i(0)\exp(-\frac{\alpha_\omega z}{2}) \quad \text{with} \quad \text{i} = 1, \ldots, \text{n}.
\end{aligned}$$

Recall that α_ω is the absorption coefficient of the fundamental field.

In the case of high-order harmonic generation for which $\mathcal{E}_i = \mathcal{E}_\omega(0)\exp(-\frac{\alpha_\omega z}{2})$ holds Eq. (4.16) becomes:

$$\frac{\partial \mathcal{E}_{n\omega}}{\partial z} = i\frac{n\omega}{2n_{n\omega}c^2}\chi^{(n)}[\mathcal{E}_1(0)]^n \exp(-\frac{n\alpha_\omega z}{2})\exp(i\Delta k z). \tag{4.17}$$

In an highly absorptive medium one can expect the high-harmonic wave to suffer some loss as the fundamental does (see Eq. (4.15)). Therefore by taking into account absorption Eq. (4.17) may written in SI units as:

$$\frac{\partial \mathcal{E}_{n\omega}}{\partial z} = i\frac{n\omega}{2n_{n\omega}c^2}\chi^{(n)}[\mathcal{E}_1(0)]^n \exp(-\frac{n\alpha_{\omega z}}{2})\exp(i\Delta kz) - \frac{n\omega\kappa_{n\omega}}{c}\mathcal{E}_{n\omega}. \quad (4.18)$$

Alternatively, in esu for which we have $4\pi\kappa$ rather than κ as in SI units Eq. (4.18) may be written as

$$\frac{\partial \mathcal{E}_{n\omega}}{\partial z} = i\frac{2\pi n\omega}{n_{n\omega}c^2}\chi^{(n)}[\mathcal{E}_1(0)]^n \exp(-\frac{n\alpha_{\omega z}}{2})\exp(i\Delta kz) - \frac{4\pi n\omega\kappa_{n\omega}}{c}\mathcal{E}_{n\omega}. \quad (4.19)$$

Eq. (4.18) and (4.19) are both ODE's that can be solved by means of the integrating factor (IF) method. They represent the main results of this section.

Their respective solutions in SI units and esu are Eq. (4.20) and (4.21):

$$\begin{aligned} I^{SI}_{n\omega}(L) &= \frac{(n\omega)^2|\chi^{(n)}|^2 I^n_\omega}{2^{n+1}\epsilon_0^{n-1}c^{n+1}n^n_\omega n_{n\omega}}\frac{[\exp(-n\alpha_\omega L/2)-\exp(-\alpha_{n\omega}L/2)]^2}{\Delta k^2+(-n\alpha_\omega/2+\alpha_{n\omega}/2)^2} \\ &+ \frac{(n\omega)^2|\chi^{(n)}|^2 I^n_\omega L^2}{2^{n+1}\epsilon_0^{n-1}c^{n+1}n^n_\omega n_{n\omega}}\frac{\exp[-(n\alpha_\omega+\alpha_{n\omega})L/2]}{1+[(-n\alpha_\omega+\alpha_{n\omega})/2\Delta k^2]^2}\mathrm{sinc}^2(\Delta \mathrm{kL}/2), \end{aligned} \quad (4.20)$$

$$\begin{aligned} I^{esu}_{n\omega}(L) &= \frac{(2\pi)^{n+1}(n\omega)^2|\chi^{(n)}|^2 I^n_\omega}{c^{n+1}n^n_\omega n_{n\omega}}\frac{[\exp(-n\alpha_\omega L/2)-\exp(-\alpha_{n\omega}L/2)]^2}{\Delta k^2+(-n\alpha_\omega/2+\alpha_{n\omega}/2)^2} \\ &+ \frac{(2\pi)^{n+1}(n\omega)^2|\chi^{(n)}|^2 I^n_\omega L^2}{c^{n+1}n^n_\omega n_{n\omega}}\frac{\exp[-(n\alpha_\omega+\alpha_{n\omega})L/2]}{1+[(-n\alpha_\omega+\alpha_{n\omega})/2\Delta k^2]^2}\mathrm{sinc}^2(\Delta \mathrm{kL}/2). \end{aligned} \quad (4.21)$$

These equations represent the high-order harmonic intensity output $I_{n\omega}$ in an absorbing media given a fundamental intensity input I_ω which suffers pump attenuation only.

4.3 Special Cases of Eq. (4.20) and (4.21).

In the case of SHG in a lossless medium. i.e $n = 2$, $\alpha_\omega = \alpha_{2\omega} = 0$, it is easy to see that Eq. (4.20) becomes Eq. (4.22) which is in agrement with the result of

P. N. Butcher and D. Cotter [1]:

$$I_{2\omega} = \frac{(2\omega)^2|\chi^{(2)}|^2}{8\epsilon_0^2 c^3 n_\omega^2 n_{2\omega}} I_\omega^2 L^2 \mathrm{sinc}^2(\Delta \mathrm{kL}/2). \tag{4.22}$$

In a similar way in a lossless medium if the second-order susceptibility is $\chi^{(2)}$, Eq. (4.21) becomes (4.23) which is the same as that obtained by Y. R. Shen [35]

$$I_{2\omega} = \frac{32\omega^2|\chi^{(2)}|^2}{c^3 n_\omega^2 n_{2\omega}} I_\omega^2 L^2 \mathrm{sinc}^2(\Delta \mathrm{kL}/2). \tag{4.23}$$

In the case where the phase-matching condition is satisfied i.e $\Delta k = 0$ and for which there is absorption Eq. (4.21) becomes Eq. (4.24) which was obtained by T-J.Chen et al. [23]

$$I_{2\omega}(L) = \frac{32\pi^2\omega^2|\chi^{(2)}|^2 I_\omega^2}{c^3 n_\omega^2 n_{2\omega}} \frac{[\exp(-2\alpha_\omega L/2) - \exp(-\alpha_{2\omega} L/2)]^2}{(-2\alpha_\omega/2 + \alpha_{2\omega}/2)^2}. \tag{4.24}$$

If one considers THG in the case of a lossless medium. i.e $n = 3$, $\alpha_\omega = \alpha_{3\omega} = 0$. We get Eq. (4.25) in the SI units which corresponds to the same result as that obtained by P. N. Butcher and D. Cotter [1]:

$$I_{3\omega} = \frac{9\omega^2|\chi^{(3)}|^2}{16\epsilon_0^2 c^4 n_\omega^3 n_{3\omega}} I_\omega^3 L^2 \mathrm{sinc}^2(\Delta \mathrm{kL}/2). \tag{4.25}$$

For a tight, focused beam Eq. (4.25) may written in esu as Eq. (4.26) in terms of the third-harmonic power by letting $P_\omega = \frac{I_\omega}{\sigma}$ and $P_{3\omega} = \frac{I_{3\omega}}{\sigma}$, where $\sigma \approx \pi^2\omega^2$ is the cross-section of the laser beam, P_ω and $P_{3\omega}$ are the fundamental and third-harmonic power respectively. Therefore [34, 36],

$$P_{3\omega} = \frac{2304\pi^6|\chi^{(3)}|^2}{n_\omega^3 n_{3\omega}\lambda^4 c^2} P_\omega^3 L^2 \mathrm{sinc}^2(\Delta \mathrm{kL}/2). \tag{4.26}$$

4.4 Transmission Configuration

The transmission configuration consists of an input beam that illuminates the surface at $z = 0$ to produce a higher harmonic wave. The output beam is monitored at $z = L$ and $\mathcal{E}$ travels in the forward (+) direction. See Fig. (4.1).

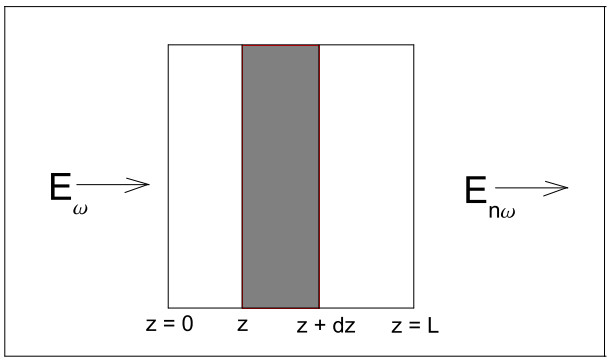

Figure 4.1: Transmission Configuration. Adapted from T-J. Chen et al. [23]

If one considers the case in which there is a very strong absorption i.e $(n\alpha_\omega/2 - \alpha_{n\omega}/2)L \gg \Delta kL$. It follows that Eq. (4.20) reduces to:

$$I_{n\omega}(L) = \frac{(n\omega)^2|\chi^{(n)}|^2 I_\omega^n}{2^{n+1}\epsilon_0^{n-1}c^{n+1}n_\omega^n n_{n\omega}} \frac{[\exp(-n\alpha_\omega L/2) - \exp(-\alpha_{n\omega}L/2)]^2}{(-n\alpha_\omega/2 + \alpha_{n\omega}/2)^2}. \tag{4.27}$$

Let L_c be the length at which $I_{n\omega}$ reaches its maximum $I_{n\omega}^{max}$
To find L_c for Eq. (4.27) we demand that $\frac{\partial I_{n\omega}(L)}{\partial L}|_{L_c} = 0$. It follows that:

$$L_c = \frac{\ln(n\alpha_\omega/\alpha_{n\omega})}{[(n\alpha_\omega - \alpha_{n\omega})/2]}, \tag{4.28}$$

$$I_{n\omega}^{max}(L) = \frac{(n\omega)^2|\chi^{(n)}|^2 I_\omega^n}{2^{n+1}\epsilon_0^{n-1}c^{n+1}n_\omega^n n_{n\omega}} \frac{\exp(-\alpha_{n\omega}L_c)}{(n\alpha_\omega/2)^2}. \tag{4.29}$$

Note that I_ω is raised to the power n.

In the case of Au-VO_2 nanocomposite the optimized characteristic length for different volumetric concentration of Au ranges from 60 to 100Å.

In a strongly absorbing medium Eq. (4.28) and (4.29) reduce in SI and esu respectively to:

$$L_c = 2/n\alpha_\omega, \tag{4.30}$$

$$I_{n\omega}^{max}(L) = \frac{(n\omega)^2|\chi^{(n)}|^2 I_\omega^n}{2^{n+1}\epsilon_0^{n-1}c^{n+1}n_\omega^n n_{n\omega}} \frac{\exp(-2)}{(n\alpha_\omega/2)^2},$$

$$I_{n\omega}^{max}(L) = \frac{(2\pi)^{n+3}n^2|\chi^{(n)}|^2 I_\omega^n}{c^{n+1}n_\omega^n n_{n\omega}\lambda_\omega} \frac{\exp(-2)}{(n\alpha_\omega/2)^2}. \tag{4.31}$$

In the special case for which $k_i \sim 1 (i = 1, 2)$ and $\alpha_\omega \sim \alpha_{2\omega}/2$. Eq. (4.31) leads to the same result as that obtained by T-J. Chen et al. [23].

It can be demonstrated that although the phase-matching condition is crucial for conventional high-order harmonic generation [1, 9, 10, 34-36], this is not the case for thin-films. To see that we consider the strong absorption case for which the phase matching condition fails. Eq. (4.20) and (4.21) reduce to:

$$I'_{n\omega}(L) = \frac{(n\omega)^2 |\chi^{(n)}|^2 I_\omega^n}{2^{n+1}\epsilon_0^{n-1} c^{n+1} n_\omega^n n_{n\omega}} \exp(-n\alpha_\omega L) \quad \mathrm{sinc}^2(\Delta \mathrm{kL}/2), \tag{4.32}$$

$$I'_{n\omega}(L) = \frac{(2\pi)^{n+1}(n\omega)^2 |\chi^{(n)}|^2 I_\omega^n}{c^{n+1} n_\omega^n n_{n\omega}} \exp(-n\alpha_\omega L) \quad \mathrm{sinc}^2(\Delta \mathrm{kL}/2). \tag{4.33}$$

$I'_{n\omega}(L)$ represents the high-order harmonic intensity output in the case which the phase matching is not satisfied $\Delta k \neq 0$. It reaches its maximum when $\frac{\partial L'_{n\omega}}{\partial I'_{n\omega}}|_{L'_c} = 0$.

It follows that in SI units and esu:

$$L'_c = \frac{2\lambda_\omega}{n(n_\omega - n_{n\omega})} \tan^{-1}[(n_\omega - n_{n\omega})/\lambda_\omega \alpha_\omega], \tag{4.34}$$

$$I'^{max}_{n\omega}(L) = \frac{(n\omega)^2 |\chi^{(n)}|^2 I_\omega^n}{2^{n+1}\epsilon_0^{n-1} c^{n+1} n_\omega^n n_{n\omega}} \frac{\lambda_\omega^2}{n^2[\alpha_\omega^2 \lambda_\omega^2 + (n_\omega - n_{n\omega})^2]} \exp(-n\alpha_\omega L'_c), \tag{4.35}$$

$$L'_c = \frac{\lambda_\omega}{\pi n(n_\omega - n_{n\omega})} \tan^{-1}[(n_\omega - n_{n\omega})/\lambda_\omega \alpha_\omega], \tag{4.36}$$

$$I'^{max}_{n\omega}(L) = \frac{(2\pi)^{n+1}(n\omega)^2 |\chi^{(n)}|^2 I_\omega^n}{c^{n+1} n_\omega^n n_{n\omega}} \frac{\lambda_\omega^2}{n^2[\alpha_\omega^2 \lambda_\omega^2 + 4\pi^2 (n_\omega - n_{n\omega})^2]} \exp(-n\alpha_\omega L'_c). \tag{4.37}$$

It is easy to show that phase-matching has little effect on the high-order harmonic intensity output, $I_{n\omega}$, in the case of thin-film. This is proved by Eq. (4.38) which compares $I'^{max}_{n\omega}(L)$ which represents the high-order harmonic intensity output from a strongly absorbing thin-film ($L \ll \lambda$) in the case of phase mismatch i.e $\Delta k \neq 0$ and $I^{max}_{n\omega}(L)$ which is the high-order harmonic intensity output from a strongly absorbing thin-film in the case of perfect phase matching condition i.e $\Delta k = 0$ in SI units and esu:

$$\frac{I'^{max}_{n\omega}(L)}{I^{max}_{n\omega}(L)} = \frac{1}{1 + (n_\omega - n_{n\omega})^2/4} \exp \frac{(2 - 4\tan^{-1}[(n_\omega - n_{n\omega})/2])}{(n_\omega - n_{n\omega})}. \tag{4.38}$$

This result agrees with that of T-J. Chen et al. [23]. In the case $n_\omega - n_{n\omega} = 0.5$. It follows that $I'^{max}_{n\omega}(L) \approx 0.979 \times I^{max}_{n\omega}(L)$. This shows that phase-matching has little effect on the output beam if the medium is a thin-film [23].

During a high-order harmonic generation process only a fraction of initial fundamental light converts into the high-order harmonic radiation [1, 9, 10, 34, 35].

This is expressed trough the so-called conversion coefficient defined as $\eta = I^{max}_{n\omega}/I_\omega$. It follows that:

$$\eta_{SI} = \frac{(n\omega)^2|\chi^{(n)}|^2 I_\omega^{n-1}}{2^{n+1}\epsilon_0^{n-1}c^{n+1}n_\omega^n n_{n\omega}} \frac{\exp(-2)}{(n\alpha_\omega/2)^2}, \tag{4.39}$$

$$\eta_{esu} = \frac{(2\pi)^{n+1}(n\omega)^2|\chi^{(n)}|^2 I_\omega^{n-1}}{c^{n+1}n_\omega^n n_{n\omega}} \frac{\exp(-2)}{(n\alpha_\omega/2)^2}. \tag{4.40}$$

4.5 Reflection Configuration

In the reflection configuration the incident beam (fundamental wave) and the higher harmonic wave propagate in opposite direction. They are both monitored at the surface $z = 0$ as shown in Fig. 4.3.

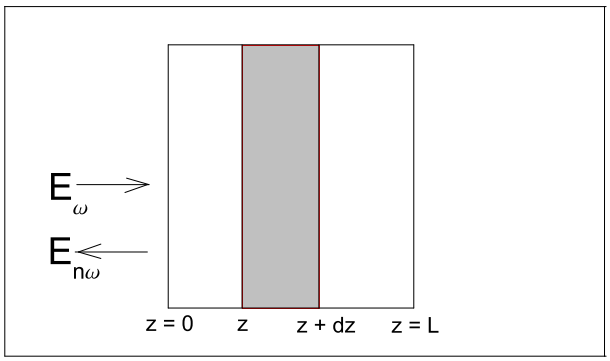

Figure 4.2: Reflection Configuration. Adapted from T-J. Chen et al. [23]

In the slowly varying envelope approximation the reflection configuration corresponds to the case for which the envelope function $\mathcal{E}$ travels in the backward

(−) direction.

High-order harmonic generation in the reflection configuration is analysed as follows:

First, consider the envelope of the fundamental harmonic wave propagating in the transmission configuration in an absorbing media according to the following equation:

$$\frac{d\mathcal{E}(\omega)}{dz} = -\frac{\alpha_\omega}{2}\mathcal{E}(\omega) \quad \text{where} \quad \alpha_\omega = \frac{2\omega}{\mathrm{c}}\kappa.$$

Next, consider the envelope of the high-order harmonic wave propagating in the transmission configuration in an absorbing media according to Eq. (4.16) [1]:

$$\frac{\partial\mathcal{E}_{\omega_\sigma}}{\partial z} = i\frac{\omega_\sigma^2}{2k_P c^2}\chi^{(n)}\mathcal{E}_1 \ldots \mathcal{E}_n \exp(i\Delta k z).$$

For the sake of simplicity we let $A = i\frac{\omega_\sigma^2}{2\kappa_P c^2}\chi^{(n)}\mathcal{E}_1 \ldots \mathcal{E}_n$, therefore the above equation may be written as:

$$d\mathcal{E}_{\omega_\sigma} = A\exp(i\Delta k z)dz. \tag{4.41}$$

Note that one may replace the partial derivative by the full derivative since we aim at analysing the propagation in the z-direction only.

Now, suppose that the high-order harmonic wave envelope is reflected. To describe its differential change one needs to take into account the loss that its amplitude suffers only and not its phase change. Recall that A represents the amplitude of the envelope of the high-order harmonic wave. Therefore, the loss suffered during the reflection by this amplitude may be described in a similar fashion to the loss suffered by the envelope of the fundamental wave ($\frac{d\mathcal{E}(\omega)}{dz} = -\frac{\alpha_\omega}{2}\mathcal{E}(\omega)$). Hence the loss suffered by the amplitude of the envelope of the high-order harmonic wave $A(z)$ is described over the distance z by:

$$\frac{d}{dz}A(z) = -\frac{\alpha_{n\omega}}{2}A(z). \tag{4.42}$$

Eq. (4.42) admits the solution $A(z) = A(0)\exp(-\alpha_\omega z/2)$, where $A(0) = A$ (See Eq. (4.41)). Therefore the differential change of the high-harmonic in the reflection configuration is

$$d\mathcal{E}_{\omega_\sigma} = A(z)\exp(i\Delta k z)dz \tag{4.43}$$

with $A(z) = A(0)\exp(-\alpha_\omega z/2)$ and $\Delta k = nk_\omega + k_{n\omega}$ [1].

It follows that

$$\frac{\partial \mathcal{E}_{\omega_\sigma}}{\partial z} = i\frac{\omega_\sigma^2}{2\kappa_P c^2}\chi^{(n)}\mathcal{E}_1 \ldots \mathcal{E}_n \exp[(-\alpha_\omega/2 + i\Delta k)z], \tag{4.44}$$

with

$$\begin{aligned}
\Delta k &= k_P + k_\sigma, \\
k_P &= k_1 + k_2 + \ldots + k_n, \\
k_n &= \frac{n\omega n_\omega}{c}, \\
\mathcal{E}_i &= \mathcal{E}_i(0)\exp(-\frac{\alpha_\omega z}{2}) \quad \text{with} \quad \text{i} = 1, \ldots, \text{n}.
\end{aligned}$$

Eq. (4.44) admits the solution in Eq. (4.45) in SI and esu units. They represent the main results of this section.

$$I_{n\omega}^r = \frac{(n\omega)^2|\chi^{(n)}|^2 I_\omega^n}{2^{n+1}\epsilon_0^{n-1}c^{n+1}n_\omega^n n_{n\omega}} \frac{\lambda_\omega^2}{[(2\kappa_\omega + n\kappa_{n\omega})^2 + n^2(n_\omega + n_{n\omega})^2]}, \tag{4.45}$$

$$I_{n\omega}^r = \frac{(2\pi)^{n+1}(n\omega)^2|\chi^{(n)}|^2 I_\omega^n}{c^{n+1}n_\omega^n n_{n\omega}} \frac{\lambda_\omega^2}{[(2\kappa_\omega + n\kappa_{n\omega})^2 + n^2(n_\omega + n_{n\omega})^2]}. \tag{4.46}$$

4.6 Conclusion

High-order harmonic generation in a strongly absorbing medium has been analysed by means of the SVEA method [1]. It is assumed that there is pump attenuation only.

According to G. Veres et al. [37] the phenomenon of harmonic generation has been investigated in an opaque medium in the so-called tight focusing limit only. This work investigates high-order harmonic generation in strongly absorbing media by taking into account the pump attenuation only due to the absorptive property of the material.

The general formula that describes the high-order harmonic intensity output from the absorbing medium in the transmission configuration is given in SI units and esu as Eq (4.20) and Eq. (4.21). In the case of SHG in a lossless medium Eq (4.20) reduces to the same result as that obtained by P. N. Butcher and D. Cotter [1] whereas Eq. (4.21) reduces the result of Y. R. Shen [35]. In the case where the phase matching is satisfied $\Delta k = 0$ Eq. (4.21) reduces to the same result as that of T-J. Chen et al. [23]. In the case of THG in a lossless media Eq (4.20) reduces to the same result as that obtained by P. N. Butcher and D. Cotter [1] meanwhile Eq. (4.26) is similar to the result of J. F. Reintjes [34].

It is worth pointing out that although the phase-matching condition is crucial for conventional high-order harmonic generation [1, 9, 10, 34-36] this is not the case for thin-films. In the case of THG in the reflection configuration the phase matching condition simply cannot be satisfied.

In the reflection configuration, the general formula that describes the high-order harmonic intensity output from the absorbing medium is given in SI units and esu by Eq. (4.45) and Eq. (4.46). It is easy to see that in the case of SHG Eq. (4.46) and Eq. (4.47) are similar to the results of T-J. Chen et al. [23].

Chapter 5

Model Calculation of THG and Heat Dissipation in Au-VO_2 Thin-Films

5.1 Model Calculation of THG in Au-VO_2 Thin-Films

5.1.1 Introduction

This chapter presents calculation of the conversion coefficients [23] or conversion efficiencies [34] in the transmission configuration as well as the reflection one for Au-VO_2 nanocomposite. The size of the nanogold particles is within the range 50Å-500Å. Recall that for the Au nanoparticles: THG $\chi^{(3)}_{(intra)} = -i10^{-13}$ esu and the THG $\chi^{(3)}_{(inter)} = -i1.7 \times 10^{-12}$ esu, meanwhile $\chi^{(3)}_{(hot-electron)}$ does not contribute to THG. Therefore, for the Au nanoparticles the overall effective THG $\chi^{(3)}$=THG $\chi^{(3)}_{(intra)}$ + THG $\chi^{(3)}_{(inter)}$=1.8×10^{-12} esu. Note that the Au-VO_2 thin-film thickness is equal to 1000Å.

The conversion efficiency is a measure of harmonic conversion i.e the proportion of waves of fundamental frequency ω that convert into waves of high-order harmonic frequency $n\omega$.

Note that the calculations take into account a pulsed laser source whose peak laser intensity is equal to 7.4×10^5 W/cm^2 and average intensity over on and off periods is equal to 0.45 W/cm^2, given a laser whose pulse energy is 3.4 μJ/cm^2 and the gap between successive pulses duration is 7.5 μs, see page 89. The laser intensity has been chosen in such a way that one may avoid saturation on one hand and the damage of the sample through overheating on the other. This will be elaborated in the next section which is concerned with the heat dissipation in our Au-VO_2 thin-films.

5.1.2 Discussion about η in the Transmission Configuration

The calculations show that η is bigger when the value of the effective THG third-order nonlinear susceptibility $\chi^{(3)}$ is computed using the model of Ricard et al. [6] than that of Sipe and Boyd [2]. The reason for this difference follows from the fact that the local field effect in the former is greater than that in the latter. See Fig. 5.1 and 5.2.

It is also clear that η is greater when computed below T_t rather than above that temperature. See Fig. 5.1 to Fig. 5.4. It is reported to be of the order of 10^{-19} below T_t and 10^{-22} above that temperature.

It should be pointed out that the calculations reported here are performed for the laser light input at its peak intensity. When the laser light input is taken as continous at average intensity, the conversion efficiency is minuscule, with $\eta = 10^{-31}$ for Au-VO_2 thin-films below 68 ^{0}C, it is of the order of 10^{-34} when the thin-films are above 68 ^{0}C. This confirms the fact that it does not make sense to consider the average intensity of the laser for the nonlinear effect which reacts instantaneously on the instant power level of the laser. THG occurs during the high intensity periods of the pulses, and the heat generated is conducted away during the much longer period between the pulses.

5.1.3 Model Calculation of the Conversion Coefficient η of THG in the Transmission Configuration

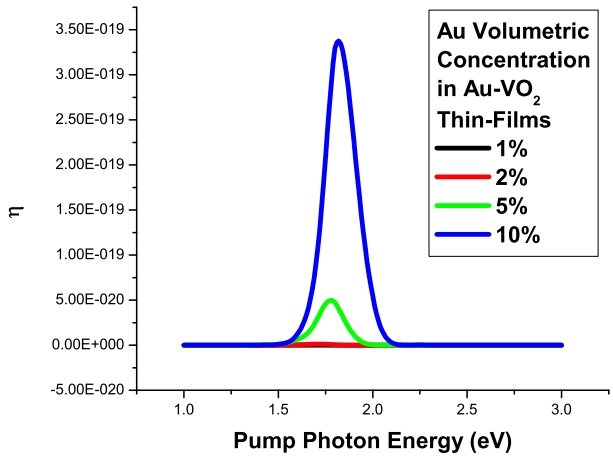

Figure 5.1: Calculation of THG of Au-VO_2 thin-films below 68 ^{0}C in the Transmission Configuration with input laser at peak intensity of 7.4×10^5 Wcm^{-2} using the Model of Ricard et al. [4]. The size of the nanogold particles is within the range 50Å-500Å. The TF thickness is equal to 1000Å.

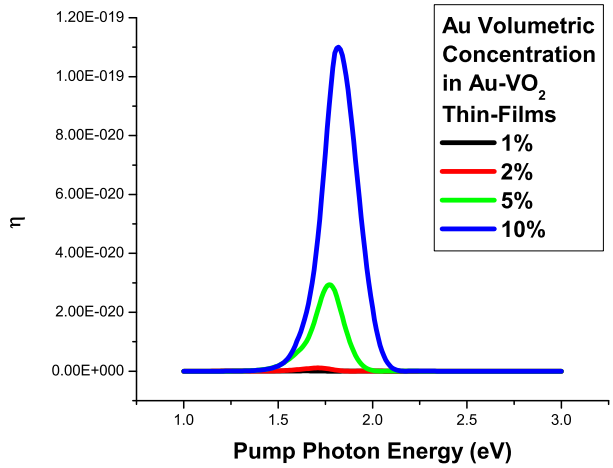

Figure 5.2: Calculation of THG of Au-VO_2 Thin-Films below 68 ^{0}C in the Transmission Configuration with input laser at peak intensity of 7.4×10^5 Wcm^{-2} using the Model of Sipe and Boyd [2]. The size of the nanogold particles is within the range 50Å-500Å. The TF thickness is equal to 1000Å.

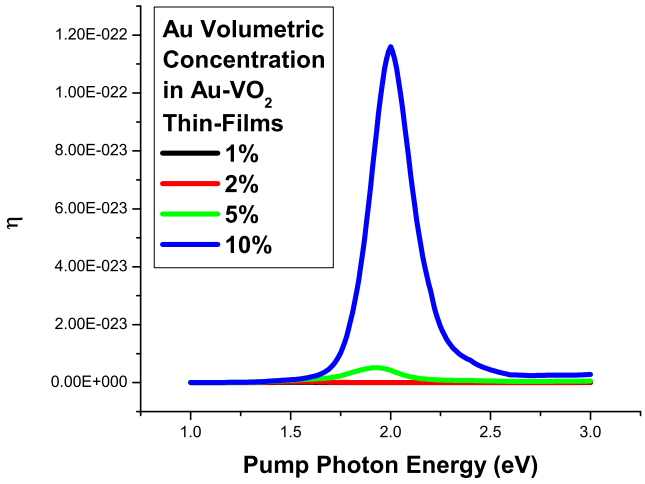

Figure 5.3: Calculation of THG of Au-VO_2 Thin-Films above 68 ^{0}C in the Transmission Configuration with input laser at peak intensity of 7.4 $\times$ 10^5Wcm^{-2} Wcm^{-2} using the Model of Ricard et al. [4]. The size of the nanogold particles is within the range 50Å-500Å. The TF thickness is equal to 1000Å.

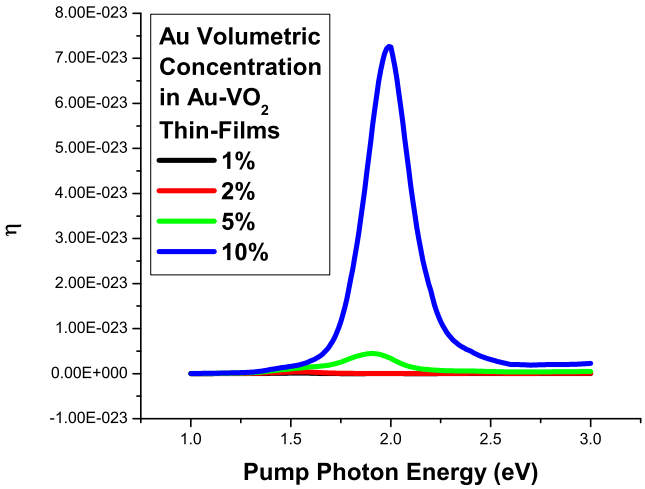

Figure 5.4: Calculation of THG of Au-VO_2 Thin-Films above 68 ^{0}C in the Transmission Configuration with input laser at peak intensity of 7.4$\times$$10^5$ Wcm^{-2} using the Model of Sipe and Boyd [2]. The size of the nanogold particles is within the range 50Å-500Å. The TF thickness is equal to 1000Å.

5.1.4 Discussion about η in the Reflection Configuration

The calculations shows that η is bigger when the value of the effective THG third-order nonlinear susceptibility $\chi^{(3)}$ is computed using the model of Ricard et al. [6] than that of Sipe and Boyd [2]. The reason for this difference follows from the fact that the local field effect in the former is greater than that in the latter. See Fig. 5.5 and 5.6.

It is also clear that η is greater when computed below T_t rather than above that temperature. It is reported to be of the order of 10^{-17} below T_t and 10^{-18} above that temperature. See Fig. 5.5 to Fig. 5.8.

It is worth pointing out that the calculations reported here are performed for the laser light input is at peak intensity of 7.4×10^5 Wcm^{-2}. When the laser light input is at average intensity $\eta = 10^{-29}$ for Au-VO_2 thin-films below 68 ^{0}C, η is negligible, of the order of 10^{-30} when the thin-films are above 68^0 C. As mentioned earlier, this confirms the fact that it does not make sense to consider the average intensity of the laser for the nonlinear effect which reacts instantaneously on the instant power level of the laser.

5.1.5 Model Calculation of the Conversion Coefficient η of THG in the Reflection Configuration

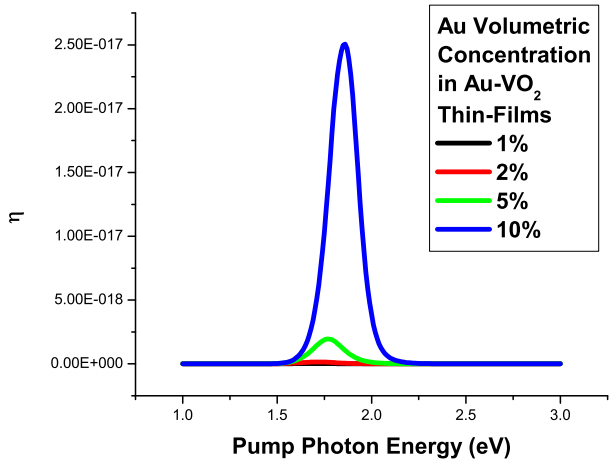

Figure 5.5: Calculation of THG of Au-VO_2 Thin-Films below 68 ^{0}C in the Reflection Configuration with input laser at peak intensity of 7.4×10^5 Wcm^{-2} using the Model of Ricard et al. [4]. The size of the nanogold particles is within the range 50Å-500Å. The TF thickness is equal to 1000Å.

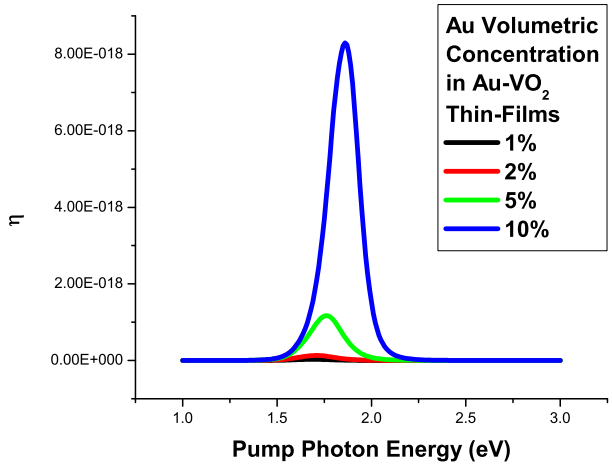

Figure 5.6: Calculation of THG of Au-VO_2 Thin-Films below 68 ^{0}C in the Reflection Configuration with input laser at peak intensity of 7.4×10^5 Wcm^{-2} using the Model of Sipe and Boyd [2]. The size of the nanogold particles is within the range 50Å-500Å. The TF thickness is equal to 1000Å.

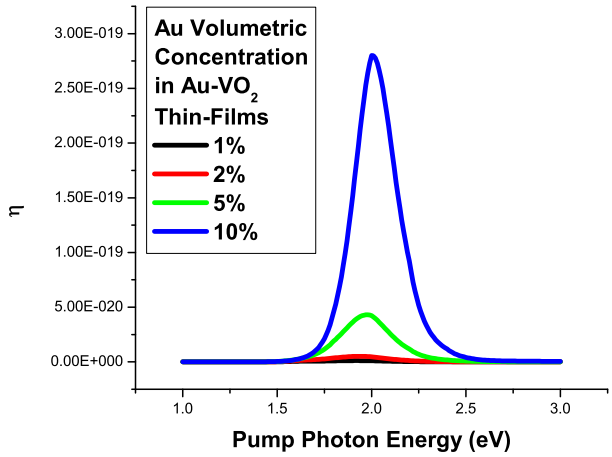

Figure 5.7: Calculation of THG of Au-VO_2 Thin-Films above 68 ^{0}C in the Reflection Configuration with input laser at peak intensity of 7.4×10^5 Wcm^{-2} Wcm^{-2} using the Model of Ricard et al. [4]. The size of the nanogold particles is within the range 50Å-500Å. The TF thickness is equal to 1000Å.

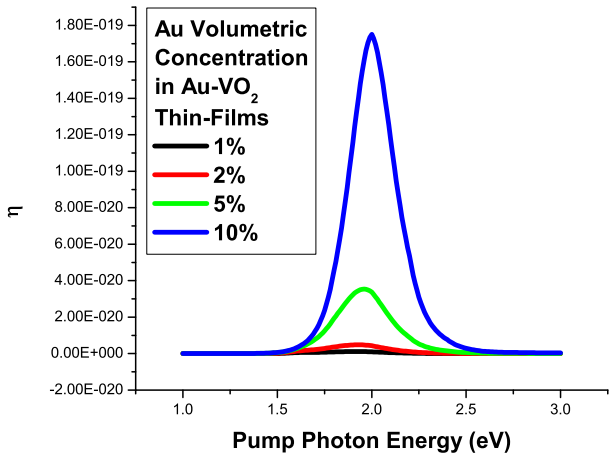

Figure 5.8: Calculation of THG of Au-VO_2 Thin-Films above 68 ^{0}C in the Reflection Configuration with input laser at peak intensity of 7.4×10^5 Wcm^{-2} using the Model of Sipe and Boyd [2]. The size of the nanogold particles is within the range 50Å-500Å. The TF thickness is equal to 1000Å.

5.1.6 Conclusion

The model calculations of the conversion efficiencies of THG in the transmission and reflection configurations allows one to conclude that they are greater in the reflection configuration compared to the transmission one in the photon energy range $1.0 - 3.0$ eV.

The conversion efficiency η is bigger when the value of the effective $\chi^{(3)}$ is computed using the model of Ricard et al. [6] than that of Sipe and Boyd [2]. The reason for this difference follows from the fact that the local field effect in the former is greater than that in the latter. It is also clear that η is greater when computed below T_t rather than above that temperature in the transmission and the reflection configuration. See Fig. 5.1 to 5.8.

It is essential to note that in the transmission configuration the THG light output has an exponential decay factor dependent on the thin-film thickness L see Eq. (4.20) and Eq. (4.21). This indicates that the THG radiation exponentially decreases as L increases, recall that in the transmission configuration $\eta = 10^{-22}$ above 68 ^{0}C and $\eta = 10^{-19}$ below T_t. A higher conversion efficiency will be obtained by using thin-film with optimized coherence length as shown in Fig. 4.2. In the reflection configuration the conversion coefficient does not depend upon the thin-film thickness. Consequently, η does not suffer any loss as L increases, because the THG output does not depend on the thin-film thickness. In the reflection configuration $\eta = 10^{-17}$ below T_t and $\eta = 10^{-18}$ above 68 ^{0}C.

There is negligible THG when the laser light input is taken as continous at average intensity. The whole point in using a pulsed laser is to achieve high intensities, albeit only for short periods, and to avoid excessive heating of the sample because the average intensity is much lower. The reason for this will become apparent in the next section.

5.2 Heat Dissipation in Au-VO_2 Thin-Films

5.2.1 Introduction

Heat generation arises as a consequence of the illumination of a thin-film (TF) by a giant laser pulse [23]. Such temperature rise may damage the thin-film by raising the temperature to the melting point [23] or plasma creation threshold [32].

During a THG process in an absorbing medium, the greatest proportion of the light of fundamental frequency ω does not convert into light of third-order harmonic frequency 3ω. This fraction is expressed quantitatively as (1-η), where η is the fraction of light of fundamental frequency ω converted into light of third-order harmonic frequency 3ω. This proportion of the light may be either completely absorbed by the material if it is strongly absorptive (for example isolants) i.e $\eta \simeq 0$, or partly absorbed if the medium is weakly absorptive i.e $\eta \neq 0$.

The crucial problem is to ensure that the temperature rise of the sample due to the absorption of light may be controlled in some way with a simple cooling system and not be more than 5 ^{0}K. This is required by the fact that if the Au-VO_2 thin-film is below 68 ^{0}C and if the temperature rise is large during the THG process, one will be dealing with a Au-VO_2 thin-film above 68 ^{0}C.

To remove the heat generated, one may deposit the thin-film on a substrate whose heat conductivity is very high. In the transmission configuration the thin-film is deposited on a transparent substrate and in the reflection configuration it is deposited on an opaque material. See Fig. 5.9.

According to J. E. Parrot and A. D. Stuckes [40]: The thermal conductivity of different solids ranges over five orders of magnitude. Crystallines materials generally have much higher thermal conductivity than non-crystallines ones. Consequently, they will always be preferred as heat sinks. Isotopically pure diamond has the highest thermal conductivity around the room temperature, it is reported to be ~ 20 $\mathrm{Wcm^{-1}K^{-1}}$ compared to crystalline silver which is about 4 $\mathrm{Wcm^{-1}K^{-1}}$.

The subsections are organised as follows: Subsection 5.2.2 deals with the problem formulation and discussion of heat dissipation in Au-VO_2 thin-films deposited on a substrate. Section 5.2.3 deals with the calculation of heat dissipation. Finally, Section 5.2.3 is the conclusion.

5.2.2 Problem Formulation and Discussion of heat dissipation in Au-VO_2 thin-films

We consider a pulsed laser which delivers temporarily separated pulses of wavelength 0.7μm, with pulse duration of 5 *ps* and pulse energy of ~ 3.4 μJ per cm^{-2}. Therefore the laser peak intensity is equal to 7.4×10^5 W/cm^2, which we show below does not cause excessive heating. The pulse duration has been chosen to be of the order of picoseconds, because the nonlinear response time of Au nanoparticles is of the order of picoseconds see Table 1.1.

Heat transfer modelling is investigated by means of the heat conduction equation [48] also known as Fourier's equation [48] or Fourier's first law [40]. P. L. Komarov and P. E. Raad [48] have shown that Fourier's equation is applicable in the range of laser heating pulses widths of the order of picoseconds (recall that the above mentioned laser has heating pulses of 5 *ps* duration). According to P. L. Komarov and P. E. Raad [48], the Fourier equation describes heat propagation from the illuminated TF into the substrate as follows: Consider a pulsed laser with short pulse duration of the order of picoseconds, see Fig. (5.9) and Fig. (5.10). During each pulse a given volume known as "volumetric heat source" on the TF heats up as a consequence of the laser light energy absorbed into the TF. The heating area, A, of the volumetric heat source is specified by adjusting the pulsing laser aperture and the optics of the system. It is assumed to be equal to 1 cm^2 in the heat dissipation calculation. The depth of the volumetric heat source is equal to the light penetration depth which is equal to $\delta_\lambda = \frac{1}{\alpha_{TF}}$. It is in the range of 148 Å-189 Å for α_{TF} in the range of 5.29×10^7-6.75×10^7 m^{-1} where α_{TF} is the absorption coefficient of the TF, with different Au volumetric concentration. After each pulse is completed, the TF begins to cool down to its initial temperature. During this process the heat generated in the TF and propagating into the substrate is described by Eq. (5.1). The thermal penetration depth during a time period t through the substrate whose thermal diffusivity, is $\gamma = \frac{K_S}{\rho_s C_S}$ can be estimated by Eq. (5.1) [48]. The substrate's temperature change, $\Delta\theta_S(t)$ over a time period t is almost equal to substrate's temperature change at the surface, $\Delta\theta_S(0,t)$, as a consequence of the high thermal conductivity of the substrate. The substrate has been assumed to be 100 μm in thickness. In any practical situation, it would probably be thicker. Note that

$$\delta(t) = \sqrt{\frac{K_S}{\rho_S C_S}(t - t')}, \tag{5.1}$$

where K_S is the thermal conductivity of the substrate. It is equal to 419 Wm^{-1}K^{-1} in the case of Ag and 2000 Wm^{-1}K^{-1} in the case of Diamond. $\rho_S C_S$ is the specific heat of the substrate. It is equal to 7 $\times 10^6$ Jm^{-3}K^{-1} in the case of Ag and 4.4 $\times 10^6$ Jm^{-3}K^{-1} in the case of Diamond.
$\delta(t)$ is the thermal penetration depth during a time period t through the substrate. t' is approximately equal to 2 *ps* as it shall be shown later.

P. L. Komarov and P. E. Raad [48] have shown that provided $\delta(t) \leq 100$ μm, it is acceptable to describe the heat transfer by the one-dimensional heat equation, Eq. (5.2) [48] where heat propagates in the z-direction as shown in Fig. (5.9):

$$\begin{aligned} \rho C_P \frac{\partial \theta}{\partial t} &= \frac{\partial}{\partial z}(K \frac{\partial \theta}{\partial z}) + Q(z,t), \\ Q(z,t) &\approx I(t)\alpha \exp(-\alpha z), \\ I(t) &= \frac{2E}{\tau\sqrt{\pi}} \exp[-4((t-t_0)/\tau)^2]. \end{aligned} \tag{5.2}$$

where
ρC is the specific heat of the TF and substrate system,
$\Delta\theta$ is the change of temperature of the TF and substrate system,
K is the thermal conductivity of the TF and substrate system,
Q is the laser energy absorbed by the thin-film's volumetric heat source,
$I(t) = 7.4 \times 10^5$ Wcm^{-2} is the heating laser intensity,
α is the absorption coefficient of the TF and substrate system,
z is a coordinate that is normal to the thin-film surface,
$E = 3.38$ μJ is the pulse energy,
$\tau = 5$ ps is the pulse duration,
t is the time,
$t_0 = \tau/2$ is the value of t where the laser intensity reaches its maximum.

Since the heat energy penetrates entirely through the TF, it is imperative to take into account the thermal properties of the TF as well as that of the substrate. For this reason the heat transfer equation is solved numerically due to the complexity of the analytical solution. In the numerical solution of Eq. (5.2) which is Eq. (5.3) below [48], the knowledge of the overall specific heat of the TF and substrate system, ρC, of the overall thermal conductivity of the TF and substrate system, K, as well as that of the overall absorption coefficient of TF and substrate system, α, is not required. Therefore one obtains:

$$\frac{\Delta\theta_{TF}(t)}{\Delta\theta_{TF}(t_0)} = 1 + [\frac{\rho_S C_S K_S}{\rho_{TF} C_{TF} K_{TF}}]^2 [(\frac{t_0}{t'} - 1)^{\frac{1}{2}} \frac{\Delta\theta_S(t_0)}{\Delta\theta_{TF}(t_0)} - (\frac{t}{t'} - 1)^{\frac{1}{2}} \frac{\Delta\theta_S(t)}{\Delta\theta_{TF}(t_0)}], \tag{5.3}$$

where $\Delta\theta_{TF}(t)$ is the change of temperature of the thin-film at time t; $\Delta\theta_{TF}(t_0)$ is the change of temperature of the thin-film at time t_0; $\Delta\theta_S(t)$ is the change of temperature of the substrate at time, t. The thermal penetration depth $\delta(t)$ into substrate is equal to 95 μm for diamond when $t = 7.5$ μs and 85 μm for Ag, when $t = 42$ μs, as it shall be shown later. $\Delta\theta_S(t_0)$ is the change of temperature of the substrate at time, $t_0 = \tau/2$, with thermal penetration depth of $\delta(t_0)$ into substrate. $\delta(t_0) = 246$ Å for a diamond substrate and $\delta(t_0) = 81$ Å for a silver substrate. $t' = L_{TF}^2 \frac{\rho_{TF} C_{TF}}{K_{TF}} = 2$ ps is the time required for heat to propagate through the TF. Finally, $K_{TF} = 27$ Wm^{-1}K^{-1} and $\rho_{TF} C_{TF}$=5 $\times 10^5$ Jm^{-3}K^{-1}.

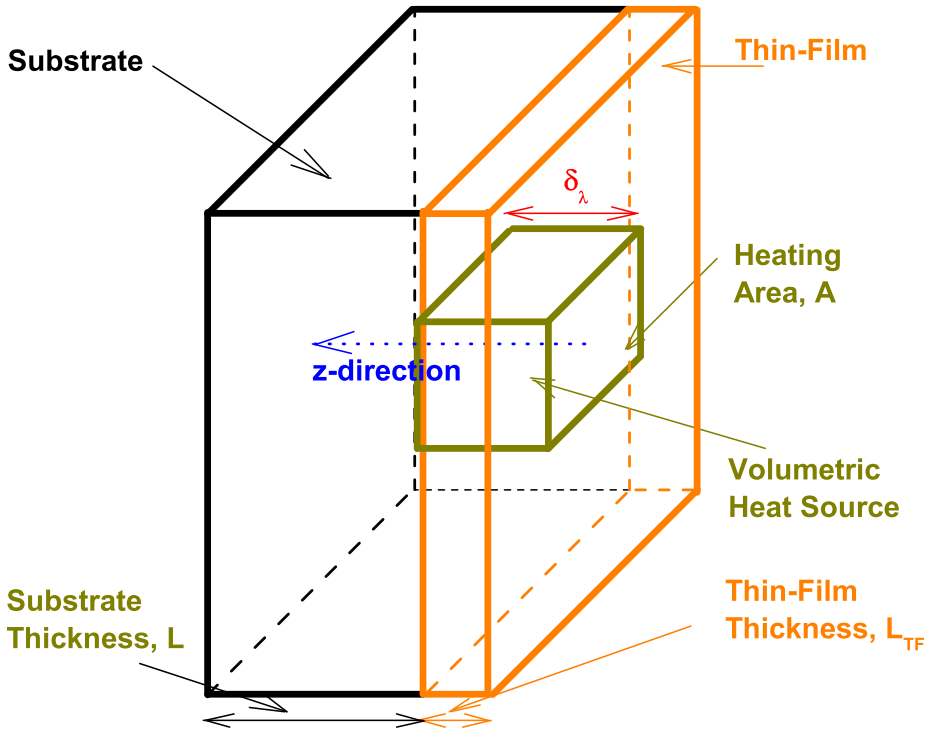

Figure 5.9: Illuminated Au-VO_2 Thin-Film deposited on a Substrate after P. L. Komarov and P. E. Raad [48].

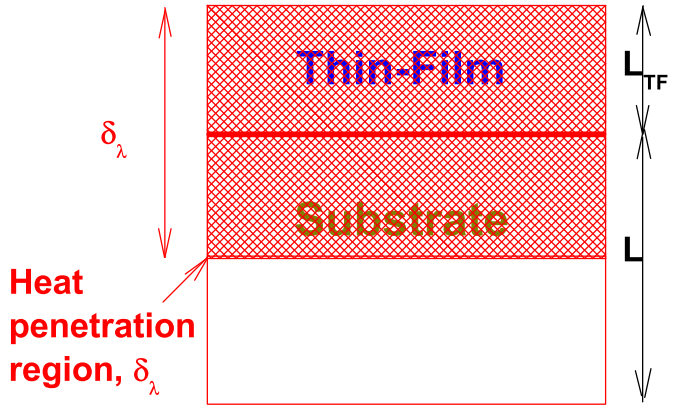

Figure 5.10: Transversal view of the Illuminated Au-VO_2 Thin-Film deposited on a Substrate after P. L. Komarov and P. E. Raad [48].

5.2.3 Calculation of Heat Dissipation

Eq. (5.3) can be used to determine the necessary time required for both the thin-film and the substrate to cool down to ambient temperature, this is done by letting $\Delta\theta_{TF}(t) = \Delta\theta_S(t) \approx 0^0K$, which is our desired change of temperature. Next, $t_0 = \tau/2$, this is justified by the fact that the temperature reaches its maximum when the laser intensity reaches its maximum at $\tau/2$. According to P. L. Komarov and P. E. Raad [48] $\Delta\theta_{TF}(t_0) \approx \Delta\theta_{TF}(0, t_0)$ and $\Delta\theta_S(t_0) \approx \Delta\theta_S(0, t_0)$ with:

$$\Delta\theta(0,t) = \frac{2E\alpha}{\pi\tau\sqrt{\rho CK}} \int_0^t \int_0^\infty \frac{\exp[-4(\frac{t_0-t'}{\tau})^2]}{\sqrt{t-t'}} \exp[-z'(\alpha + \frac{z'}{4\alpha(t-t')})]dz'dt'. \quad (5.4)$$

Consequently, $\Delta\theta_{TF}(t_0)$ and $\Delta\theta_S(t_0)$ could be computed by solving Eq. (5.4) with the appropriate parameters for the TF and the substrate. Eq. (5.4) is solved numerically using a QuasiMonteCarlo method and it is found that the temperature of the TF monotonically increases with the Au volumetric concentration in the Au-VO_2 nanocomposite TF as shown in Fig. (5.11). Moreover, $\Delta\theta_S(t_0) \approx \Delta\theta_{TF}(t_0)$, this follows as a consequence of the high thermal conductivity of the substrate [48].

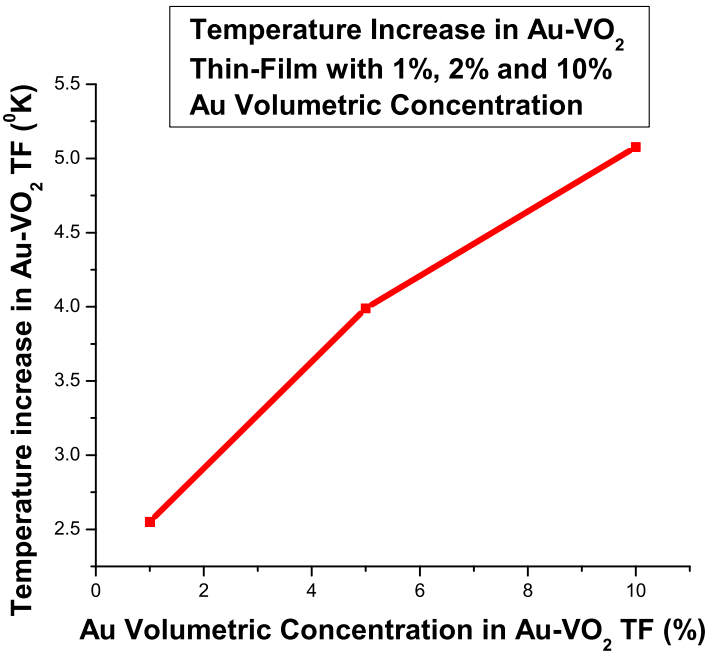

Figure 5.11: Thin-Film Temperature increase, $\Delta\theta_{TF}(t_0)$, in ^{0}K versus Au volumetric concentration in Au-VO_2 Thin-Film. The Laser Input Intensity is $7.4 \times 10^5 \mathrm{Wcm}^{-2}$ and the pulse duration is 5 ps.

Next [49], given $K_{Diamond} = 2000$ $\mathrm{Wm^{-1}K^{-1}}$, $K_{Ag} = 419$ $\mathrm{Wm^{-1}K^{-1}}$, $K_{Au} = 320$ $\mathrm{Wm^{-1}K^{-1}}$, $K_{VO_2} = 31$ $\mathrm{Wm^{-1}K^{-1}}$, $\rho_{Diamond} = 3515$ $\mathrm{Kgm^{-3}}$, $\rho_{Ag} = 10490$ $\mathrm{Kgm^{-3}}$, $\rho_{Au} = 19300$ $\mathrm{Kgm^{-3}}$, $\rho_{VO_2} = 6110$ $\mathrm{Kgm^{-3}}$, $C_{Diamond} = 471$ $\mathrm{JKg^{-1}K^{-1}}$, $C_{Ag} = 234$ $\mathrm{JKg^{-1}K^{-1}}$, $C_{Au} = 125$ $\mathrm{JKg^{-1}K^{-1}}$ and $C_{VO_2} = 300$ $\mathrm{JKg^{-1}K^{-1}}$ one may calculate $\rho_{TF} = p\rho_{Au} + (1-p)\rho_{VO_2}$, it is in the range of $4890 - 5836$ $\mathrm{Kgm^{-3}}$ for p varying in the range of $p = 0.01 - 0.10$ where p is the volumetric concentration of Au nanoparticles, ρ_{Au} is the density of Au and ρ_{VO_2} is the density of VO_2, the heat capacities of the TF is found to be in the range of 145-189 $\mathrm{JKg^{-1}K^{-1}}$ from:

$$C_{TF} = \frac{1}{\rho_{TF}} \frac{\rho_{Au}\rho_{VO_2}C_{Au}C_{VO_2}}{(\rho_{Au}C_{Au} + \rho_{VO_2}C_{VO_2})}, \tag{5.5}$$

where C_{Au} and C_{VO_2} are respectively the heat capacities of Au and VO_2. Finally, $K_{TF} = 27$ $\mathrm{Wm^{-1}K^{-1}}$ is equal to [40]:

$$K_{TF} = K_{VO_2} \frac{1 + 2\beta - 2p_{Au}(\beta - 1)}{1 + 2\beta + p_{Au}(\beta - 1)}, \tag{5.6}$$

$$\beta = \frac{K_{VO_2}}{K_{Au}}. \tag{5.7}$$

It is now easy to compute the necessary time for heat to propagate from the TF into the substrate. Hence the TF will cool down to the original ambient temperature, whereas the substrate temperature rise is negligible. This follows from the fact that the substrate thickness is much greater than that of the TF. The necessary time interval, t, between two successive pulses is equal to 7.5 μs for a diamond substrate and 42 μs for a silver substrate. The thermal penetration depth $\delta(t)$ in the diamond and silver substrate is found by substituting the appropriate values of t, $t^{'}$, $K_{diamond}$, K_{Ag}, $\rho_{diamond}C_{diamond}$ and $\rho_{Ag}C_{Ag}$ into Eq. (5.1). Therefore, $\delta(t)$ is found to be equal to 95 μm for diamond and 85 μm for Ag. It is clear that the required time interval between two successive pulses is shorter in the case of diamond than that of silver while the thermal penetration depth is greater in the diamond substrate compared to the silver substrate. This is due to the higher thermal conductivity of the diamond compared to the thermal conductivity of silver.

5.2.4 Conclusion

It may be concluded that the heat generated by a single pulse is manageable within limits by letting the time interval between successive pulses to be of the order of μs given a laser source whose peak intensity is 7.4×10^5 $\mathrm{Wcm^{-2}}$. Heat calculations have also been shown to be dependent of the Au volumetric concentration. In conclusion heat dissipation calculation in the thin-film and substrate system show that the heat generated by a single pulse in Au-VO_2 thin-films deposited on a diamond or silver substrate is controllable within limits.

Chapter 6

Conclusion

The estimated and computed Optical Kerr Effect (OKE) of Au-VO_2 nanocomposite thin-films has yielded a high value, comparable to that found in Au-SiO_2, Au-TiO_2 and Au-Al_2O_3 thin-films [29, 33], despite the fact that the Au volumetric concentration in the Au-VO_2 composites considered here is 10 percent at most. The main feature of the model calculations of the real and imaginary parts of the effective nonlinear susceptibilities is their monotonically increasing magnitudes as the Au volumetric concentration increases. This follows from the fact that the Au is responsible for the optical nonlinearity. The value of the effective OKE $\chi^{(3)}$ is of the order of 10^{-6} esu when the Au-VO_2 thin-films is below 68 ^{0}C. It is of the order of 10^{-7} esu when the Au-VO_2 thin-films is above T_t.

The overall effective THG $\chi^{(3)}_{Au-VO_2}$ is several orders of magnitude smaller than the overall effective OKE $\chi^{(3)}_{Au-VO_2}$. The reasons for this are: Firstly, there is no contribution from the hot-electron effect in the pure Au nanoparticles, secondly, the intraband effect in the pure nanogold particles is smaller in the case of THG compared to the OKE one by three orders of magnitude, and lastly the interband effect in the nanogold particles during THG process is smaller than that in the OKE by four orders of magnitude. Hence, THG $\chi^{(3)}_{Au}$=THG $\chi^{(3)}_{(intra)}$+THG$\chi^{(3)}_{(inter)}$ $= 1.8 \times 10^{-12}$ esu meanwhile OKE $\chi^{(3)}$ =OKE $\chi^{(3)}_{(intra)}$+ OKE $\chi^{(3)}_{(inter)}$ + OKE $\chi^{(3)}_{(hot-electron)} = 1.2 \times 10^{-7}$ esu.

The modelling here of high-order harmonic generation in strongly absorbing media, as regards the amplitude of the primary beam, takes into account *pump attenuation* only, due to the absorption of light by the media. It is not concerned with *pump depletion* which is a consequence of the transfer of energy to the harmonics and which is small by comparison with attenuation in absorbing media. The modelling is applied to the so-called transmission and reflection configurations. The former refers to the case in which the high-order harmonic wave is monitored in the same direction as the input fundamental wave, whereas the latter describes the situation in which the fundamental wave is in the opposite

direction to the high-order harmonic one.

The general formula that describes the high-order harmonic intensity output from the absorbing medium in the transmission configuration is given in SI units and esu as Eq (4.20) and Eq. (4.21). In the case of SHG in a lossless medium Eq (4.20) reduces to the same result as that obtained by P. N. Bucther and D. Cotter [1] whereas Eq. (4.21) reduces to the result of Y. R. Shen [35]. In the case where the phase matching is satisfied $\Delta k = 0$ Eq. (4.21) reduces to the same result as that of T-J. Chen et al. [23]. In the case of THG in a lossless medium Eq (4.20) reduces to the same result as that obtained by P. N. Bucther and D. Cotter [1] meanwhile Eq. (4.26) is similar to the result of J. F. Reintjes [34]. In the reflection configuration, the general formula that describes the high-order harmonic intensity output from the absorbing medium is given in SI units and esu by Eq. (4.45) and Eq. (4.46). It is easy to see that in the case of SHG Eq. (4.46) and Eq. (4.47) are similar to the results of T-J. Chen et al. [23].

The ratio of the third-harmonic intensity to the fundamental intensity is termed the *conversion coefficient* or the *conversion efficiency*, and it is denoted by η [23, 34]. It is useful in the sense that it expresses quantitatively the amount of input light of frequency ω converted into light of frequency $n\omega$, where n is the order of nonlinear polarisation [1]. The model calculations of the conversion efficiencies of THG in the transmission and reflection configurations allow one to conclude that they are greater in the reflection configuration compared to the transmission one above and below T_t in the photon energy range $1.0 - 3.0$ eV, see Fig. 5.1 to 5.8. Moreover, the conversion efficiency η is bigger when the value of the effective $\chi^{(3)}$ is computed using the model of Ricard et al. [6] than that of Sipe and Boyd [2]. The reason for this difference follows from the fact that the local field effect in the former is greater than that in the latter. Next, η is greater when computed below T_t rather than above that temperature in the transmission configuration but not in the reflection configuration. Finally, there is negligible THG when the laser light input is continous at average intensity of 0.45 Wcm^{-2}.

It is essential to note that in the transmission configuration the THG light output has an exponential decay factor dependent on the thin-film thickness L see Eq. (4.20) and Eq. (4.21). This indicates that the THG radiation exponentially decreases as L increases, recall that in the transmission configuration $\eta = 10^{-22}$ above 68 ^{0}C and $\eta = 10^{-19}$ below T_t. A higher conversion efficiency will be obtained by using thin-film with optimized characteristic length. In the reflection configuration the conversion coefficient does not depend upon the thin-film thickness. Consequently, η does not suffer any loss as L increases, because the THG output does not depend on the thin-film thickness. In the reflection configuration $\eta = 10^{-17}$ below T_t and $\eta = 10^{-18}$ above 68 ^{0}C.

The heat generated as a consequence of the illumination of the thin-film by the laser [23] may be controlled by using a simple cooling device which consists of a substrate on which the thin-film is deposited and by limiting the laser pulse energy. The choice of such a substrate depends on whether THG is monitored in the transmission or reflection configuration. In the former a transparent substrate must be used (for example Diamond) whereas in the latter an opaque substrate may be used (for example Ag). Calculations pertaining to the removal of heat from the illuminated film are shown to be dependent of the Au volumetric concentration. By letting the time interval between successive pulses to be of the order of μs given a laser source whose peak intensity is 7.4×10^5 Wcm^{-2} and pulse duration is 5 ps, it has been shown that heat generated by a single pulse is manageable.

The main conclusion here is that η is extremely weak for the Au-VO_2 thin-films. It is of the order of 10^{-17} under the best of circumstances and it is difficult to see a potential use of this system as a tunable frequency converter. N. A. Papadiogannis et al. [32] have reported η to be in the range of $10^{-10} - 10^{-13}$ for pure Au, using a laser of intensity 10^{11} Wcm^{-2}. According to T-J. Chen et al. [23] and G. I. Petrov et al. [36] , it is clear that, in order to achieve high conversion efficiency it is preferable to have a transparent material so that a negligible proportion of the incident light will be absorbed by the medium so that the light intensity can be pushed very high before encountering heating problems. Moreover, the thickness of the transparent material must be chosen to be a few milimiters [23, 36] to achieve the phase-matching condition. Finally, It is desirable to use a material with the highest possible THG $\chi^{(3)}$. They have also pointed out that an increase of the laser intensity above a certain threshold level will damage the material. The heat dissipation calculation performed in this work have shown that with a short pulse duration of 5 ps and pulse energy of 3.4 μJ, the heat generated by a single pulse is tolerable. This leads one to suggest that by reducing the pulse duration and keeping constant the pulse energy a higher laser intensity will be achieved and consequently a higher conversion efficiency will be obtained. Note that this suggestion is the same as that of N. A. Papadiogannis et al. [32]. They suggested to use ultrashort laser pulses to avoid excessive temperature rise or plasma creation in the TF, while producing third-order harmonics.

Bibliography

[1] Paul N. Butcher and D. Cotter, *The Elements of Nonlinear Optics*, Cambridge University Press, 1990.

[2] J. E. Sipe and R. W. Boyd, *Phys. Rev. A* **46,** 1614-1629 (1992).

[3] C. F. Bohren and D. R. Huffman, *Absorption and Scattering of Light by Small Particles*, Wiley, New York, 1983.

[4] D. Ricard, P. Roussignol and C. Flytzanis, *Opt. Lett. A* **10,** 511 (1985).

[5] R. W. Boyd, J. G. Gehr, G. L. Fisher and J. E. Sipe, *Pure Appl. Opt. A* **5,** 505-512 (1996).

[6] F. Hache, D. Ricard, C. Flytzanis, and U. Kreibig, *Appl. Phys. A* **47,** 347-357 (1988).

[7] F. Hache, D. Ricard, C. Flytzanis, *J. Opt. Soc. Am. B* **3,** 1647-1655 (1986).

[8] H. W. Verleur, A. S. Barker, Jr., C. N. Berglund, *Phys. Rev.* **172,** 788 (1968).

[9] R. W. Boyd, *Nonlinear Optics*, Academic, Boston, 1992.

[10] R. A. Fisher, *Optical Phase Conjugation*, Academic, New York, 1983.

[11] C. Flytzanis, F. Hache, M. C. Klein, D. Ricard, P. Roussignol, *Nonlinear Optics in Composite Materials*, E. Wolf. Progress in Optics XXIX, Elsevier Science Publishers B. V., 1991.

[12] J. F. Ward and G. H. C. New, *Phys. Rev. A* **185,** 57-72 (1969).

[13] G. C. Bjorklund, *IEEE J. Quant. Elecron. A* **QE-11,** 287-296 (1975).

[14] P. Drude, *Ann. Phys. A* **1,** 566 (1900).

[15] A. Sommerfeld, *Ann. Phys. A* **4,** 28 (1909).

[16] N. W. Ashcroft and N. D. Mermin, *Solid State Physics*, Holt-Saunders, Philadelphia. Pa., 1976.

[17] C. Sonnischen, *Thesis.,* 2001.

[18] J. C. Maxwell-Garnett, *Phil. Trans. Roy. Soc. A A* **203,** 385 (1904).

[19] A. Lakhtakia, *Optik* **103,** 85-87 (1996).

[20] R. Ruppin, *Optics Communication* **182,** 273-279 (2000).

[21] G. Mie, *Ann. Phys. A* **25,** 377 (1908).

[22] L. Genzel, T. P. Martin and U. Kreibig, *Z. Phys. B* **21,** 339-346 (1975).

[23] T-J. Chen, R. N. Zitter and R. Rao, *Phys. Rev. A***51,** 706 (1995)

[24] G. J. Hyland, *J. Phys. C (Proc. Phys. Soc.)* **1,** ser. 2 (1968)

[25] S. Berthier, *Optique des Milieux Composites*, Polytechnica, 1993.

[26] J. H. Weaver and H. P. R. Frederikse, *Optical Properies of Seclected Elements*, *Handbook of Chemistry and Physics* **84,** (2003-2004)

[27] D. Compton, L. Cornish and E. van der Lingen, *Gold Bulletin* **36/1,** 10 (2003)

[28] M. Thomas and E. E. Chain, *Thin Solid Films* **204,** L1-L4 (1991)

[29] S. Scheistel, C. M. Cotell, C. A. Carossa, K. S. Grabowski and G. K. Hubler, *Nucl. Instrum. Meths. Phys. Res. B***566,** 127-128 (1997)

[30] L. Banyai, Y. Z. Hu, M. Lindberg and S. W. Koch, *Phys. Rev. B* **38,** 1842 (1988).

[31] G. L. Eesley, *Phys. Rev.B* **33,** 2144 (1986).

[32] N. A. Papadogiannis, P. A. Loukakos and S. D. Moustaizis, *Opt. Comm.* **166,** 133 (1999)

[33] H. B. Liao, R. F. Xiao, J. S. Fu, H. Wang, K. S. Wong and G. K. L. Wong, *Opt. Lett.* **23, No. 5,** 388 (1998)

[34] J. F. Reintjes, *Nonlinear Optical Parametric Processes in Liquids and Gases*, Academic, Boston, 1984.

[35] Y. R. Shen, *The Principles Of Nonlinear Optics*, Wiley, New York, 1993.

[36] G. I. Petrov, V. Shcheslavsky and V. V. Yakvlev, *Appl. Phys. Lett.* **83,** 3393 (2003)

[37] G. Veres, S. Matsumoto, Y. Nabakawa and K. Midorikawa, *Appl. Phys. Lett.* **81,** 3714 (2002)

[38] H. Verleur, *J. Opt. Soc. Am.* **58, No. 10,** 1356 (1968).

[39] W. K. Burns and N. Bloembergen, *Phys. Rev.B* **4,** 3437 (1971).

[40] J. E. Parrott and A. D. Stuckes *Thermal Conductivity of Solids*, Pion, London, 1975.

[41] P. B. Johnson and R. W. Christy, *Phys. Rev. B* **6,** 12 (1972).

[42] N. J. Weber, D. Milan and W. L. Smith, *Opt. Eng.* **17,** 466 (1978).

[43] S. R. Friberg and P. W. Smith, *IEEE J. Quantum Electron* **QE-23,** 2089 (1987).

[44] R. Adair, L .L. Chase and S. A. Payne, *J. Opt. Soc. Am. B* **4,** 875 (1987).

[45] W. E. Williams, M. J. Soileau and E. W. van Stryland, *Opt. Comm.* **50,** 256 (1984).

[46] J. R. Hill, G. Parry and A. Miller, *Opt. Comm.* **43,** 151 (1982).

[47] D. C. Hanna, M. A. Yuratich and D. Cotter, *Nonlinear Optics of Free Atoms and Molecules*, Springer Series in Optical Sciences **17,** Berlin: Springer-Verlag, 1979.

[48] P. L. Komarov and P. E. Raad, *International Journal of Heat and Mass Transfer* **47,** (2004).

[49] www.matweb.com.

Glossary of mathematical symbols

c is the velocity of light in vacuum.
e is the modulus of electronic charge.
$\mathbf{e}, \mathbf{e_j}$ is the unit vector in polarization direction of the field $\mathbf{E}_\omega, \mathbf{E}_{\omega_\mathbf{j}}$.
$exp(x)$ is the exponential (e^x).
E_F is the Fermi energy.
$E(t), E_j(t)$ are the scalar amplitudes of $\mathbf{E}_\omega, \mathbf{E}_{\omega_\mathbf{j}}$.
$\mathbf{E_t}$ is the optical field.
$\mathbf{E}_\omega$ is the Fourier transform of the electric field.
E_t is the amplitude of the monochromatic electric-field component at frequency ω.
$f(\omega)$ is the local field factor at frequency ω in medium with isotropic or cubic symmetry.
$g_1(\nu), g_2(\nu)$ and $g_3(\nu)$ are dimensionless quantities of the order one.
$\hbar$ is the Dirac constant.
$I_{n\omega}$ is the intensity of monochromatic travelling wave at frequency $n\omega$.
k is the magnitude of $\mathbf{k}$.
k_j is the magnitude of the wave vector of optical wave with frequency ωj.
k_P is the sum of constants $k_1, k_2 + \ldots + k_n$.
$\mathbf{k}$ is the wave vector of optical wave.
$\mathbf{k_j}$ is the wave vector of optical wave with frequency ωj.
$\mathbf{k_P}$ is the vector sum of wave vector $\mathbf{k_1} + \mathbf{k_2} + \ldots + \mathbf{k_n}$.
$K(-\omega_\sigma; \omega_1, \ldots, \omega_n)$ is the conventional numerical factor in expression for n-th order polarization at frequency ω_σ.
m is the electro rest mass.
n is the order of nonlinearity.
$n(\omega)$ is the refractive index at frequency ω.
$n_j(\omega)$ is the refractive index at frequency ω_j.
$n_2^I(\omega)$ is the nonlinear refraction coefficient defined with respect to optical intensity I.
$n_0(\omega)$ is the nonlinear refractive index at frequency ω.
$P(t), P_j(t)$ are the scalar amplitudes of $\mathbf{P}_\omega, \mathbf{P}_{\omega_\mathbf{j}}$.
$\mathbf{P}_\omega$ is the Fourier transform of $P(t)$.

$P_{\omega_j}^{(n)}$ is the amplitude of the monochromatic component at frequency ω_j of nth-order polarization.
$P_{\omega_j}^{(NL)}$ is the amplitude of the monochromatic component at frequency ω_j of nonlinear polarization.
$\mathbf{P^{(n)}(t)}$ is the nth-order component of $P(t)$.
$\mathbf{P^{(n)}}(\omega)$ is the Fourier transform of $P(t)$.
$\mathbf{P^{(NL)}(t)}$ is the total nonlinear polarization.
$\mathbf{P^{(NL)}}(\omega)$ is the Fourier transform of $\mathbf{P^{(NL)}(t)}$.
$P_\omega, P_{3\omega}$ are the powers of optical beam at frequency $\omega, 3\omega$.
$\mathbf{R}$ is the coordinate axis transformation matrix.
$\mathbf{R_n}$ is the nth-order polarization response function.
$\mathbf{s}$ is the unit vector in the direction of optical wave propagation.
SPR is the surface plasmon resonance.
t is the time variable.
T_1 is the energy lifetime.
T_2 is the dephasing time.
$T_1^{'}$ is the energy lifetime of a two level system.
$T_2^{'}$ is the dephasing time of a two level system.
z is a coordinate that is normal to the thin-film surface.
α, α_ω is the intensity absorption coefficient.
δk is the magnitude of phase mismatch.
$\delta \mathbf{k}$ is the vector phase mismatch.
$\epsilon(\omega)$ is the dielectric constant.
ϵ_0 is the permittivity of free space.
$\epsilon(\omega)$ is the dielectric tensor.
η is the conversion coefficient.
$\kappa(\omega)$ is the imaginary component of the refractive index at frequency ω.
$\chi^{(n)}(-\omega_\sigma; \omega_1, \ldots, \omega_n)$ is the nth-order scalar susceptibility.
$\chi^{(\mathbf{n})}(-\omega_\sigma; \omega_\mathbf{1}, \ldots, \omega_\mathbf{n})$ is the nth-order tensor susceptibility.
ω is the frequency in eV.
ω_n is the carrier density parameter related to the plasma frequency.
ω_c is the collision frequency.
s_i is the strength of the i'th harmonic oscillator.
ω_i is the frequency of the i'th oscillator.
Γ_i is the linewidth of the i'th oscillator.
$< \ldots >$ is the cycle average.
$\Delta\theta$ is the change of temperature of the TF and substrate system
Δ is the vector del operator.
ρC is the specific heat of the TF and substrate system.
$\Delta\theta$ is the change of temperature of the TF and substrate system.
K is the thermal conductivity of the TF and substrate system.
Q is the laser energy absorbed by the thin-film's volumetric heat source.
τ ps is the pulse duration.